



**Politecnico
di Torino**

Master's degree in Mechanical Engineering

**Optimal cabin thermal management
strategy for battery life extension in
electric vehicles**

Mattia Mauro

December 2023

Advisors

Prof. Ali Emadi

Prof. Ezio Spessa

Co-advisors

Ph.D. Atriya Biswas

Ph.D. Federico Miretti

Prof. Vittorio Ravello

This thesis project was conducted at McMaster Automotive Resource Center (MARC), and it was the result of a collaboration with Stellantis.



Abstract

In recent years, the transportation sector has witnessed a shift away from traditional combustion-based propulsion, driven by growing concerns over air pollution and climate change. Among the multitude of emerging technologies, battery electric vehicles (BEVs) have emerged as a prominent and highly supported solution. However, despite their increasing popularity, questions persist regarding their practical benefits in the current scenario. Challenging aspects are electric energy mix, battery longevity, and BEVs driving range. In this context, the following project aims to improve battery durability in BEVs. Then, to achieve this target, the main focus is on the Heating Ventilation and Air Conditioning (HVAC) unit, the most impacting auxiliary in terms of battery loads. Specifically, this system handles the cabin's thermal conditions in order to fulfill the passengers comfort request. In the literature efforts attempting to face similarly this problem can be evidenced, i.e. [1] , [2], [3]. Building upon these previous works, our aim was to develop a simplified solution that could potentially be implemented and executed in real-time. The proposed Integrated Energy and Thermal Management (IETM) strategy effectively minimizes the battery degradation rate at each instant. The IETM controller intelligently allocates battery power to the HVAC system, ensuring both thermal comfort and traction power needs as required by the driver. The key innovations in this model turn around the battery's State of Health (SOH) model, which relies on real data from A123 26650 battery cells tested to the end of their lifespan. This provides a realistic foundation for estimating the benefits of the IETM strategy. An important part for the project involved the implementation of a realistic model for the cabin thermodynamics, the HVAC system layout and its respective control logic. After the assessment of all the models and after checking the effectiveness of the IETM controller, the results about the advantages brought by the intelligent allocation of power to the HVAC were quantified over both WLTP cycle and EPA (UDDS and HWFET) drive schedules. Our findings demonstrated both reduced battery degradation and a positive impact on energy consumption. The improvements due to the IETM controller, depending on the cabin comfort settings, ranged from 3.1 % to 4.5 % in terms of battery capacity degradation reduction and from 0.5 % to 2.8 % in energy consumption improvement. At the end of this work, also the results found by using the IETM controller together with

the eco-driving controller, namely Cooperative Adaptive Cruise Control (CACC), developed within the same comprehensive project are given. They evidence a slightly dependency for the IETM controller on the CACC, but the total benefits are almost the exact sum of the two. Future research could involve real-time assessment of the IETM strategy using onboard vehicle systems. Additionally, an analysis can be conducted to spot which are the most impacting inputs to be predicted for finding the best benefits by using the IETM controller, i.e. solar radiation, external temperature and so on.

Contents

1	Introduction	1
1.1	Transportation sector, pollution and climate change	1
1.2	Moving steps towards transport decarbonisation	4
1.3	Transport electrification	6
1.4	Project foundation	7
1.5	Project outlines	9
2	Vehicle plant model	11
3	Cabin and HVAC models	14
3.1	Simscape™ cabin model	14
3.1.1	Convection and conduction contribution	16
3.1.2	Solar radiation contribution	18
3.1.3	Air fluxes contribution	20
3.1.4	Passengers contribution	21
3.1.5	Free cabin temperature evolution	22
3.2	HVAC model	23
3.2.1	HVAC system architecture	23
3.2.2	HVAC control logic	25
3.3	Lumped parameters cabin model	29
3.4	Tuned lumped parameters cabin model's results	31
3.4.1	Free temperature evolution	31
3.4.2	Reference temperature variability	32
3.5	Energy consumption related to cabin thermal comfort	36
4	Battery model	39
4.1	Battery pack design	39
4.2	Battery fading model	42
5	IETM strategy	48
5.1	IETM controller integration in HVAC control architecture	49
5.2	Mathematical formulation	50
5.3	Tuned IETM results	55
5.3.1	WLTP-based results	57
5.3.2	EPA-based results	60

5.3.3	Results comment	62
5.4	IETM-related benefits	64
5.4.1	Battery degradation improvements	64
5.4.2	Energy consumption improvements	65
6	Combined effect of eco-driving and IETM strategies	68
6.1	Battery degradation improvements	69
6.2	Energy consumption improvements	70
7	Future developments	72
8	Conclusions	72

List of Tables

1	Boundary conditions for the free cabin temperature evolution test of the Simscape TM model	22
2	Boundary conditions for the set of testes aimed at assessing the lumped parameters cabin model	33
3	Boundary conditions for the set of testes aimed at quantifying the HVAC impact on the energy consumption	36
4	HVAC system impact on the energy consumption at different reference temperatures	37
5	Pre-exponential factor table	44
6	Tuned weighting factor vector values	55
7	Boundary conditions for the set of simulations conducted for checking the effectiveness of the IETM controller	56

List of Figures

1	Sources of primary air pollutants and their relative weight	1
2	Earth's atmosphere energy budget	2
3	Global CO ₂ emissions from energy combustion and industrial processes, 1900-2022 [6]	3
4	Global energy-related CO ₂ emissions by sector [8]	3
5	Global CO ₂ emissions from transport by sub-sector in the Net Zero Scenario from 2000 to 2030 [9]	4
6	Worldwide electric car sales from 2016 to 2023 [11]	5
7	World gross electricity production by source, 2019 [12]	6
8	Range of battery energy used as function of weather conditions [13]	8
9	Vehicle Control - Simulink® Flowchart	11
10	Vehicle Plant - Simulink® Flowchart	11
11	Energy interactions of cabin's air volume and HVAC systems among them and with external environment	14
12	Energy interactions of the cabin's air volume with the external environment	15
13	One single layer's thermal model	16
14	Roof Simscape™ thermal model	17
15	Floor Simscape™ thermal model	17
16	Side walls Simscape™ thermal model	17
17	Glass windows Simscape™ thermal model	17
18	Radiation absorbed by the roof - Simscape™ thermal model	19
19	Radiation absorbed by the windows - Simscape™ thermal model	19
20	Radiation transmitted through the windows - Simscape™ thermal model	19
21	Air mass flow rate blown out of the HVAC system - Simscape™ thermal model	20
22	Air mass flow rate drawn from the cabin for recirculation - Simscape™ thermal model	21
23	Cabin's air leakages - Simscape™ thermal model	21
24	Sensible heat power generated by passengers - Simscape™ thermal model	22
25	Free cabin's temperature evolution - Simscape™ thermal model	23
26	Widespread architecture of HVAC system for EVs and HEVs	23
27	Psychrometric chart of humid air	27
28	Air flux temperature at cooler outlet and HVAC outlet	28
29	HVAC internal controller flow-chart	29
30	HVAC overall control flow-chart	29

31	Free cabin temperature evolution - models comparison	31
32	Free cabin temperature evolution - models comparison magnification	32
33	External ambient conditions: solar irradiance (a), outdoor temperature (b) . . .	33
34	Lumped parameters vs. Simscape TM : from 26 °C to 23 °C	34
35	Lumped parameters vs. Simscape TM : from 28 °C to 23 °C	34
36	Lumped parameters vs. Simscape TM : from 45 °C to 25 °C	35
37	Lumped parameters vs. Simscape TM : from 57 °C to 23 °C	35
38	Lumped parameters vs. Simscape TM : reference temperature variability	36
39	Original battery pack model - Simulink [®] flowchart	39
40	Battery R-circuit model	40
41	OCV battery characteristic surface - Simulink [®] look-up-table	41
42	Internal resistance battery characteristic surface - Simulink [®] look-up-table . . .	42
43	Final battery pack model - Simulink [®] flowchart	45
44	Battery capacity degradation along one cycle: WLTP vs. EPA	46
45	Battery loads along a WLTP cycle. Total battery load (blue) and HVAC battery load (red) to keep the cabin temperature at 18 °C	48
46	Cabin thermal comfort control architecture including IETM controller	50
47	Number of iterations undergone by the GSS algorithm to find the minimum of the cost function along a WLTP cycle	54
48	Weighting factor profile as function of the reference temperature	55
49	WLTP traction power request to the battery	56
50	EPA traction power request to the battery	57
51	Temperature and HVAC battery power profiles with a target temperature of 18°C (upper panel) and 19°C (lower panel) along the WLTP cycle	57
52	Temperature and HVAC battery power profiles with a target temperature of 20°C (upper panel) and 21°C (lower panel) along the WLTP cycle	58
53	Temperature and HVAC battery power profiles with a target temperature of 22°C (upper panel) and 23°C (lower panel) along the WLTP cycle	58
54	Temperature and HVAC battery power profiles with a target temperature of 24°C (upper panel) and 25°C (lower panel) along the WLTP cycle	59
55	Temperature and HVAC battery power profiles with a target temperature of 26°C (upper panel) and 27°C (lower panel) along the WLTP cycle	59
56	Temperature and HVAC battery power profiles with a target temperature of 18°C (upper panel) and 19°C (lower panel) along the EPA cycle	60
57	Temperature and HVAC battery power profiles with a target temperature of 20°C (upper panel) and 21°C (lower panel) along the EPA cycle	60

58	Temperature and HVAC battery power profiles with a target temperature of $22^{\circ}C$ (upper panel) and $23^{\circ}C$ (lower panel) along the EPA cycle	61
59	Temperature and HVAC battery power profiles with a target temperature of $24^{\circ}C$ (upper panel) and $25^{\circ}C$ (lower panel) along the EPA cycle	61
60	Temperature and HVAC battery power profiles with a target temperature of $26^{\circ}C$ (upper panel) and $27^{\circ}C$ (lower panel) along the EPA cycle	62
61	Battery degradation benefits with HVAC controlled through IETM controller rather than PI controller	64
62	Energy consumption benefits with HVAC controlled through IETM controller rather than PI controller	65
63	Battery degradation benefits with HVAC controlled through IETM controller and CACC enabled over HVAC controlled through PI controller and CACC disabled	69
64	Energy consumption benefits with HVAC controlled through IETM controller and CACC enabled over HVAC controlled through PI controller and CACC disabled	70

Glossary

BEV Battery electric vehicle. 5

BMS Battery management system. 40

CH₄ Methane. 1

CO Carbon monoxide. 1

CO₂ Carbon dioxide. 1

COP Coefficient of performance. 24

HEV Hybrid electric vehicle. 5

HVAC Heating, ventilation and air conditioning. 7

LCA Life cycle assessment. 6

N₂O Nitrous oxide. 1

NH₃ Ammonia. 1

NO_x Nitrogen oxides. 1

PM Particulate matter. 1

SO_x Sulphur oxides. 1

SOC State of charge. 12

VOC Volatile organic compounds. 1

1 Introduction

In recent years, the research in the field of transportation has been, and is going to be, mainly directed towards eco-driving technologies and more eco-friendly propulsion systems. Some countries are adopting always more stringent frameworks to contrast ground level pollutants and carbon-dioxide emissions. It is well known the unhealthy effect that emissions coming from human activities, including the transportation sector, have on the Earth's atmosphere. This adverse effect is not only harmful to human health, but in general to the whole bio-diversity.

1.1 Transportation sector, pollution and climate change

These human activities emissions can be split into *primary pollutants* (e.g. NO_x , SO_x , PM, CO, VOCs, NH_3), *secondary pollutants* (e.g. ground-level ozone, photo-chemical smog, acid rains), and greenhouse gases (e.g. CO_2 , CH_4 , N_2O). Primary pollutants are responsible, together with atmospheric agents, for secondary pollutants generation. Making reference to trusted data provided by the IEA, a weight for the impact of any human activities over the primary pollutants generation can be assigned. [4]

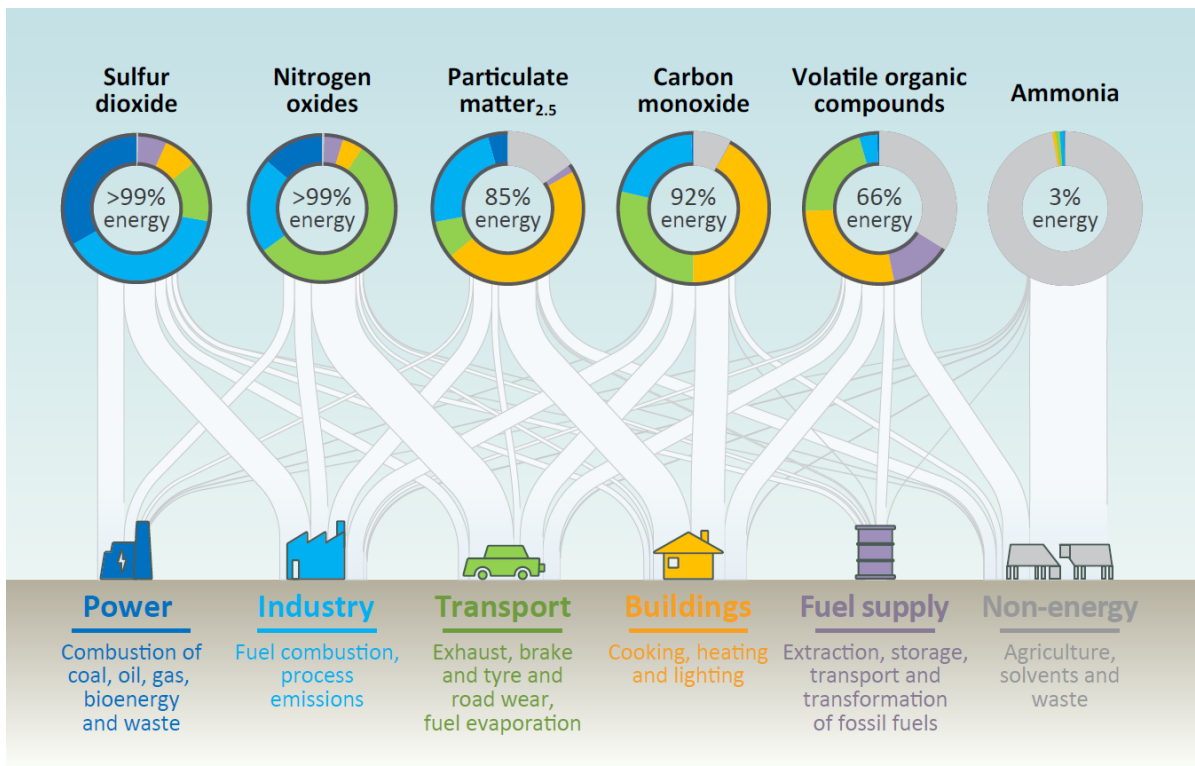


Figure 1: Sources of primary air pollutants and their relative weight

Looking at the Figure 1, it can be appreciated as energy sources are the main causes for air pollutants generation. The transportation sector has a relevant impact over all the primary pollutants, except for ammonia. The vital conditions on the low level of the atmosphere are a consequence of the energy budget among incoming solar radiation and outgoing radiations, as depicted schematically in Figure 2. To ensure this latter, a very important role is played by the gases composing the air. Always in Figure 2, it is possible to understand the importance of greenhouse gases. The reason why carbon-dioxide became a concern in the last decades, is because of its growing increase into the air mix, that leads to keep an higher portion of radiation into the atmosphere, thus resulting in a rise of the average Earth's temperature. The air mix is mainly composed of nitrogen (N_2) and oxygen (O_2), then, there are lots of other gases present in very low quantities. Among these ones, CO_2 is very important, even considering its very small quantity, because of its greenhouse property. Taking as reference value the carbon-dioxide volume concentration at the beginning of the Industrial Age (approximately 280 *ppm*), nowadays the concentration has risen of more than 45% (about 410 *ppm*). Most of this growth is caused by fossil fuels burning [5], and the main problem is the increase of the growing rate of this trend. Even the methane concentration in the air is becoming higher. Anyway, the main difference among these two is the length of the period their effects will endure, which is much higher for the carbon-dioxide than for the methane.

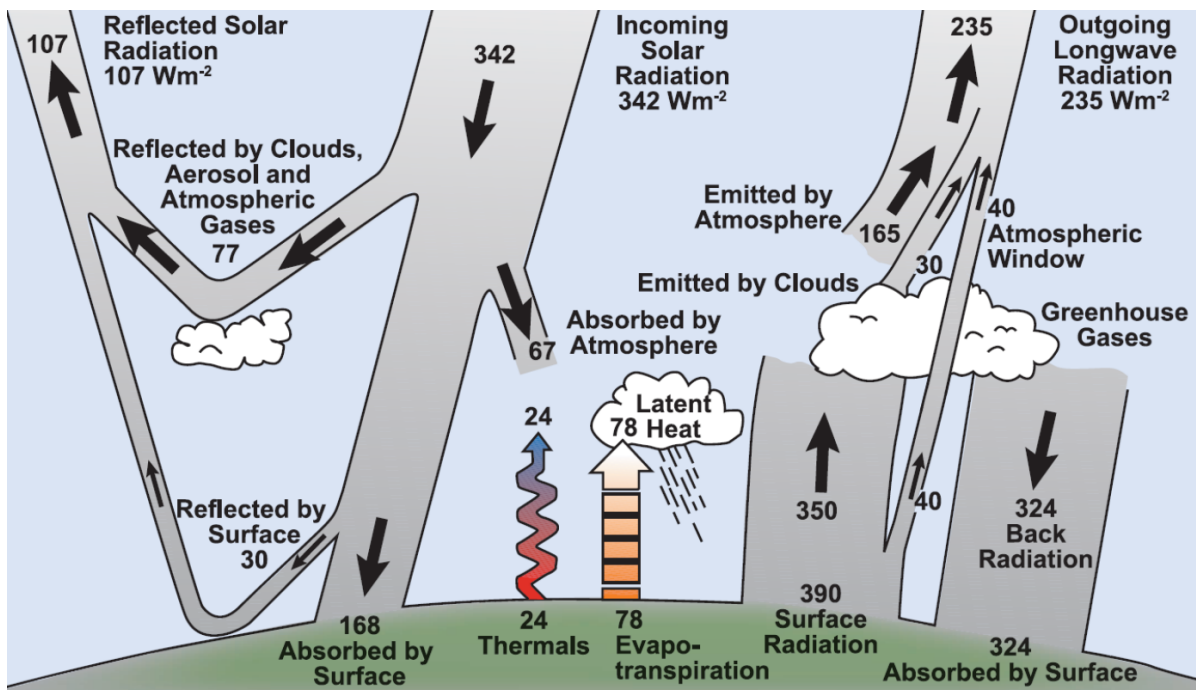


Figure 2: Earth's atmosphere energy budget

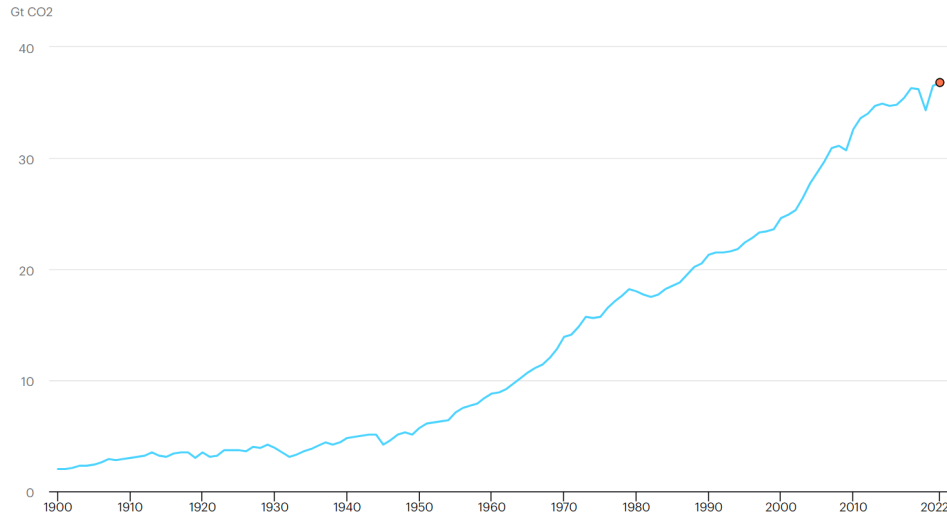


Figure 3: Global CO₂ emissions from energy combustion and industrial processes, 1900-2022 [6]

The problem of the current average transportation fleet is represented by the carbon-dioxide emission in the atmosphere. It has just been explained as these emissions can be strongly correlated to the amount of fossil fuels burnt. From the website of the IEA, it is possible to get the trend of CO₂ emitted from energy combustion and industrial processes, as shown in Figure 3, since the beginning of the XX century. It can be noticed as the increase is constantly becoming steeper, and the amount of carbon-dioxide emitted per year has passed from 24.6 *Gt* registered in 2000, to 36.8 *Gt* registered in 2022. Always IEA provides, from his annual reports [7], the impact of each energy sector on the CO₂ (see Figure 4). It is possible to get important

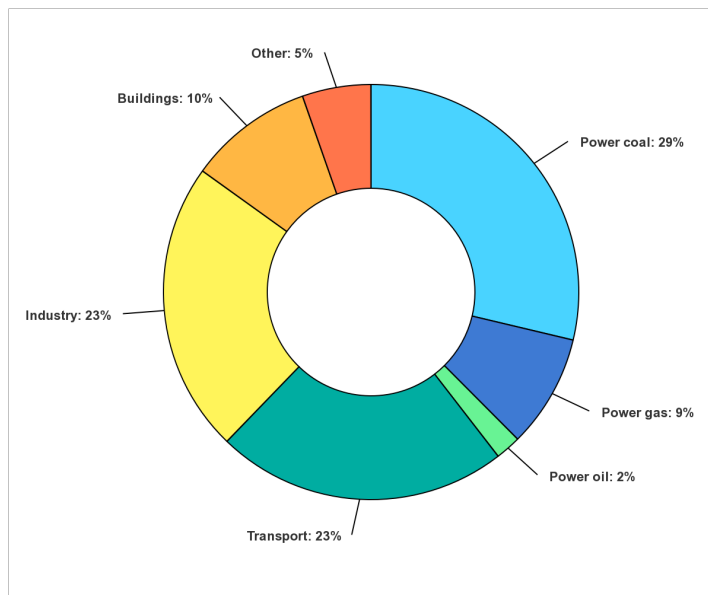


Figure 4: Global energy-related CO₂ emissions by sector [8]

information concerning the transportation sector. This is one of the energy sectors most affecting carbon-dioxide emissions, impacting for almost one quarter of the entire set of sectors. Moreover, examining this latter, its contribution can also be split among five classes: road, rail, shipping, aviation and pipeline transport. Of all these, as depicted in Figure 5, *road transport* gives one of the highest contribution to the global CO₂ budget. The reduction highlighted from 2018 to 2021 is to be considered an outlier, as strictly linked to Covid-19 pandemic, which had

tough economical implications, obviously reflected on partial blockages of transports and industries. Apart from this, the chart also contains an outlook for the emissions of carbon-dioxide in 2030 according to the Net Zero Emission (NZE) scenario. This is a normative IEA scenario that shows a pathway for the global energy sector to achieve net zero CO₂ emissions by 2050.

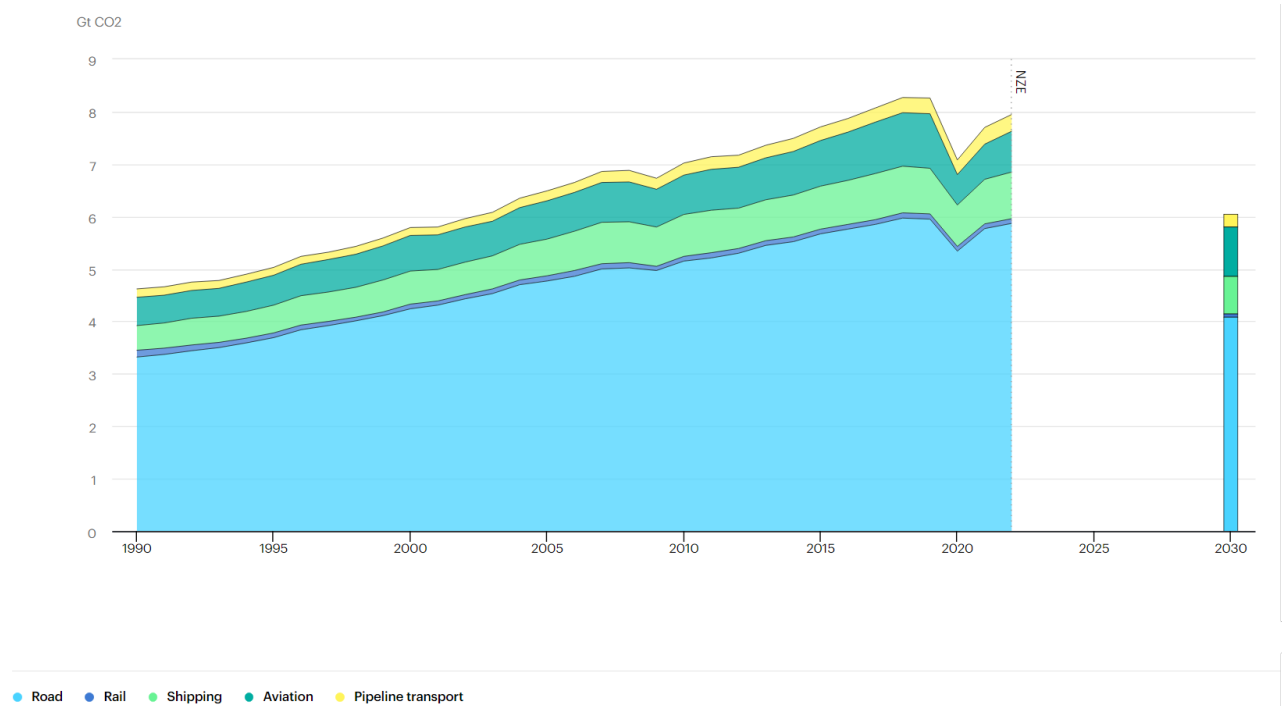


Figure 5: Global CO₂ emissions from transport by sub-sector in the Net Zero Scenario from 2000 to 2030 [9]

1.2 Moving steps towards transport decarbonisation

According to current data, transport accounts for about one quarter of the global energy-related CO₂ emissions. Unfortunately, due to the rise of the world population and the subsequent obvious intensification of trades, without any strong global action, the amount of carbon-dioxide global emission is expected to grow more and more. Thus, it is necessary to accelerate the transition of all energy sectors, included the transportation, towards sustainability. For the field of interest of the following work, this can be done only acting on many directions, such as using low-CO₂ fuels, improving vehicles energy efficiency and changing the way we use to travel. In addition to this, it has been noticed the extremely importance of including Carbon capture, utilisation and storage (CCUS) technologies to efficiently reach a global transition [10]. In accordance with this, the major international economies have issued policies to contrast this tendency and lead the transportation sector towards decarbonisation.

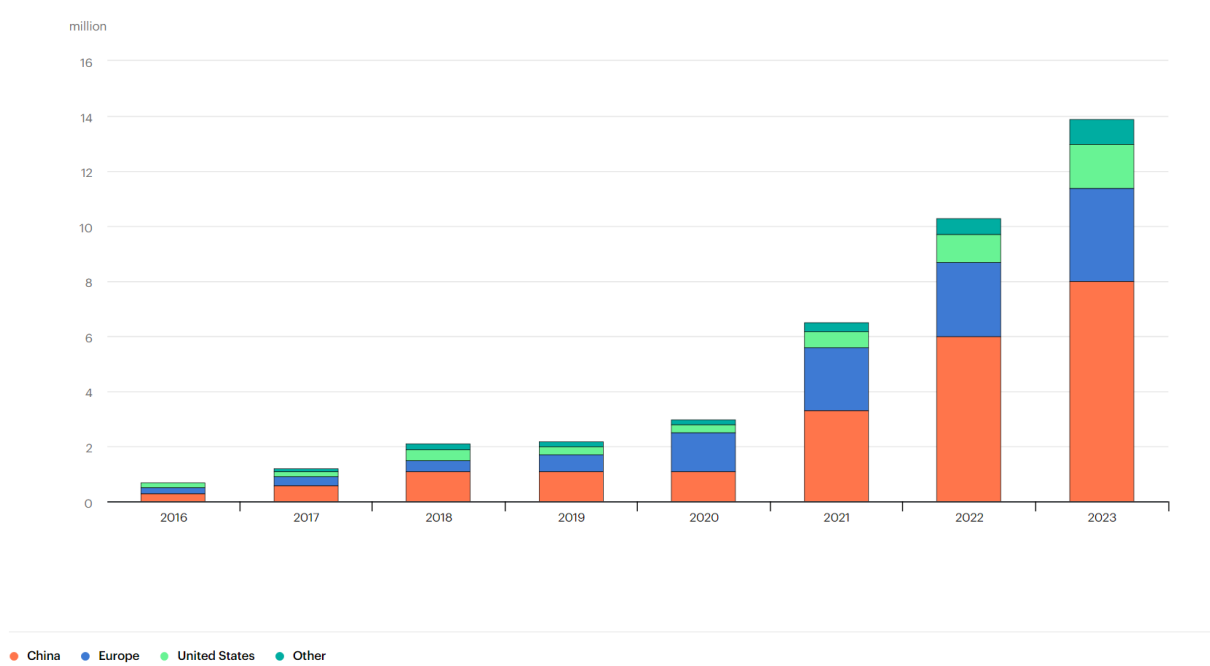


Figure 6: Worldwide electric car sales from 2016 to 2023 [11]

Currently, the most trusted pathway for doing this has been identified in transport electrification. Figure 6 reported above illustrates, to prove what has just been stated, the growth registered in electric car sales for the last few years, in different regions of the world. It is possible to appreciate as, in a relatively short period, the volume of brand-new registered electric cars has steeply increased. The problem that such transition towards electrification is asked to face, is the rising rare minerals (Li, Ni, Co, Mn) supply demand, whose reserves are limited and also condensed in a few regions of the world. Then, a series of socio-economical concerns may derive from this. Such an uneven distribution, in case of a further growth in sales of vehicles equipped with batteries, could lead to instabilities of the price of batteries, and inevitably also of the respective brand-new vehicles. Not only BEVs need a medium or large battery pack, but also, for instance, HEVs, and hydrogen fuel cell vehicles.

1.3 Transport electrification

About the electricity, this must not be improperly associated to “renewable energy” and it is extremely important to increase the consciousness of people about this fact, and to provide them with real data about the way electricity is currently produced. As a matter of fact the adjective

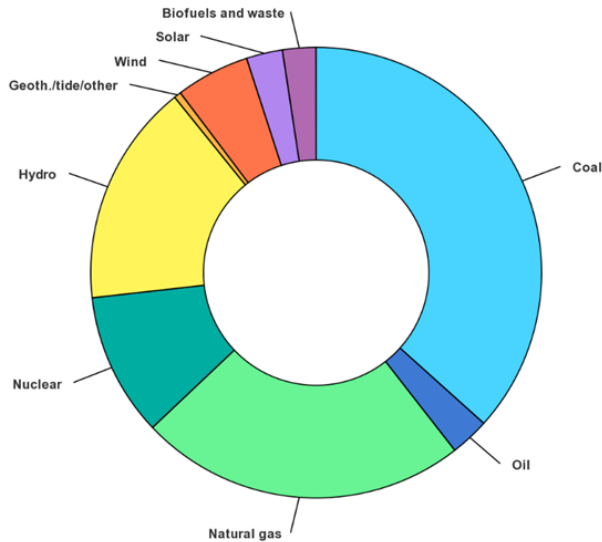


Figure 7: World gross electricity production by source, 2019 [12]

renewable must be associated to the source, and not to the energy itself. The pie-chart in Figure 7, even referring to the electricity production sources mix of a few years ago, clearly shows as globally the electric energy is not produced only by renewable sources (solar, wind, hydro) but still, more than one half is produced by non-renewable energy sources (coal, oil, natural gas). This is another challenging aspect to consider when, speaking about transport decarbonisation, we mention the electrification of the transportation sector. Other aspects necessarily to be enhanced concern the volume specific energy and mass specific energy of the

batteries, as well as volume specific power and mass specific power of the same, which are still too low, leading to low drive ranges. Also, further carbon emissions are associated to battery building and disposal. Thus, if one considered an LCA analysis within the current scenario, it is not stated that BEVs would have the upper hand on HEVs or conventional vehicles. Given the challenges discussed above regarding a complete transition to electrification in the current scenario, and considering the various pieces of legislation issued in favour of BEVs deployment, it is sensible to continue intensive research in this field to address potential issues that may arise in the event of a widespread electrification. The following list summarise the greatest advantages of BEVs over conventional ICE vehicles:

- regenerative braking
- no idling loss
- eliminate clutch losses
- improved motor efficiency
- power auxiliaries electrically driven

1.4 Project foundation

Across the previous section have been thoroughly underlined the main pros and cons which could arise from an intensive electrification of the transportation fleet. Then, in the very likely event that this should occur, kinds of problems strictly linked to the concerns discussed before could verify. The right way of thinking, that was the conductive thread of such project, would be to leverage the several advantages of the BEVs to further improve their energy efficiency, as well as to elongate the useful life of the batteries. This research work was conducted as part of a broader project involving a small-sized BEV (Chevrolet e-Spark 2015) with the following general objectives:

1. improving vehicle's energy efficiency through an eco-driving technology
2. reducing the battery degradation acting on the power delivered to the auxiliaries

Because the introduction on the market of BEVs is a recent matter, the same legislative frameworks do not consider any kind of threshold for the minimum endurance period of the battery pack yet. However, that is one of the most discussed points for the next legislative update. In the wake of such a possibility, the following master's thesis focused around the reduction in battery degradation.

In a BEV the entire power required by both traction and auxiliaries must come from the battery, differently from what happens in conventional ICE vehicles, whose auxiliaries are driven by the ICE through an alternator. Indeed, in a BEV the battery represents the only energy source. Consequently, in high-demand situations, such as when significant power is needed for traction, this can lead to an overload on the battery. Under this detrimental conditions the rate of battery fading can steeply increase. However, it is worth noting that among all the auxiliaries, the HVAC system ranks as the most energy-consuming one in a vehicle, which can lead to a huge reduction in its range. The role of this auxiliary system is to heat the cabin in winter and to cool it in summer, and also dehumidifying the air if necessary. This is the auxiliary system whom the cabin's thermal comfort management controller of a vehicle relies on to meet the passengers thermal request. To fulfill its commitment, generally compressors, heat exchangers and fans are involved in such system, leading to a considerable power demand.

Looking at the next picture, one can find a perfect summary of what has just been mentioned in the last paragraph. Figure 8 shows as, of total energy stored into the battery, the portion that can be allocated to power the drive-wheels of the vehicle is toughly affected by the weather conditions. More in detail, considering the Seville scenario, one can appreciate a reduction up to 40 % in extremely hot months. With such a climate combining a high temperature with a very intense incoming solar radiation, the energy required to chill the cabin's volume increases a lot.

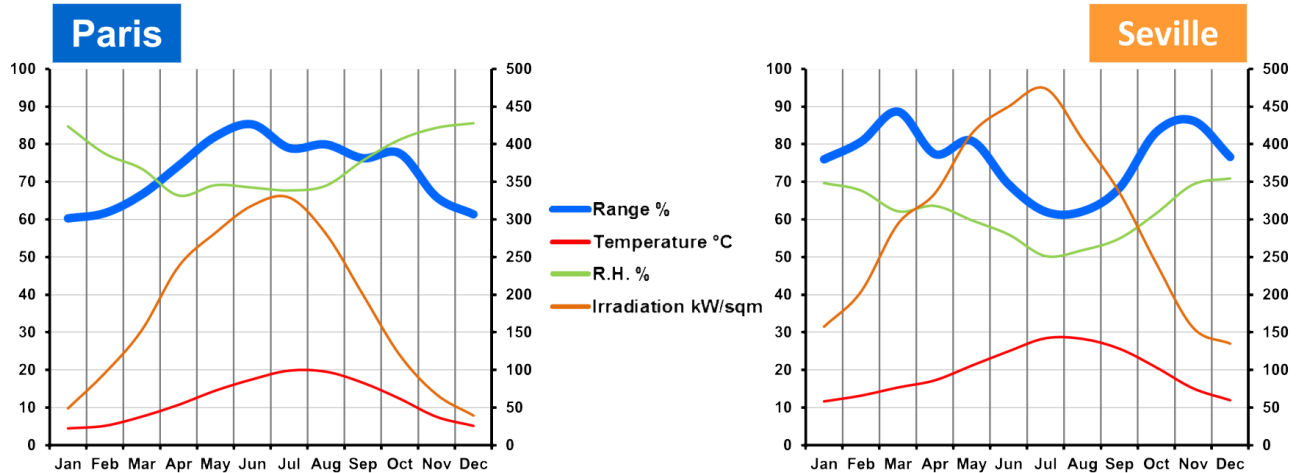


Figure 8: Range of battery energy used as function of weather conditions [13]

Taking into account all the things which have been reported up to this point, the idea of intelligently control the power delivered to the HVAC by the battery, in order to limit the detrimental effect of such auxiliary on the battery health, might come to mind. One can think about a clever supervisory control for the cabin thermal comfort, that is able to consider the battery state of health as well. Seeking around in the literature, it is possible to appreciate as the efforts taken towards such a direction start to get more extensive only by a few years. Concerning the exact topic that is matter of discussion, some papers took important step forwards, which is worth to be mentioned inside this work. The first to be mentioned focuses around the energy consumption reduction related to the HVAC system. An innovative real-time strategy based on Model Predictive Climate Control (MPCC) is developed. This strategy is able of performing an optimum splitting of the battery power between the heating and cooling, and the fan power is identified as a function of ambient temperature through an offline optimization process [1]. Another research proposes an innovative climate control system to account for the dynamics of the HVAC model while considering the importance of the ambient temperature and route behavior on the power usage that is needed to provide a comfortable climate in the cabin. This is done together with an accurate prediction of the external ambient temperature. This strategy claims improvements in energy efficiency and battery state of health [2]. The last one that we would like to mention, analysed the same problem in a similar way. The main difference is that, instead of using predictive algorithms, within this work the authors decided to rely on reinforcement learning to face the same issues, finally finding similar improvements [3].

This section served to introduce the reader to the subject that has been the primary foundation of this thesis project, and to provide whom it may concerned with a scientific argumentation about the reason for the work developed.

The idea behind this master's thesis starts from the steps moved forward in this subject. The

main purpose was to succeed in developing an energy management strategy, comparable to the ones from the papers cited but much simpler in formulation. The strategy developed, reported as **Integrated Energy and Thermal Management** (IETM) strategy, is capable of recognising if the overall instantaneous power request would lead to a high load on the battery, and then, if the conditions for compromising the thermal comfort subsisted, the IETM controller reduce to some extent the power forwarded to the HVAC while entirely fulfilling the traction request. Essentially, the feasibility of such a kind of control arises from the slowly varying of the cabin temperature compared to the fast dynamics of traction power. Then, the IETM controller can instantaneously spot if the battery could be asked to face an overloading condition, and if it is so, to re-shape the power allocated to the HVAC system, thus reducing the detrimental effect on the battery. In this way, by introducing the awareness of the battery fading on the top of the system components control, the same targets for cabin thermal comfort and vehicle's propulsion can be achieved with additional improvements on the battery exploitation.

1.5 Project outlines

After a comprehensive description of both the problem and the solution thought, it is now possible to provide the reader with a summary of what will be explained in the following chapters, which will delve into the technical work conducted and the results obtained. Across the first following chapters there will be the description of all the models preliminary developed and implemented from scratch in Simulink[®] environment, namely:

- Cabin thermodynamic model
- HVAC model and control architecture
- Battery model

All of these elements served as a crucial foundation for implementing the previously mentioned strategy, meaning IETM strategy. They were also essential for quantifying the observed benefits in comparison to a baseline. This baseline refers to the same vehicle in which the HVAC system was controlled without the application of the IETM strategy. In the end, this thesis will delve into the outcomes of the smart HVAC control strategy (IETM) and also discuss the results stemming from the integration of the two strategies (eco-driving and IETM) developed as part of the broader project as mentioned earlier.

2 Vehicle plant model

To simulate the strategy implemented in this work, it was necessary to rely on a vehicle dynamics model capable of reproducing the realistic behavior of the vehicle while following a predefined drive cycle. It is important to note that, in this thesis project, all the results presented in the final chapters are derived from simulations of only the *vehicle longitudinal dynamics* of the Chevrolet e-Spark 2015.

Since the primary objective was not to develop this specific model, it was provided pre-implemented in Simulink[®].

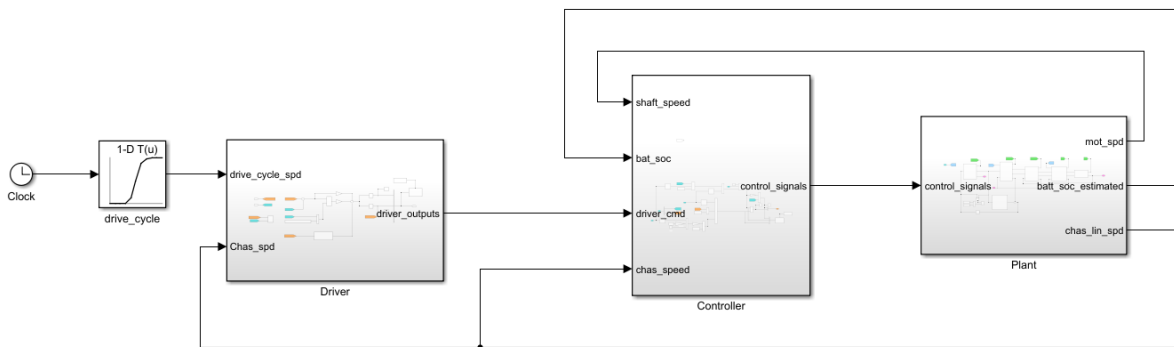


Figure 9: Vehicle Control - Simulink[®] Flowchart

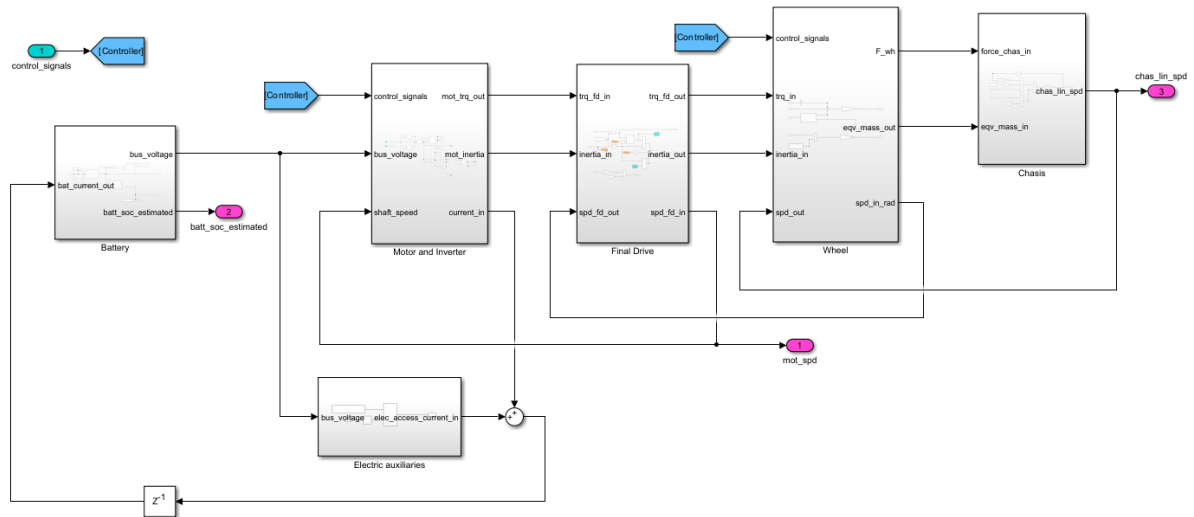


Figure 10: Vehicle Plant - Simulink[®] Flowchart

Although not a part of the work developed, the following paragraph will provide a brief but comprehensive description of this model. It is a *forward vehicle model*, meaning that the vehicle speed (*chas_lin_speed* in Figure 9 and Figure 10) is not exactly followed at each instant. Instead, a driver can generate a torque command based on the difference between the actual vehicle speed and the desired speed. To execute this command, the driver is represented by a PI controller, which takes the speed error and reacts by returning the sum of a term proportional to the current error, and a term proportional to the integration of the error over the time. This model, compared to a *backward vehicle model* that assumes the vehicle can precisely follow the desired velocity trajectory, is more accurate and realistic. In this model, the command is sent to the engine, passes through the mechanical transmission, the wheels, and ultimately affects the vehicle's longitudinal dynamics. Additionally, since the electric motor is powered by the battery pack, the power required by the driver for the motor is computed at each time step ($f = 10 \text{ Hz}$), directly affecting the amount of residual energy stored inside the battery, i.e. battery SOC. For the entire project, the model just depicted for the plant of the BEV has been used as a solid frame on which building the additional models, which will be explained in detail in the next chapters.

3 Cabin and HVAC models

Considering that the final objective of this work involved controlling the cabin’s ambient temperature, as a preliminary step, due to the lack of data regarding real cabin temperature evolution and the impracticality of conducting real experiments, it became necessary to develop a realistic model for the cabin’s environment, that was able to grasp accurately the dynamic behaviour of the temperature evolution under any weather conditions. Moreover, since one of the objectives was to have the possibility of running *real-time* the strategy, this initial model served as a reliable foundation for fine-tuning a simplified lumped-parameters cabin model. While the second model was less precise than the first, it offered a much simpler mathematical formulation, making it significantly less computationally intensive. Furthermore, a model for the HVAC system was implemented, along with an internal control architecture capable of manipulating its internal control variables.

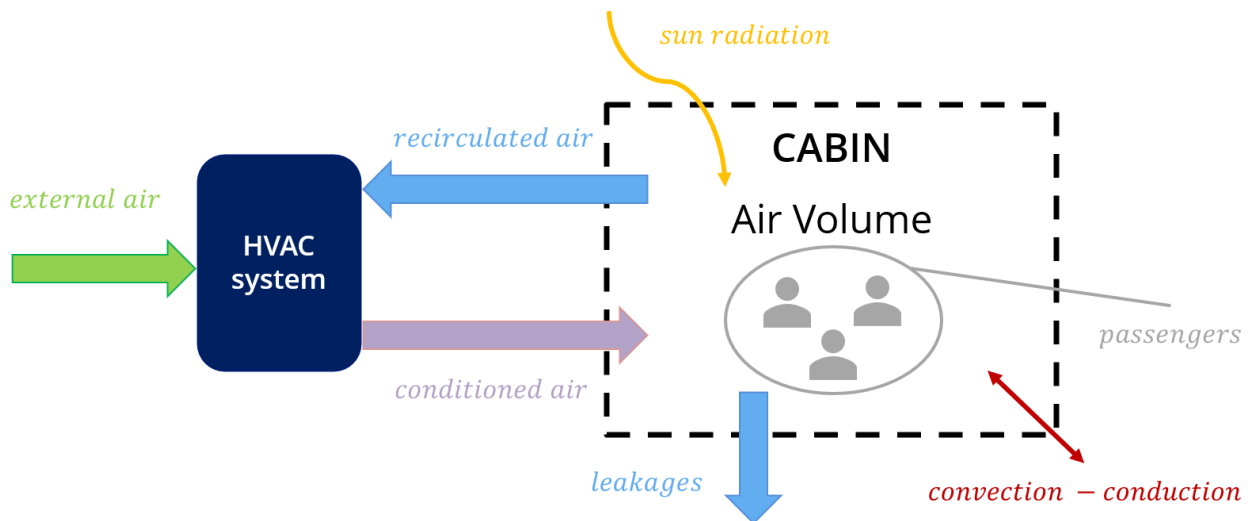


Figure 11: Energy interactions of cabin’s air volume and HVAC systems among them and with external environment

In Figure 11 reported above, it is possible to spot all the incoming and out-coming energy fluxes (heat and mass) involving the cabin air volume, and also its connections with the HVAC system. It is easy to visualize in the figure as the way by means the HVAC system acts on the cabin’s volume, for ensuring the thermal comfort required by the passengers, is by blowing a certain conditioned air mass flow rate inside it.

3.1 SimscapeTM cabin model

This cabin thermodynamic model that has been developed in Simulink[®] accessing the SimscapeTM’s libraries, can be considered a high-fidelity model of reality, because capable to

capture many physical phenomena involved in heat transfer. The only assumption at the base of the model is that the cabin's volume, as well as the incoming and out-coming air mass flow rates, are all made of dry air. The humidity of the air has been neglected, and also driver and passengers inside the cabin have simply been modeled as a heat source internal to the cabin volume. As a matter of fact, even for these latter, it should be considered separately, a contribution coming from convective heat transfer among cabin's body surface and cabin's air, and a generated humid air mass flow rate representing the humid mixture flow blown by breathing. Apart from this, the model does not rely on other simplified assumptions that could distance it from achieving realistic results.

For the implementation, the Simscape™'s blocks have been used, that are very user-friendly, but on the other side they cover many physical aspects otherwise too challenging to be considered.

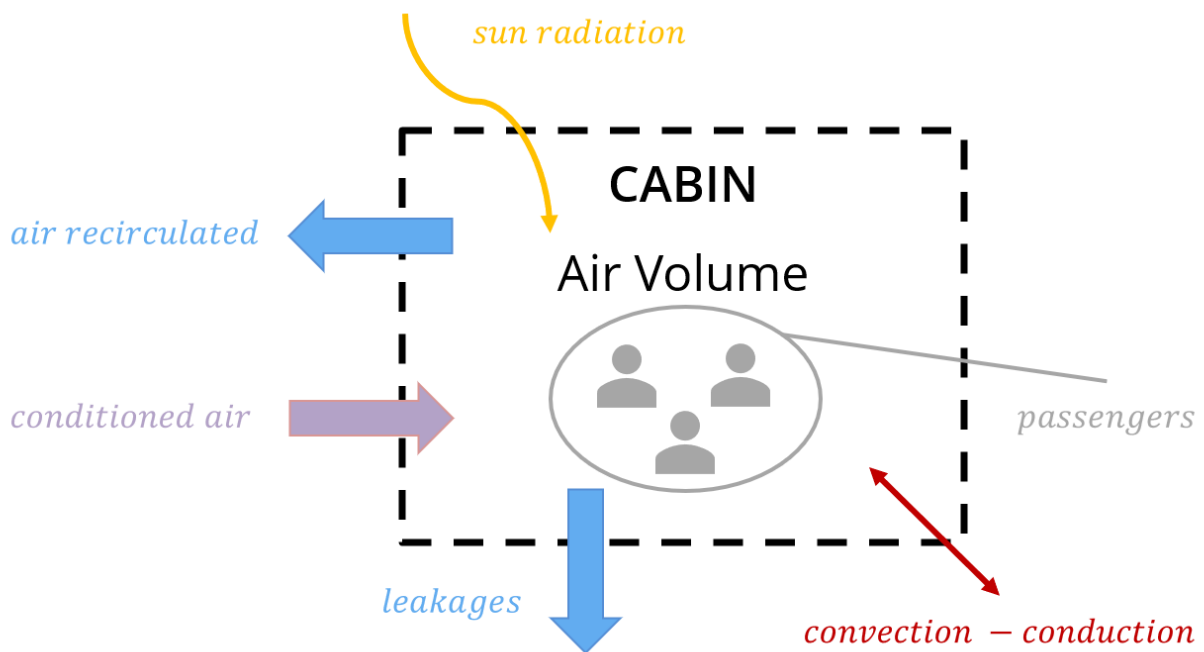


Figure 12: Energy interactions of the cabin's air volume with the external environment

Then, it is possible to turn the attention to the thermodynamic problem of the cabin's air volume, and going to analyse how all its energy exchanges have been modeled, namely:

- convection and conduction
- sun radiation
- air fluxes
- sensible heat

Apart from the physical aspects behind the cabin thermal model, which were well known, to design the layout of the Simscape™ model, a paper focusing on the implementation of a bus cabin’s model has been used as reference [14]. Furthermore, another reference has been helpful for physical parameters and dimensions about materials and composition of the perimeter cabin’s walls [15]. In this way it was possible to double check the correctness of the model.

3.1.1 Convection and conduction contribution

To properly account for the contribution given by convection and conduction heat transfer through the cabin’s boundary in touch with the external environment, it is important to design all the boundaries with a fine thermal model, like the one shown in Figure 13, considering a thermal mass between two thermal resistances. Then, the cabin’s outer boundaries have been consequently subdivided into four zones:

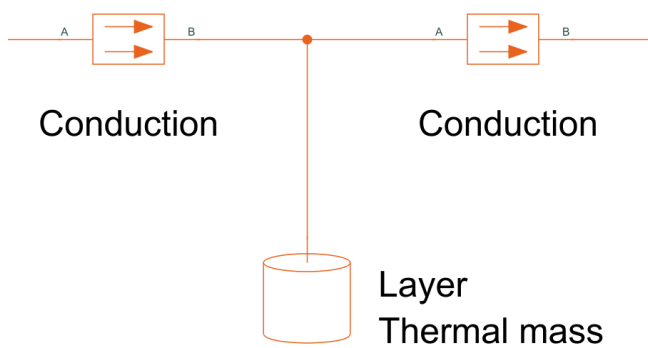


Figure 13: One single layer’s thermal model

- roof
- floor
- side walls
- glass windows

For the sake of clarity, it is worth specifying as “glass windows” includes lateral car windows, windshield and rear window, instead “side walls” does not include any glass surface,

but only frame, doors, front and rear walls. Once made this distinction among cabin’s boundary surface zones, for each of them has been considered a proper stratigraphy, using the one proposed in [15]. This is a crucial point to add to the model if one want to reproduce in a realistic manner the cabin’s air temperature evolution, because it allows to introduce the thermal inertia of the boundary walls. The figures reported below, namely 14, 15, 16 and 17, depict the exact stratigraphy considered for the different boundary zones. Now, the other points still missing are the convection contributions, to be placed at the two ends of the thermal masses chain: the outer one (external ambient) and the inner one (cabin’s environment). For the cabin’s volume, assuming the air inside as still air, a constant convective heat transfer coefficient h_{in} of $4 \frac{W}{m^2 \cdot K}$ has been selected [14]. For the external side, it has been considered a relation for the convective heat transfer coefficient h_{ext} with the vehicle speed v_{veh} , that is:

$$h_{ext} = 1.163 + 4 \cdot \left(12 + \sqrt{v_{veh} \left[\frac{m}{s} \right]} \right) \quad \left[\frac{W}{m^2 \cdot K} \right] \quad (1)$$

The justification for this relationship lies in the dependency of the convection phenomenon on the relative velocity between the fluid that touches the surface (in this case respectively external air and car's body surface), and the same surface. Both this last formula (1) and the magnitude of the h_{in} have been taken from [16].

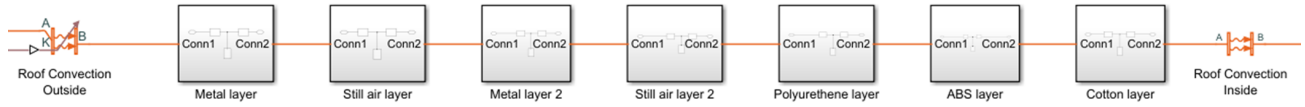


Figure 14: Roof Simscape™ thermal model

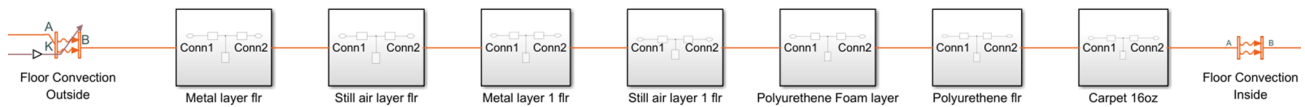


Figure 15: Floor Simscape™ thermal model

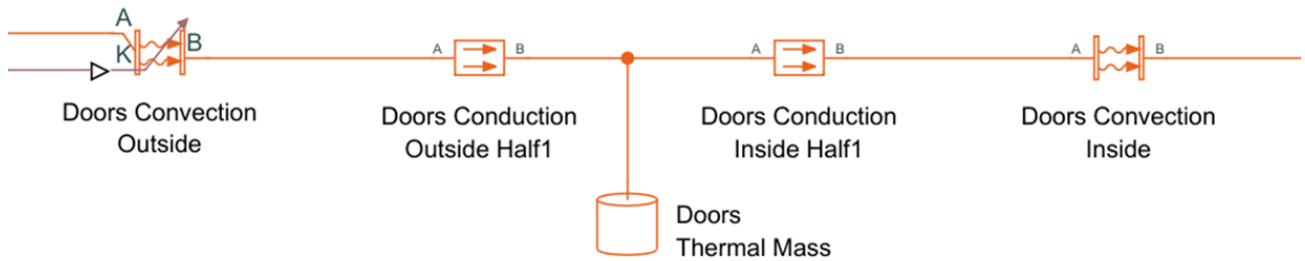


Figure 16: Side walls Simscape™ thermal model

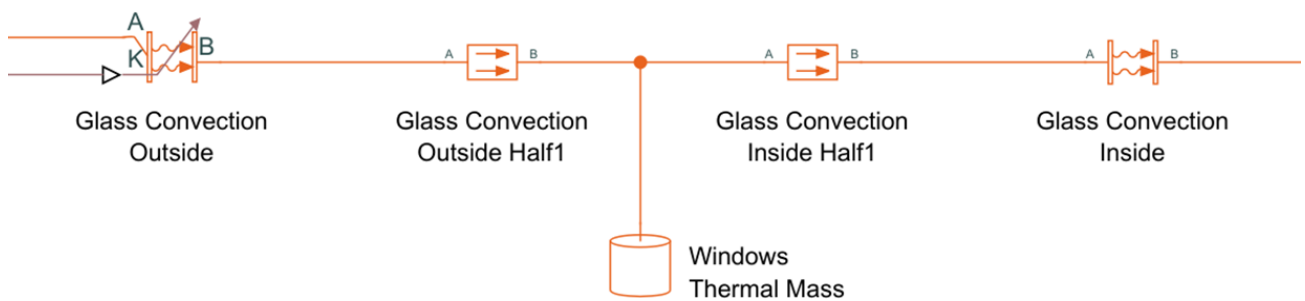


Figure 17: Glass windows Simscape™ thermal model

The previous figures show as the convection has been modeled for both the two ends. All the branches depicted are connected in parallel, and the two terminals are respectively connected to the internal and external environments.

3.1.2 Solar radiation contribution

The radiation coming from the sun $\dot{q}_{sun} \left[\frac{W}{m^2} \right]$ impinges the outer layers of the car's body surface, which are directly exposed to the sunlight, namely: roof, glass windows and lateral doors. For the theory of electromagnetic waves, only the portion of the incoming solar radiation perpendicular to the surface effectively transfers over the same.

$$\dot{Q}_{sun} = \dot{q}_{sun} \cdot S \cdot \sin(\Phi) \quad [W] \quad (2)$$

In the formula written above, S is the surface expressed in $[m^2]$, and Φ is the angle between the impinging radiation and the surface. Since for this model there was no distinction among lateral doors and front or rear walls, and considering also that for the lateral doors, which are only a portion of the side walls boundary zone, the angle Φ would be very small being the doors almost vertical $\Rightarrow \Phi \approx 0$, the contribution of the sun over these has been neglected. Otherwise, it would have complicated the model too much without giving justified benefits. Another necessary distinction considered by the model concerns the portion of power absorbed by the surface, and the portion transmitted through it. For gray bodies, such as the roof, the transmitted portion is null. Instead, for transparent surfaces, such as glass windows, it is imperative to distinguish among the two portion of the incoming radiation. Then, one can write the following equations for the transmitted \dot{Q}_{tr} and the absorbed \dot{Q}_{abs} solar radiation, considering transmissivity τ and absorptivity ρ of the material, which are constitutive properties of it.

$$\dot{Q}_{tr} = \tau \cdot \dot{Q}_{sun} \quad [W] \quad (3)$$

$$\dot{Q}_{abs} = \rho \cdot \dot{Q}_{sun} \quad [W] \quad (4)$$

Then, for the two cabin's boundary surface zones concerned, the two separate contributions have been calculated. In particular, for the glass windows, the effective area considered is the summation of all the glass effective surfaces, pre-multiplied by a shading factor. This last shading factor accounts for the position of the windows, which can take some portion of the surface to not be exposed under the solar radiation.

$$A_{wind,eff} = \sum_{i=1}^{N_{wind}} C_i \cdot A_{wind,i} \cdot \sin(\Phi_i) \approx \bar{C} \cdot \sum_{i=1}^{N_{wind}} A_{wind,i} \cdot \sin(\Phi_i) \quad [m^2] \quad (5)$$

Inside the equation (5), \bar{C} is an average shading factor for the whole set of windows. A reasonable $\bar{C} = 0.85$ has been chosen. The following pictures show the implementation of the described phenomenon.

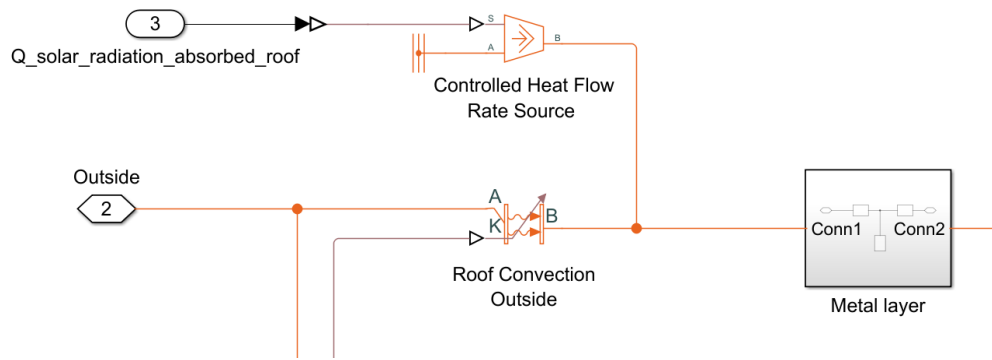


Figure 18: Radiation absorbed by the roof - Simscape™ thermal model

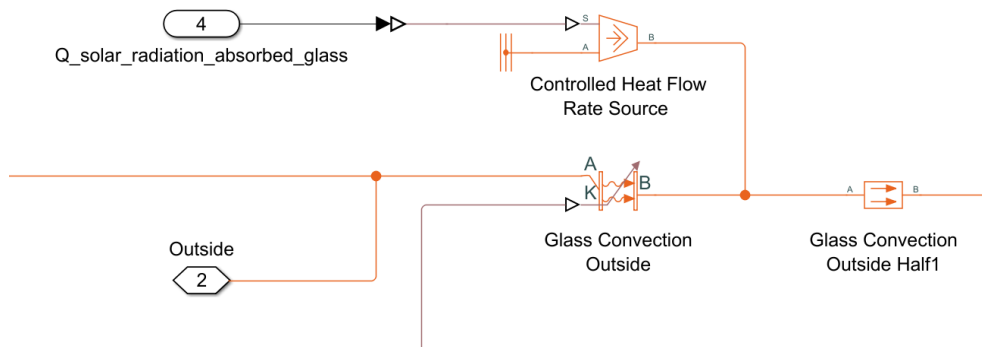


Figure 19: Radiation absorbed by the windows - Simscape™ thermal model

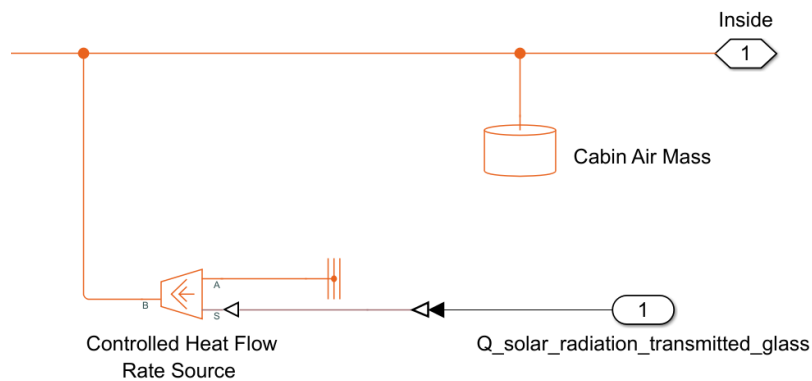


Figure 20: Radiation transmitted through the windows - Simscape™ thermal model

3.1.3 Air fluxes contribution

Looking at both Figure 11 and 12, three air mass fluxes involved in the cabin energy budget can be identified. These are:

- conditioned air mass flow rate, $\dot{m}_{HVAC,out}$

This represents the air blown into the cabin after undergoing proper conditioning as it passes through the HVAC system.

- recirculated air mass flow rate, \dot{m}_{recirc}

This accounts for the portion of air drawn by the HVAC system from the cabin, which is then mixed with fresh external air at the HVAC unit's inlet.

- leak air mass flow rate, \dot{m}_{leak}

This refers to the air that, due to the cabin not being completely sealed, can flow along the direction of the pressure gradient. Given that the mass of air blown into the cabin exceeds that drawn for recirculation from the cabin, the pressure gradient points outward, leading to air leakages.

Within SimscapeTM, it is possible to accurately describe these air fluxes and leakages. This has been done by leveraging the references mentioned earlier. Below, in Figure 21, 22 and 23, you can observe the various blocks used and their placement.

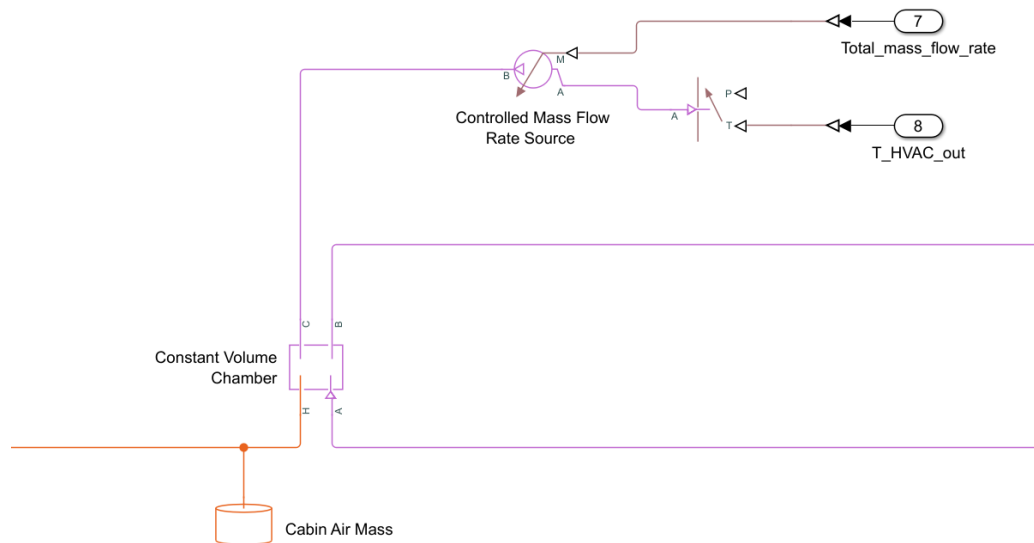


Figure 21: Air mass flow rate blown out of the HVAC system - SimscapeTM thermal model

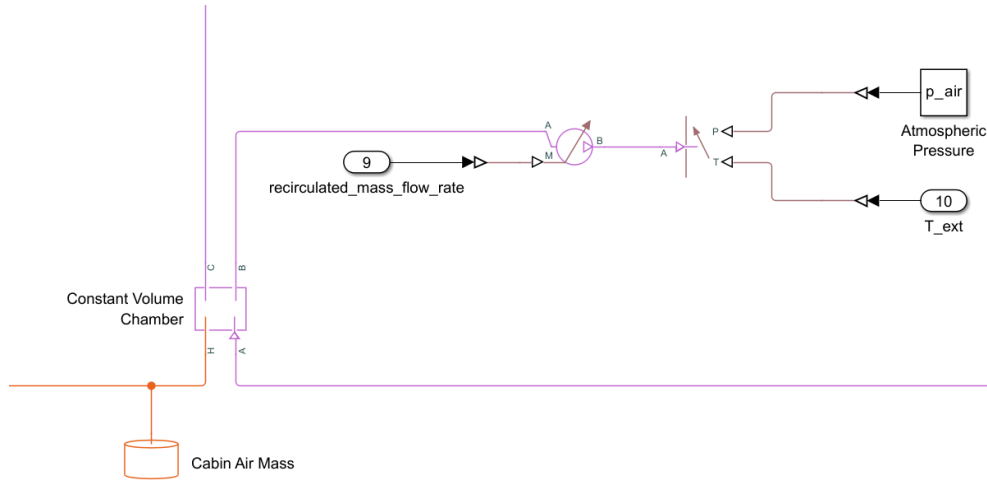


Figure 22: Air mass flow rate drawn from the cabin for recirculation - Simscape™ thermal model

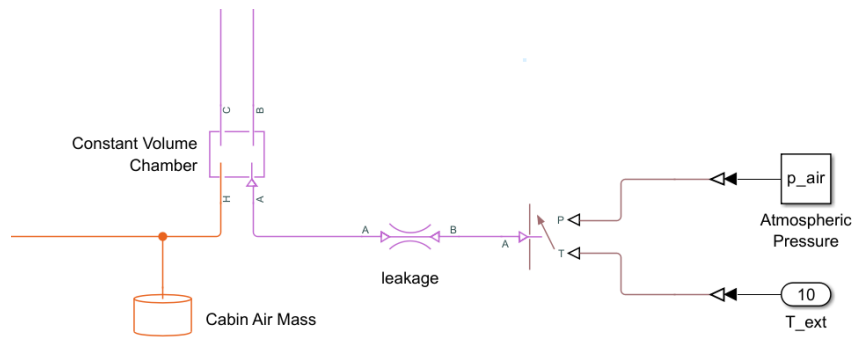


Figure 23: Cabin's air leakages - Simscape™ thermal model

3.1.4 Passengers contribution

To account for the heat gain generated inside the cabin due to passengers, many formulations had been found in the literature. In practice, all the formulas relate the total passengers sensible heat to the number thereof, namely n_p . For the model described in this thesis project, the formulation from [14] has been adopted, assuming an average passenger's body surface area A_p of 1.8 m^2 and a sensible specific heat M_s of $70 \frac{\text{W}}{\text{m}^2}$. This relationship is expressed as follows:

$$\dot{Q}_{pass} = n_p \cdot A_p \cdot M_s \quad [W] \quad (6)$$

As for the other cases, a visual representation from the Simscape™ model is provided as follows in Figure 24.

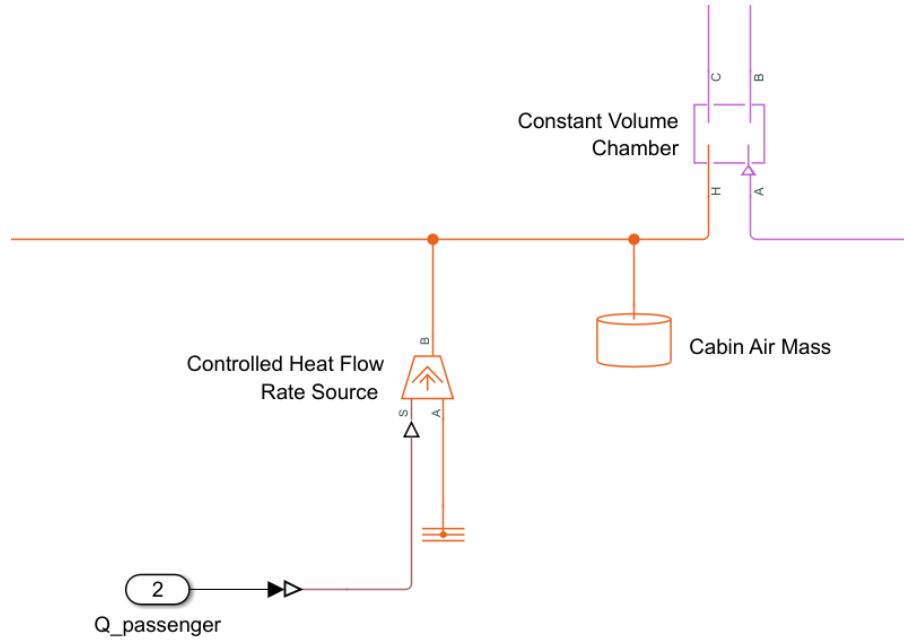


Figure 24: Sensible heat power generated by passengers - Simscape™ thermal model

3.1.5 Free cabin temperature evolution

After that the cabin thermal model was completed, without an HVAC system that would manage the air mass flow rates blown inside and drawn from the cabin, but considering only the leakages throughout the cabin's surface boundary, a check for the cabin temperature evolution has been performed keeping the vehicle at standstill. The constraints used for the simulation are reported in Table 1. From the results, sketched in Figure 25, can be seen that as the temperature raises up, the trend gets less steeper. That is because the cabin's air volume approaches a steady-state energy budget. After 1.5 hours the cabin's air reaches a temperature of about $60\text{ }^{\circ}\text{C}$. This is absolutely acceptable and realistic, then the model can be considered reliable and well implemented.

T_{ext} [$^{\circ}\text{C}$]	$T_{\text{cabin},0}$ [$^{\circ}\text{C}$]	q_{sun} [W/m^2]	n_p [-]	v_{veh} [m/s]
32	23	1000	0	0

Table 1: Boundary conditions for the free cabin temperature evolution test of the Simscape™ model

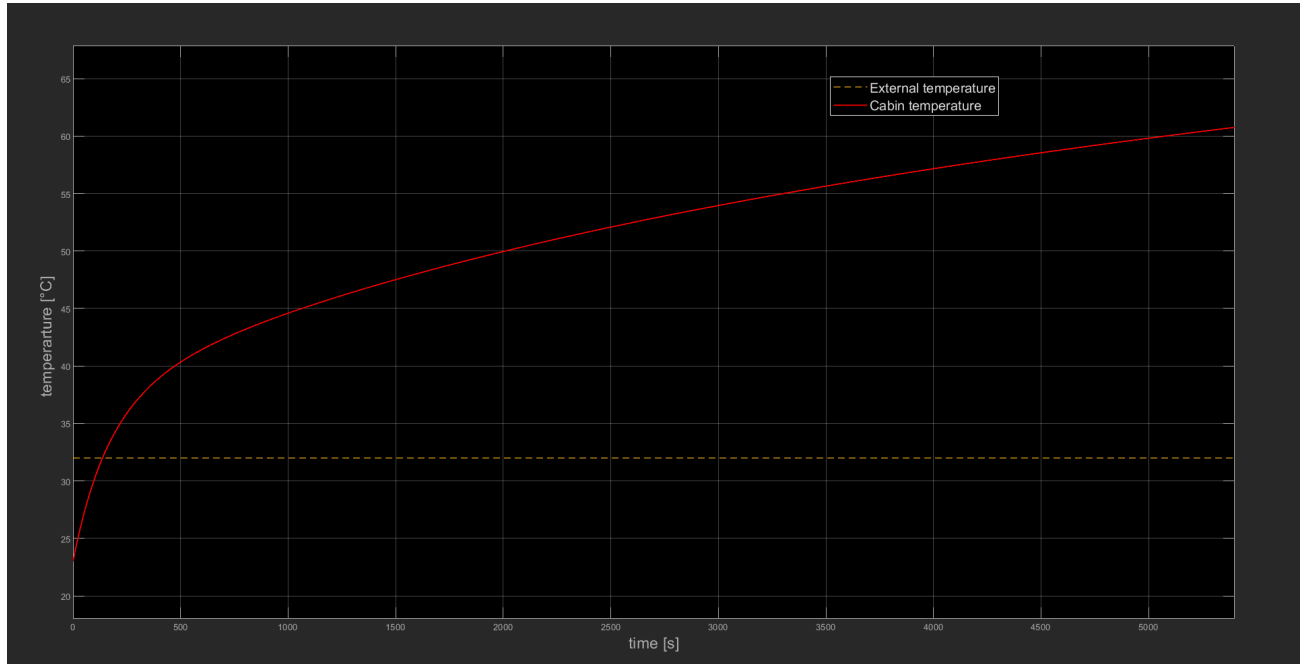


Figure 25: Free cabin's temperature evolution - Simscape™ thermal model

3.2 HVAC model

Once designed and implemented a reliable and real-behaving cabin model, the next step is to design and implement a model for the HVAC unit. This last system is able to comply with the thermal desire expressed by the driver or by the passengers.

3.2.1 HVAC system architecture

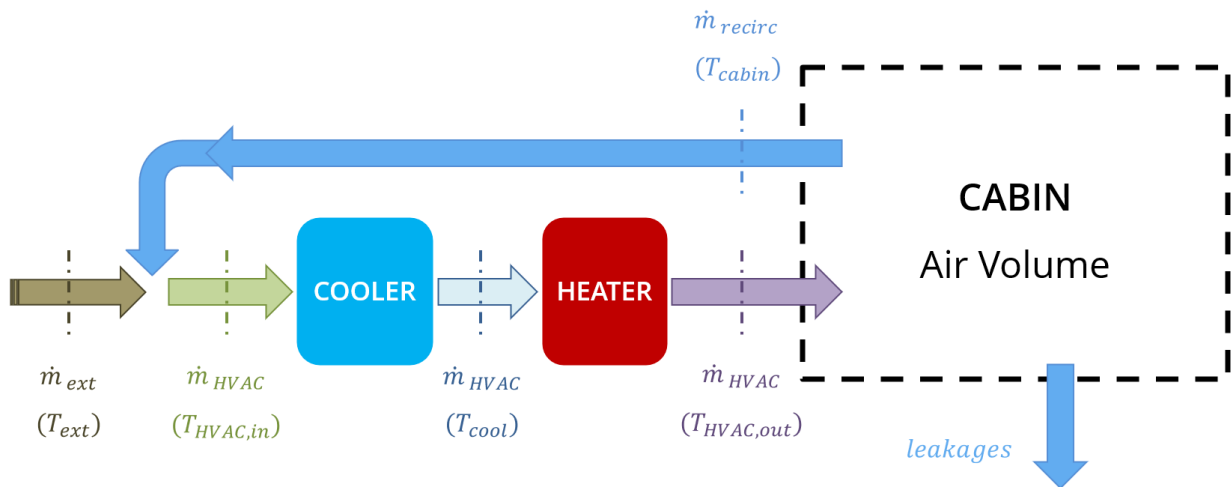


Figure 26: Widespread architecture of HVAC system for EVs and HEVs

Many architectures for the HVAC system are popular in the automotive field, there is not only one single way of proceeding with the layout design. As suggested inside [17], the most common HVAC architecture used for EVs is the one reported in Figure 26. The possible degrees of freedom of such a standard architecture are the integration of *cooler* and *heater* inside other thermal management systems for powertrain components, i.e. battery, electric motor, etc. Within this project, it was assumed that the HVAC was totally independent from the component thermal management units of the vehicle. Moreover, both cooler and heater belongs to separate heat pumps, so, for each of them is necessary to set up a compressor moved by an electric motor, in order to make the fluid flowing across the circuits. The cooler is an evaporator, and the heater a condenser. From the basics of the thermodynamics, it is possible to remind that the technical power required by an heat pump is linked to the heat power demanded through a COP.

$$P_{cooler}^{tech} = \frac{\dot{Q}_{cooler}}{COP_c} \quad [W] \quad (7)$$

$$P_{heater}^{tech} = \frac{\dot{Q}_{heater}}{COP_h - 1} \quad [W] \quad (8)$$

Inside equations (7) and (8), the heat powers are respectively:

$$\dot{Q}_{cooler} = \dot{m}_{HVAC} \cdot (T_{HVAC,in} - T_{cool}) \quad [W] \quad (9)$$

$$\dot{Q}_{heater} = \dot{m}_{HVAC} \cdot (T_{HVAC,out} - T_{cool}) \quad [W] \quad (10)$$

Then, one should consider that:

1. a *heat exchanger* is the device that physically carries out the functions of heater or cooler
2. the technical power P^{tech} does not account for the mechanical losses across compressor and electric motor

The first point leads to the need to account for an heat transfer efficiency for cooler and heater, while the second point makes necessary to account for a global combined motor-compressor efficiency, namely $\eta_{comp-em}$. Now, the power request to the battery by the HVAC is:

$$P_{HVAC}^{batt} = \frac{P_{cooler}^{tech}}{\eta_{exc,c} \cdot \eta_{comp-em,c}} + \frac{P_{heater}^{tech}}{\eta_{exc,h} \cdot \eta_{comp-em,h}} \quad [W] \quad (11)$$

Having no interest in entirely designing the heat pumps circuits with all the respective components, even though efficiencies would have a dependency on the circuit working point, constant values belonging to realistic ranges for both η_{exc} and $\eta_{comp-em}$ have been considered.

For the sake of simplicity, some simplified assumptions have been advanced:

- $COP_c = COP_h = 4 = COP$
- $\eta_{exc,c} = \eta_{exc,h} = 0.6 = \eta_{exc}$
- $\eta_{comp-em,c} = \eta_{comp-em,h} = 0.7 = \eta_{comp-em}$

Thus, the equation (11) can further be simplified, turning into the following one:

$$P_{HVAC}^{batt} = \frac{\dot{m}_{HVAC}}{\eta_{exc} \cdot \eta_{comp-em}} \cdot \left(\frac{T_{HVAC,in} - T_{cool}}{COP} + \frac{T_{HVAC,out} - T_{cool}}{COP - 1} \right) \quad [W] \quad (12)$$

3.2.2 HVAC control logic

The step moved forward, after completing the design of the architecture of the HVAC system, has been to find a suitable control logic for it. In order to satisfy the user's thermal needs, during summertime the HVAC system is asked to remove some heating capacity from the cabin. Basically, this is carried out by blowing conditioned air, with a certain temperature, inside the cabin. What has just been explained, can be easily visualized on Figure 11. Even though we assumed to deal with dry air, to suitably design an HVAC model returning reasonable power demands, the steps to follow in order to manage the air humidity cannot be neglected. Indeed, passengers sensations are strictly linked to air humidity as well. That is why the air must be properly conditioned prior to enter the cabin. To account for this, the psychrometric humid air diagram has been used.

The control variables to manage for the HVAC system are three, meaning:

- \dot{m}_{HVAC}
- $T_{HVAC,out}$
- T_{cool}

Especially the last two ones, are connected to passengers' comfort feelings. The temperature of the air blown inside the cabin must be kept below the temperature set as reference, but not too cold, avoiding passenger's discomfort. Generally, as a design rule, the air is blown inside with $6 \div 10$ °C less than the reference temperature required. About the air temperature at the outlet of the evaporator, this should be low enough to ensure a fine level of humidity inside the cabin. As extracted by [18], to make the passengers feeling comfortable, the cabin ambient should have a relative humidity, i.e. φ , ranging between 20% and 60%. These boundaries served as necessary foundations for designing the internal logic of the HVAC system.

Once given a solid overview of the HVAC system and of its internal variables to act on, it is possible to move to an insight into the overall control architecture. To do this, it is mandatory

to start from the “*First law of the Thermodynamics*” (*FLT*) applied to the cabin air volume. Keeping in mind Figure 12, one can write:

$$\dot{Q}_{sun} + \dot{Q}_{cond,conv} + \dot{Q}_{pass} = \left(\frac{\partial E_t}{\partial t} \right)_{C.V.} + (\dot{m}_{rec} + \dot{m}_{leak}) \cdot c_p \cdot T_{cabin} - \dot{m}_{HVAC} \cdot c_p \cdot T_{HVAC,out} \quad (13)$$

The partial derivative of the total energy of the thermodynamic system included into the cabin, can be written as:

$$\left(\frac{\partial E_t}{\partial t} \right)_{C.V.} = \left(\frac{\partial (M_{air} \cdot c_p \cdot T_{cabin})}{\partial t} \right)_{C.V.} \quad (14)$$

One assumption that can be made, reasonable because checked by means of the developed SimscapeTM model, is that of constant air mass inside the control volume. If this is true, the “*First law of the Thermodynamics*” turns into a first order differential equation with a single variable, i.e. T_{cabin} . Thus, one can combine the mass flow rate-related left side of equation (13), considering the heating capacity removed from the cabin as:

$$\begin{aligned} \dot{Q}_{HVAC} &= (\dot{m}_{rec} + \dot{m}_{leak}) \cdot c_p \cdot T_{cabin} - \dot{m}_{HVAC} \cdot c_p \cdot T_{HVAC,out} \\ &\approx \dot{m}_{HVAC} \cdot c_p \cdot (T_{cabin} - T_{HVAC,out}) \end{aligned} \quad (15)$$

Consequently, equation (13) can be re-formulated as follows:

$$\dot{Q}_{sun} + \dot{Q}_{cond,conv} + \dot{Q}_{pass} - \dot{Q}_{HVAC} = \left(\frac{\partial E_t}{\partial t} \right)_{C.V.} \quad (16)$$

Then, after illustrating these must-know physical and analytical foundations, it is possible to step into the control architecture. Essentially, to manage this system, it is crucial to split it into two parts:

- *external* controller
- *internal* control logic

The **external controller** is simply a PI controller that receives, with a frequency of 10 Hz, the temperature gap defined below in (17) and consequently refreshes, with the same frequency, the commanded heating capacity to be removed from the cabin, i.e. \dot{Q}_{HVAC}^{des} .

$$\Delta T = T_{cabin} - T_{ref} \quad (17)$$

Thus, the dynamics of the the cabin temperature is entrusted to the PI controller. But, the desired heating capacity \dot{Q}_{HVAC}^{des} , looking at (15), must be translated into a certain suitably conditioned air mass flow rate. Here is where the need for an **internal control logic** arises from. Basically, it is a set of rules, aimed at achieving the thermal power request fed by the PI controller. It is worth noting as the system should be able to adapt to the user request, as well

as it should be capable to fulfil this request in a comfortable way. Once the desired thermal power is fed to the HVAC system, on the basis of the T_{ref} , i.e. reference temperature, asked by the user, the internal control logic will first set a T_{cool} and a $T_{HVAC,out}$, and finally the needed \dot{m}_{HVAC} , as suggested by (15). In doing this, the recirculation ratio $\epsilon = \dot{m}_{recir}/\dot{m}_{HVAC}$ has been considered set to a constant value of 0.7. Taking into account what previously stated concerning the passengers' comfort humidity range, one can refer to the chart of Figure 27 to describe the rule that controls the T_{cool} .

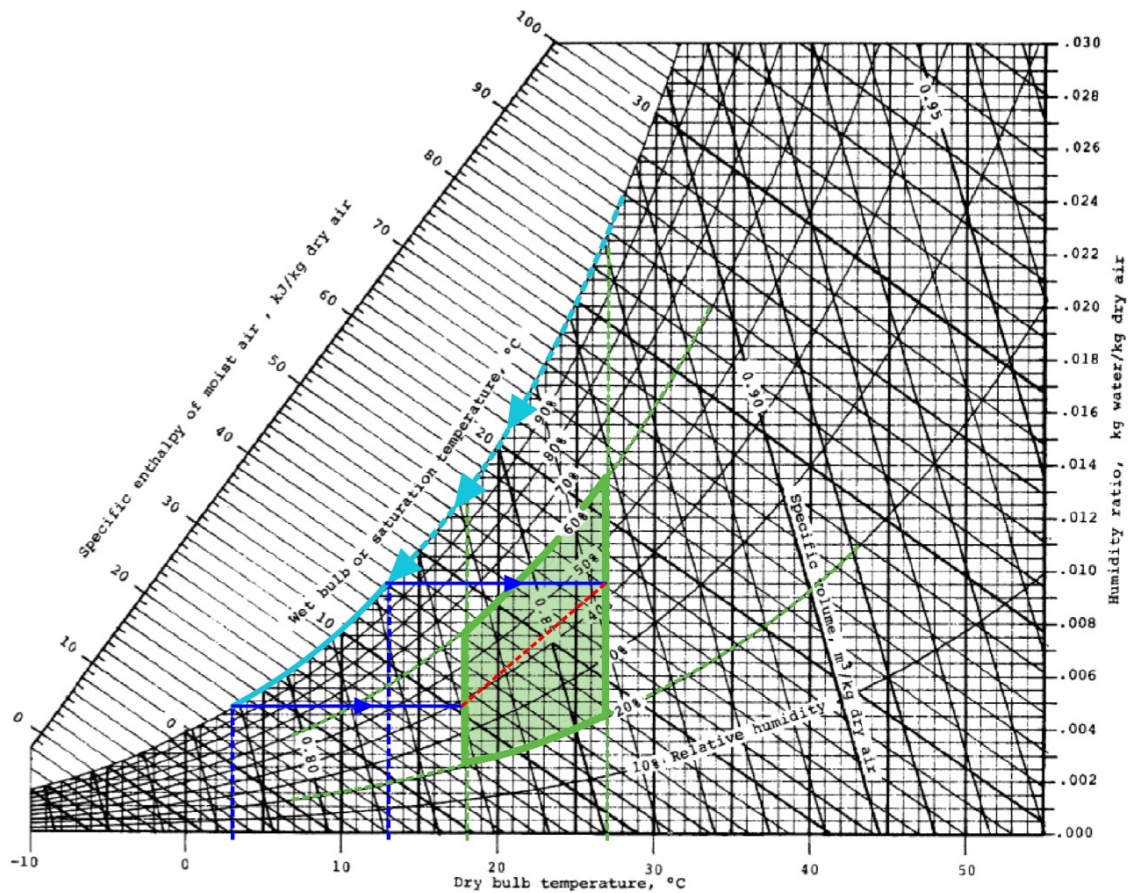


Figure 27: Psychrometric chart of humid air

In the chart shown above, the highlighted area delimited with solid green line includes the comfort conditions for the passengers for a cabin temperature ranging between $18^{\circ}C$ and $27^{\circ}C$. Therefore, to ensure such a humidity range for the cabin's volume, one should dehumidify the air flux at the inlet of the evaporator to a suitable extent. The dehumidifying process is split into two portions: first the air is cooled down to the wet bulb conditions at a constant humidity ratio, hence, the temperature is further lowered removing the unwanted water from the air. The final point of this process must be wisely identified, considering that across the next conditioning

step, and lastly inside the cabin, the air flow will be re-heated keeping constant its humidity ratio (without only caring about the amount of vapour released by the passengers). What just explained can be identified with an horizontal line, like the two blue solid ones reported on Figure 27. The final aim of the design performed within this project has been to nominally keep the cabin environment with a relative humidity of about 40%. Therefore, for each T_{ref} there is a correspondent T_{cool} as depicted by the following image.

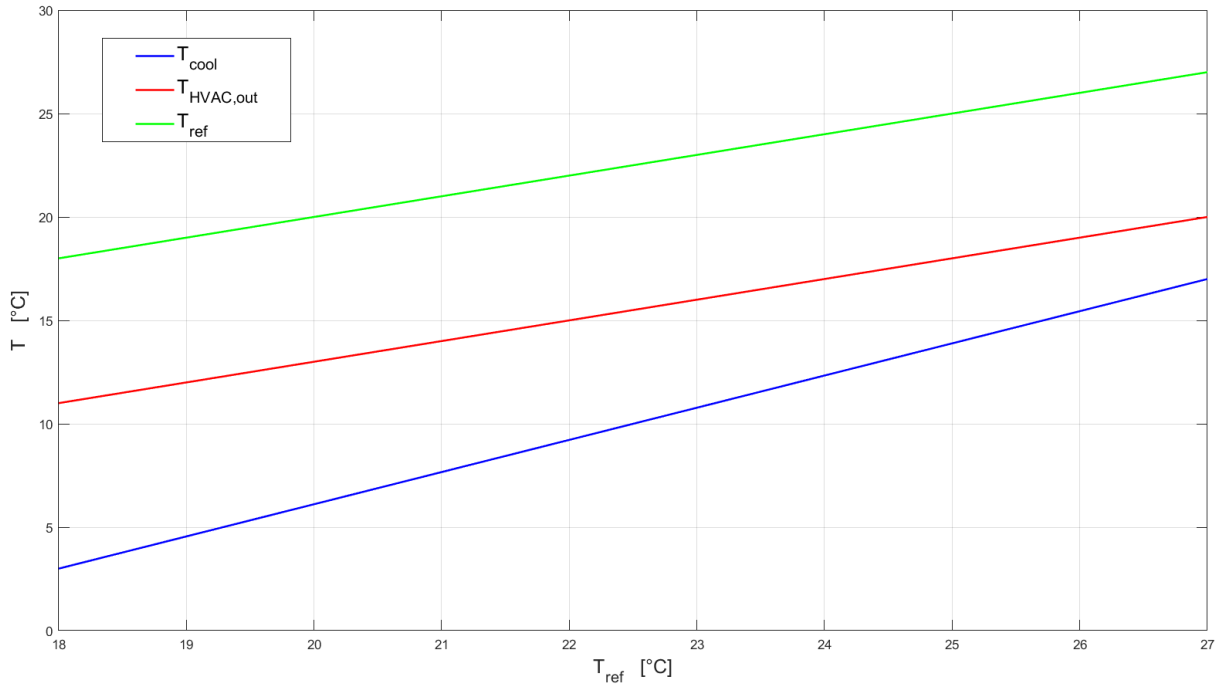


Figure 28: Air flux temperature at cooler outlet and HVAC outlet

In Figure 28, the rules chosen for the internal control logic are traced. In the wake of what just stated, it has been decided to blow the air into the cabin with a temperature $7^{\circ}C$ lower than the reference temperature, that is $T_{HVAC,out}$. Indeed, it is possible to appreciate like the green line and the red line, in the figure just above, are parallel.

In Figure 29 and Figure 30 it is possible to have respectively an overview of the *internal control logic* and of the overall control the HVAC responds to. This latter involves both external and internal controllers working in succession.

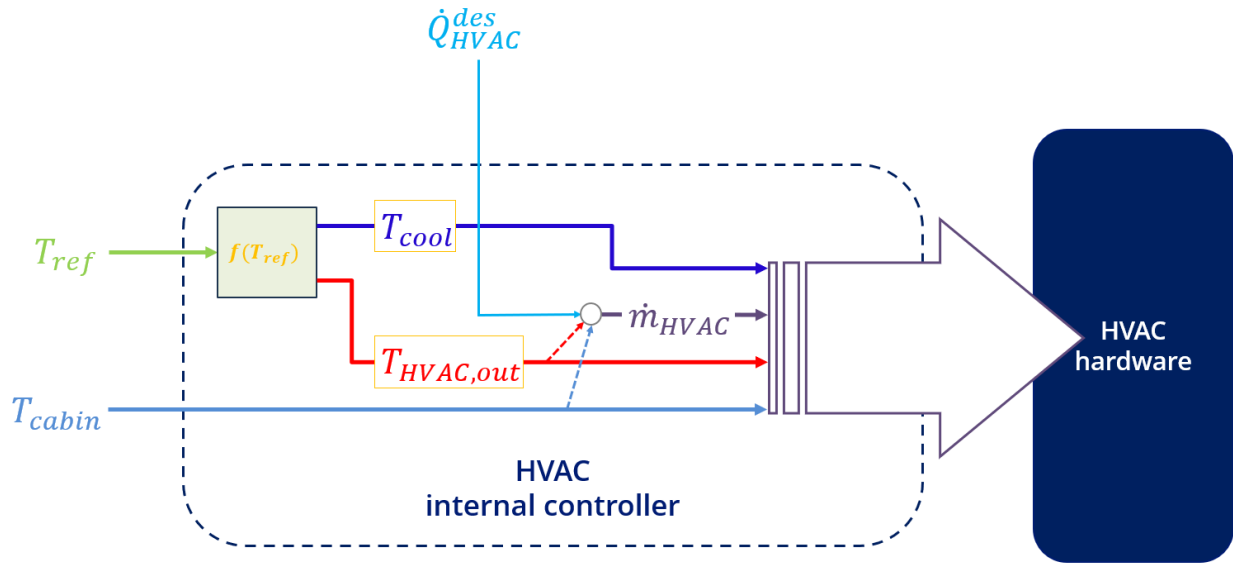


Figure 29: HVAC internal controller flow-chart

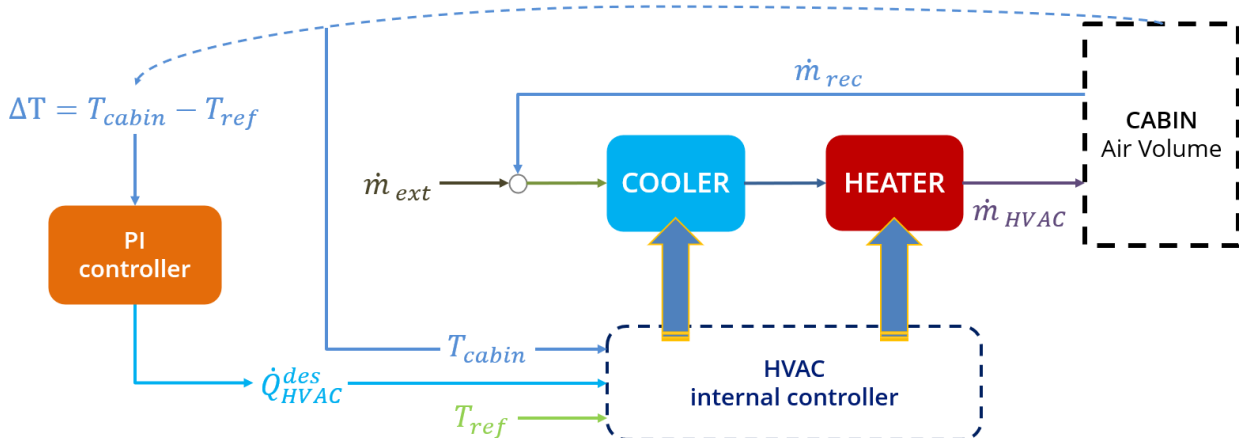


Figure 30: HVAC overall control flow-chart

3.3 Lumped parameters cabin model

After completing the implementation of the reliable thermodynamic model for the cabin and the model for the HVAC system, work commenced on the development of a faster predictive model for cabin's temperature evolution. This latter, in contrast to the more detailed one, omits certain features. Throughout the design process, it was crucial to maintain consistency with the first developed realistic model, both in terms of temperature evolution than HVAC load on the

battery. The physical foundation for this model has been the same as for the Simscape™ model, namely the *FLT*. Therefore, to by-pass the computational complexity of the first model, it has been necessary to advance some hypothesis:

- constant cabin air mass
- constant convection heat transfer coefficient for the external portion of the walls
- no walls thermal mass
- one single averaged stratigraphy for the cabin's boundary

Since these assumptions brought a tough simplification to the model, it was essential to counter-balance their effects. Examining them in the context of Figure 12, it becomes evident that they directly impact the energy fluxes related to the cabin's external interactions and the thermal inertia of the system's boundaries. The concerns which need to be addressed involve: solar radiation, convection and conduction heat transfer, and modified thermal inertia within the system. As a result, the terms in equation (16) become:

$$\dot{Q}_{sun} = \bar{C} \cdot \sum \left(A_{window,i} \cdot \sin(\phi_i) \right) \cdot \tau \cdot \dot{q}_{sun} + \sum \left(A_{boundary,i} \cdot \sin(\phi_i) \cdot \rho_i \right) \cdot \dot{q}_{sun} \quad (18)$$

$$\dot{Q}_{cond,conv} = \bar{K} \cdot A_{boundary,tot} \cdot (T_{ext} - T_{cabin}) \quad (19)$$

$$\left(\frac{\partial E_t}{\partial t} \right)_{C.V.} = M_{air} \cdot c_p \cdot \left(\frac{\partial T_{cabin}}{\partial t} \right)_{C.V.} \quad (20)$$

Hence, if one wanted to have a very similar cabin temperature behavior as for the other model, also the thermal mass of the cabin model (from (20) it is $M_{air} \cdot c_p$) would need to be revised. Then, merging together all the constants, one can re-write the *FLT* as follows:

$$C_1 \cdot \dot{q}_{sun} + C_2 \cdot (T_{ext} - T_{cabin}) + \dot{Q}_{pass} - \dot{Q}_{HVAC} = C_3 \cdot \left(\frac{\partial T_{cabin}}{\partial t} \right)_{C.V.} \quad (21)$$

Despite its easy formulation, inside this equation all the terms still hold their original physical meaning. As follows, one can find the corresponding physical property linked to each constant:

- C_1 , expressed in m^2 , it represents the effective surface of the cabin on which solar radiation has a significant impact
- C_2 , expressed in $\frac{W}{K}$, it physically stands for a thermal resistance
- C_3 , expressed in $\frac{J}{K}$, it is an equivalent thermal mass for the cabin's air volume

A fine tuning of these three constants is required to best fit the thermal cabin's behavior found with the Simscape™ model, at least within the temperature range of interest, namely below the external temperature.

The tuning ended up with the following values:

- $C_1 = 0.71 \text{ m}^2$
- $C_2 = 35 \text{ W/K}$
- $C_3 = 13000 \text{ J/K}$

Once the tuning is performed, even if the dynamics described by equation (21) does not precisely replicate the temperature trend above the outdoor temperature, it would still be satisfactory. This is because the HVAC system is responsible for maintaining the temperature at the level set by the passengers, and thus, the model will never be required to simulate temperatures above that threshold.

3.4 Tuned lumped parameters cabin model's results

In this section, the results from the tuning of the lumped parameters cabin model are presented. Before showing the temperature trend, it is imperative to list all the boundary conditions arbitrarily fixed to perform the tests, and consequently gathering the results.

3.4.1 Free temperature evolution

Exactly like previously done for the Simscape™ model, given the same external conditions reported in Table 1, the results from the test are consequently shown.

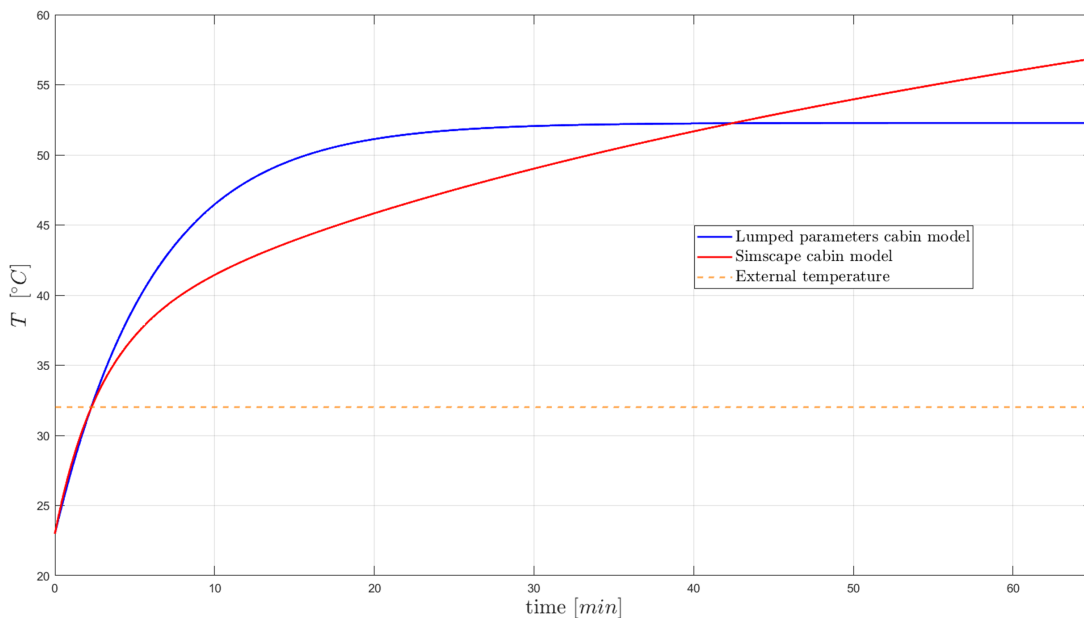


Figure 31: Free cabin temperature evolution - models comparison

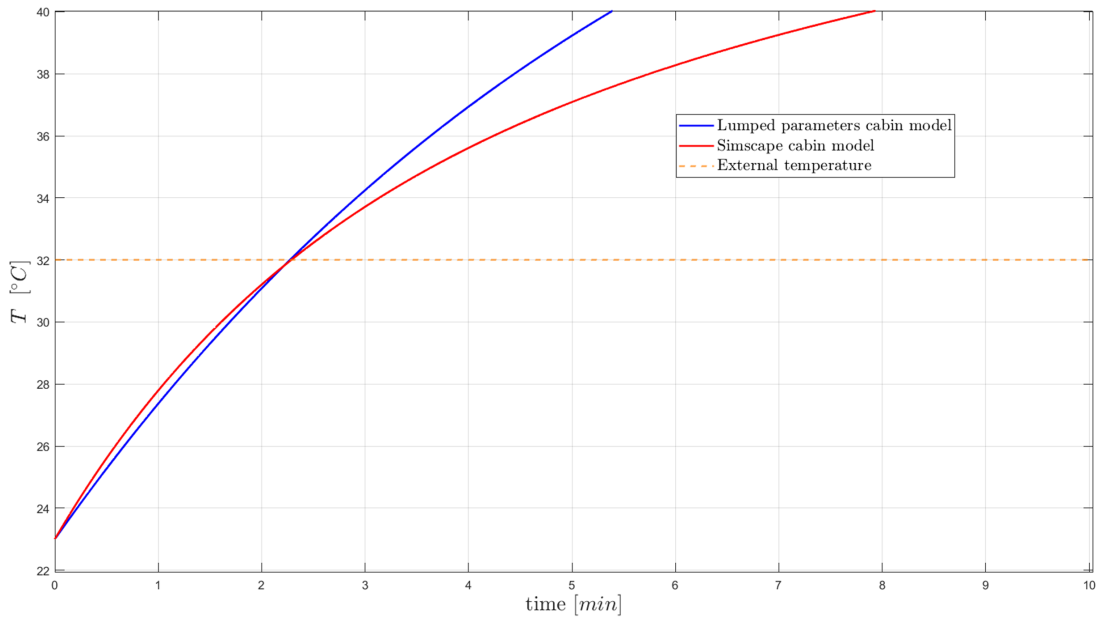


Figure 32: Free cabin temperature evolution - models comparison magnification

The two figures clearly demonstrate how the lumped-parameter cabin model accurately approximates the SimscapeTM model within the region of interest. In Figure 32, it is evident that below the reference temperature, the two behaviors closely align. This consistency was observed similarly when the test was repeated with different initial cabin temperatures.

However, as the cabin temperature exceeds the external temperature, the profile resulting from the simpler model begins to diverge, eventually leveling off toward an asymptote. This saturation trend was expected due to the mathematical formulation (21) of the lumped-parameters model, which represents a first-order differential equation. Apart from the upper region, which is not meaningful for the purpose of the controller developed during this work, the results of the test were positive and satisfactory.

3.4.2 Reference temperature variability

To trust more the last model presented, instead of considering constant solar irradiance and constant external temperature, experimental data gathered by the authors of [16] were used. By doing so, it was also possible to deeply check the model with diverse external conditions, variable over the time. Along this set of tests, the vehicle was moving following the WLTP cycle and the driver was inside the cabin.

T_{ext} [$^{\circ}\text{C}$]	q_{sun} [W/m^2]	n_p [-]
Figure 33.b	Figure 33.a	1

Table 2: Boundary conditions for the set of testes aimed at assessing the lumped parameters cabin model

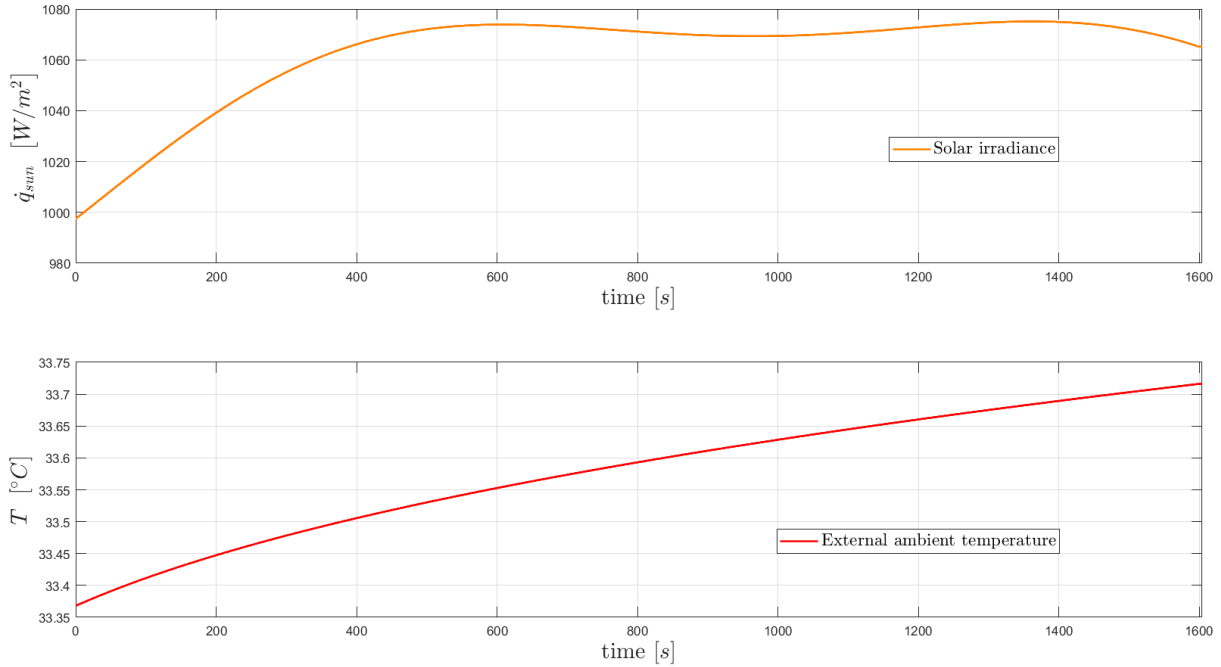


Figure 33: External ambient conditions: solar irradiance (a), outdoor temperature (b)

Given that some of the tests depicted in the following pictures extends beyond the duration of the experimental measurements for outdoor temperature and solar irradiance, a period lasting 1605 seconds, these two variables were held constant since the moment $t = 1605$ s. Likewise, once completed one WLTP cycle, another was immediately run in succession.

Along these tests the two cabin models were controlled through the same PI controller, as planned. In the tests of Figure 34, 35, 36, 37 the reference temperature was kept constant to different values, while for the one of Figure 38, the reference was changed along the test. It is obvious that, even if the profile for the lumped parameters model appears more neat than the other one, however it represents a valid approximation. The two profiles follow definitively the same trends, despite some small difference in value. The reason for these discrepancies lies in the many simplified assumptions advanced for the lumped parameters model. In the figures, one can see as the yellow profiles promptly follow the HVAC commands, instead, the blue profiles appear less responsive whenever a change in the reference occurs. This difference in responsiveness is attributable to the lack of walls thermal inertia in the lumped parameters model.

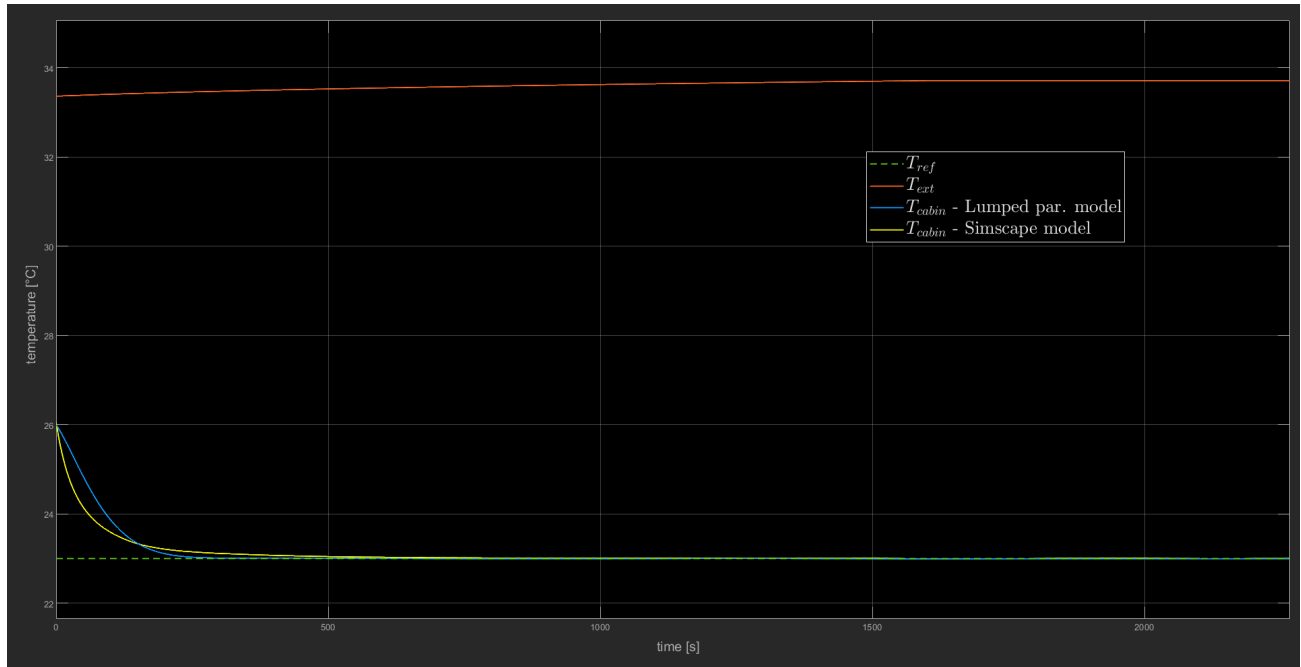


Figure 34: Lumped parameters vs. Simscape™: from 26 °C to 23 °C

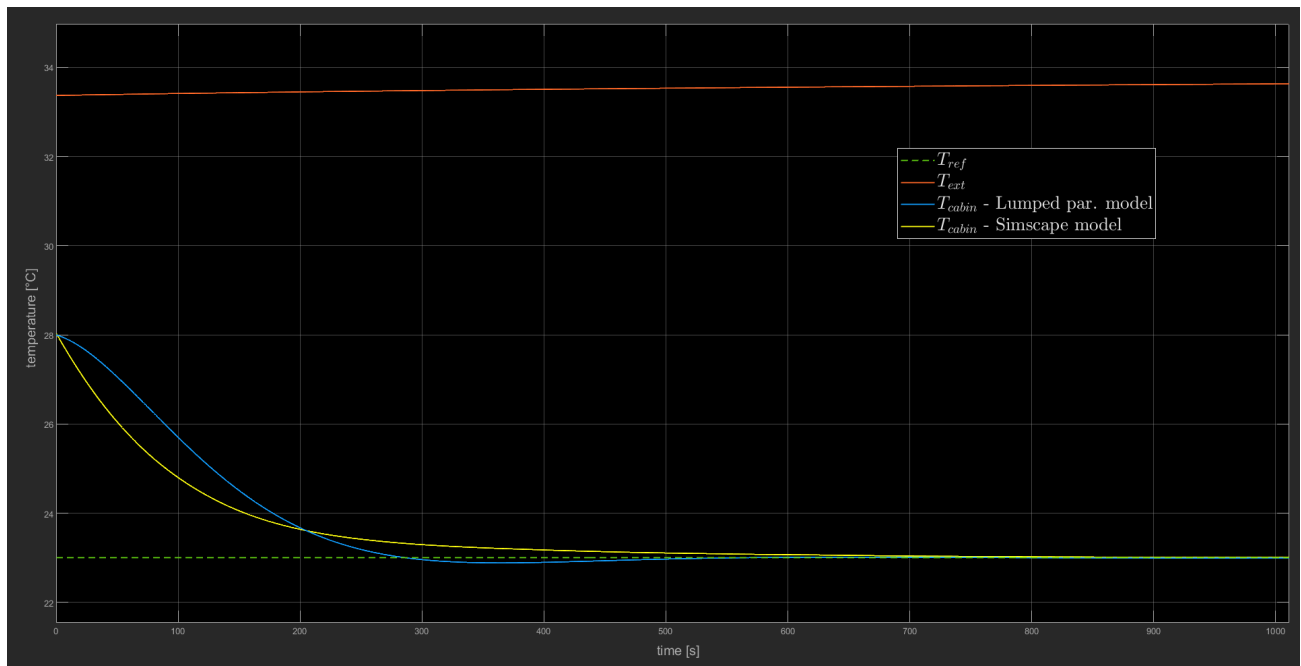


Figure 35: Lumped parameters vs. Simscape™: from 28 °C to 23 °C

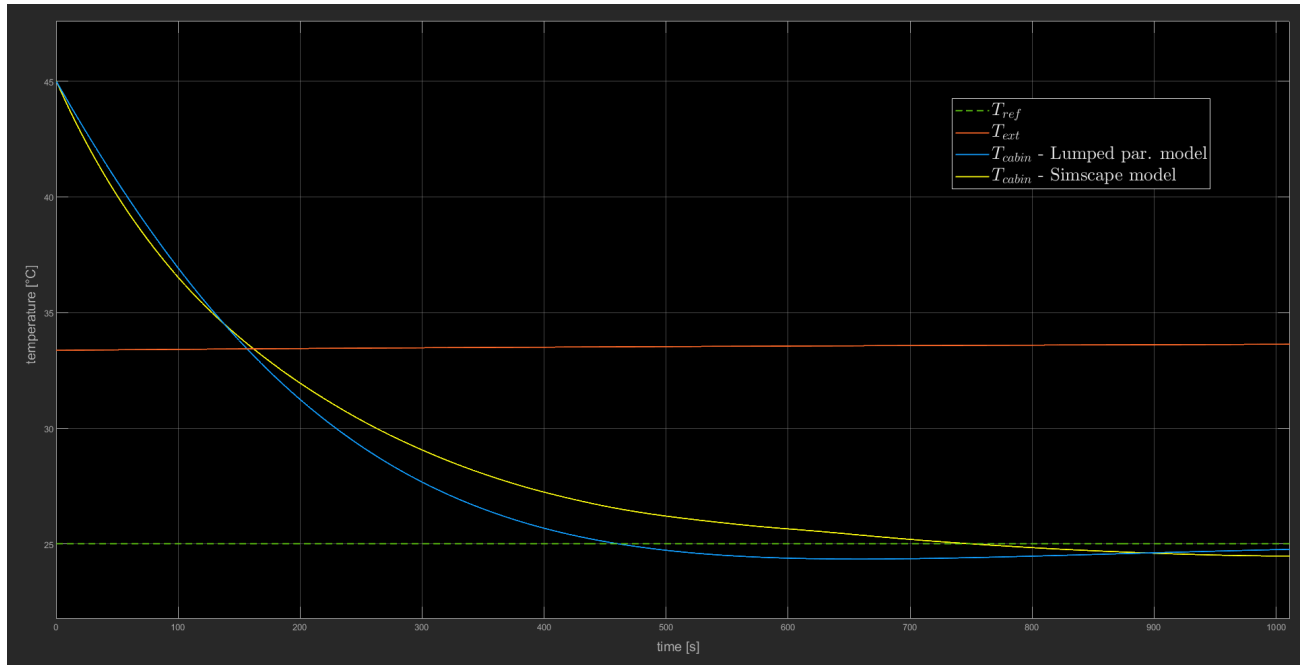


Figure 36: Lumped parameters vs. Simscape™: from 45 °C to 25 °C

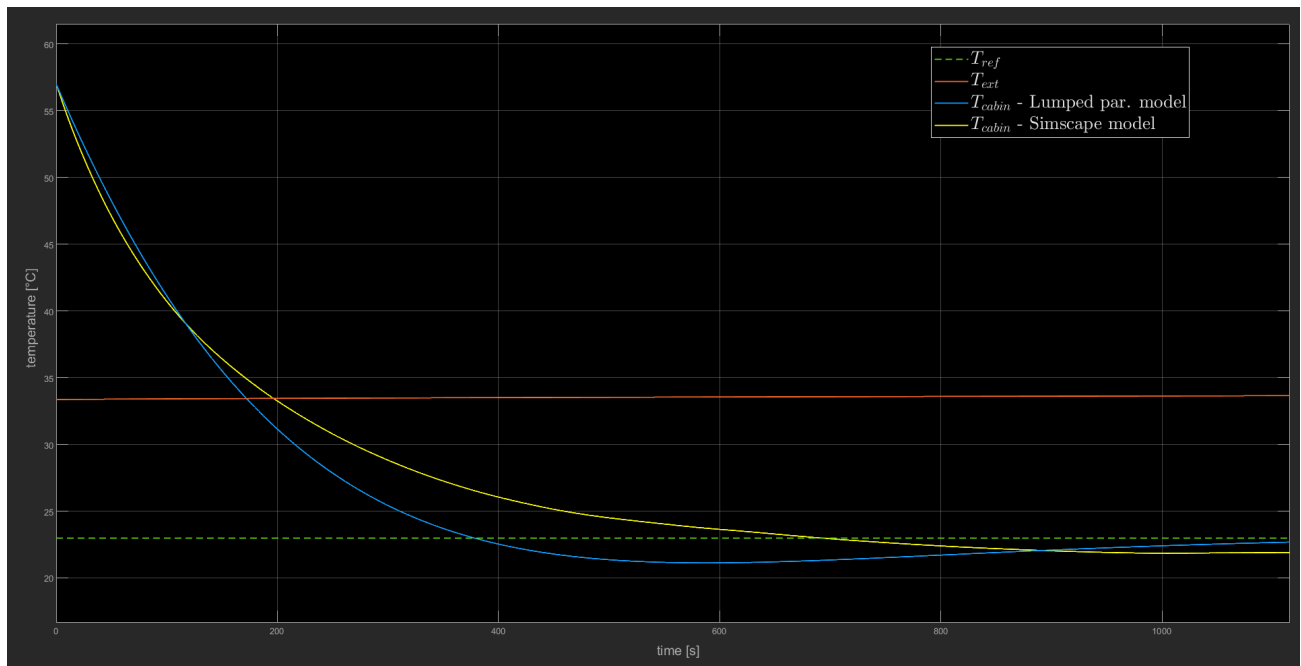


Figure 37: Lumped parameters vs. Simscape™: from 57 °C to 23 °C

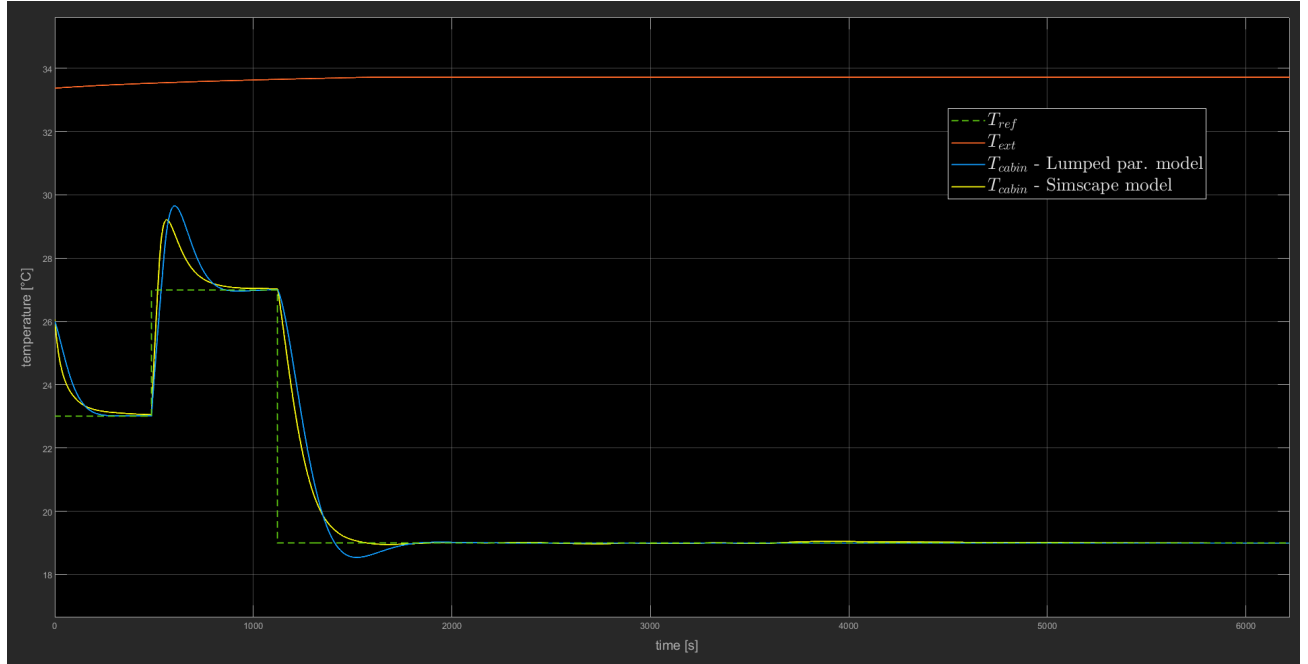


Figure 38: Lumped parameters vs. SimscapeTM: reference temperature variability

3.5 Energy consumption related to cabin thermal comfort

Here, the results from several tests conducted at different reference temperatures are presented to illustrate the influence of cabin conditioning on the drive range of the BEV under study. Before showcasing the results, it is essential to note that these tests were carried out after updating the battery pack model, which will be discussed in the following chapter. The common basis for all the tests, whose results are about to be discussed, is provided in Table 3.

T_{ext} [°C]	q_{sun} [W/m ²]	n_p [-]
32	1000	1

Table 3: Boundary conditions for the set of testes aimed at quantifying the HVAC impact on the energy consumption

The results are presented in reference to two distinct driving scenarios: the Worldwide Harmonized Light Vehicles Test Procedure (WLTP) drive cycle and the Environmental Protection Agency (EPA) drive cycle.

The WLTP cycle has a duration of 1801 seconds, covering a distance of 23.25 kilometers and is made of four regions: low, medium, high, and extra-high. The peak values for maximum acceleration and deceleration are approximately $\pm 1.6 \text{ m/s}^2$, while the maximum speed achieved is approximately 130 km/h.

The EPA cycle, on the other hand, has a total duration of 2134 seconds, covering a distance of 28.50 kilometers, and consists of two segments: the Urban Dynamometer Driving Schedule

(UDDS) and the Highway Fuel Economy Test Driving Schedule (HWFET). The maximum values for acceleration and deceleration in this cycle are approximately $\pm 1.5 \text{ m/s}^2$, with a maximum speed reached of approximately 96 km/h.

The tests were conducted, starting from a battery state of charge (SOC) of 95%, with four consecutive drive cycles run in succession. Initially, this procedure was performed with the HVAC system turned off, resulting in a SOC decrease of 49.99% for the WLTP-based test, and 52.46% for the EPA-based test. Subsequently, the HVAC system was activated, with the initial cabin temperature precisely matching the reference value. Different reference temperatures have been maintained inside the cabin while following the same driving schedules.

HVAC impact on SOC	T reference [°C]									
	18	19	20	21	22	23	24	25	26	27
WLTP	38%	36%	34%	32%	30%	28%	26%	24%	22%	20%
EPA	42%	39%	37%	35%	33%	31%	29%	26%	24%	22%

Table 4: HVAC system impact on the energy consumption at different reference temperatures

From Table 4, one can see that the HVAC has a significant impact on the drive range. As expected, because affirmed by a huge amount of researches in the literature, the consumption increases by up to 40%. This, of course, depends on the cabin conditions desired by the user, and on how closely they align with the external ambient conditions, which is clearly evident when reviewing the table above. Another notable observation from the results is that the HVAC has a more pronounced effect on the vehicle's consumption when following the EPA cycle rather than the WLTP cycle. This is not due to higher energy requirements by the HVAC system, but is simply a consequence of the EPA cycle being less aggressive compared to the WLTP cycle, resulting in lower traction-related consumption per kilometer.

4 Battery model

Throughout Chapter 2, it has already been foreshadowed that the battery model included in the Simulink[®] model of the BEV under study would have been further enhanced to make it more realistic. By examining the *Battery* system depicted in Figure 10, it appears as shown below.

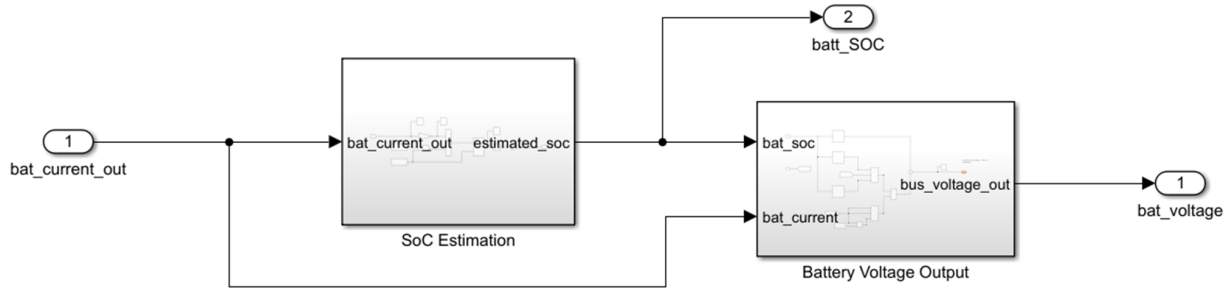


Figure 39: Original battery pack model - Simulink[®] flowchart

Of such model, for this thesis work, only the flow of data remained unchanged. Everything inside this scheme have been renovated. Nevertheless it was a good frame from which starting to build the new battery pack model. The novel model developed for this project introduces significant modifications. One involves incorporating an awareness of battery cell deterioration, while the other involves a coherent evolution of battery characteristic curves as the battery's performance degrades.

4.1 Battery pack design

A battery is a complex electro-chemical energy storage device designed to provide electrical power. At its core, a battery is composed of individual *cells*, which are the *fundamental building blocks* of the battery. These cells consist of three main components: two electrodes (an anode and a cathode) separated by an electrolyte. Once the materials and cell design are determined, the manufacturing process involves assembling the cells, typically in a series or parallel configuration, to achieve the desired voltage and capacity. The final step in battery design involves the packaging of the cells to ensure safety and protection against external factors, such as moisture and physical damage. In summary, the design of a battery starts with the selection of materials and the configuration of individual battery cells. These cells are then assembled into a battery pack, incorporating necessary components and safety measures.

Within this project, the design of the battery pack did not go through all the steps listed above, but, starting from scratch, it proceeded from the selection of suitable battery cells to choosing a configuration that would match the desired voltage and capacity. No mention

will be made about the packaging and the BMS, as along the work the battery have been considered well conditioned by an efficient BMS, constantly holding it on a temperature of $25\text{ }^\circ\text{C}$. The rated values of capacity and voltage for the battery pack were $Ah_{rated} = 55\text{ Ah}$ and $OCV_{rated} = 400\text{ V}$, which are very close to the technical data declared by the vehicle manufacturer.

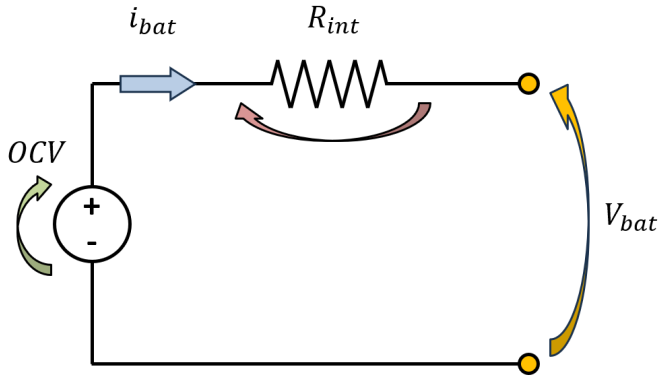


Figure 40: Battery R-circuit model

The battery cell used is an *A123 26650* with $LiFePO_4$ composition, whose rated open-circuit-voltage and capacity are respectively 3.3 V and 2.5 Ah . The equivalent circuit model considered for each cell is the one shown in Figure 40, meaning a series of a voltage generator and an internal resistance. The resistance always generate a voltage drop, then, during battery discharging $V_{bat} < OCV$, while during battery charging $V_{bat} > OCV$. The convention used for the battery current,

as well as for the battery power, is: $i_{bat} > 0$ during battery discharging, and $i_{bat} < 0$ during battery charging. Exactly as stated before, the next step followed was to fit the wished battery voltage and capacity. To do this, one can think about connecting multiple cells in series and parallel. From the Kirchhoff's laws, we can remind that electrical branches connected in parallel, among the same electric nodes, share the same voltage. Instead, the voltage within a branch is the arithmetic sum of the voltage of each dipole. Moreover, the arithmetic sum of all the currents crossing a junction is null. Keeping this in mind, it could be easily proven that, if one has n identical resistances R put in series, the equivalent resistance is:

$$R_{eq} = \sum_{i=1}^n R_i = n \cdot R \quad (22)$$

Instead, if the same are connected in parallel:

$$R_{eq} = \frac{1}{\sum_{i=1}^n \frac{1}{R_i}} = \frac{R}{n} \quad (23)$$

Considering this, it was decided, as design choice, to connect in parallel a number of branches equal to $N_{parallel}$, each made of a series of a quantity of cells that is equal to N_{series} . Thus, the equivalent rated open-circuit-voltage of the battery pack is:

$$OCV_{bat} = N_{series} \cdot OCV_{cell} \quad (24)$$

As regards the equivalent internal resistance of the battery pack, this is expressed as:

$$R_{int,bat} = \frac{N_{series} \cdot R_{int,cell}}{N_{parallel}} \quad (25)$$

Lastly, the total rated battery pack capacity:

$$Ah_{bat,rated} = N_{parallel} \cdot Ah_{cell,rated} \quad (26)$$

This theoretical discussion about the battery pack design ends up with a rated capacity of the same of $55 Ah$, and a rated open-circuit-voltage of $399.3 V$. Achieving this configuration involved a certain specific layout of connections among the cells. Specifically, it was necessary considering 22 branches in parallel, each composed of 121 cells in series, resulting in a total of 2662 cells. To create the battery model for this specific cell, we drew upon experimental data. These were provided by the authors of a paper focused on assessing the degradation of an HEV battery pack [19]. These data, which track the evolution of battery performance over its lifespan, allowed to construct a battery model whose characteristics change coherently in response to its state of aging. In essence, the entire battery lifespan has been covered in Simulink[®] by using two different look-up-tables, containing the profiles presented below.

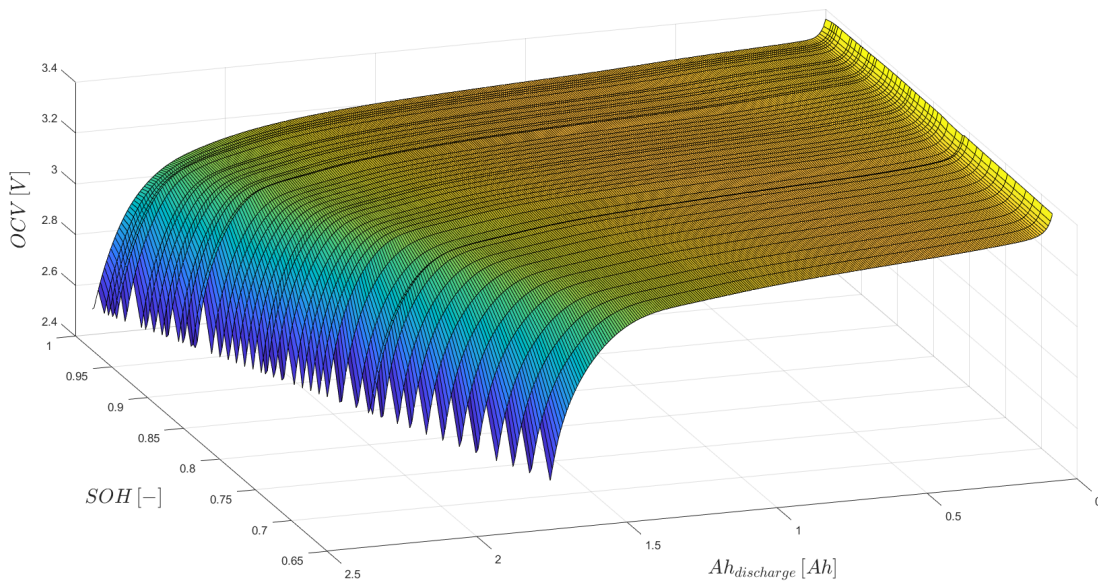


Figure 41: OCV battery characteristic surface - Simulink[®] look-up-table

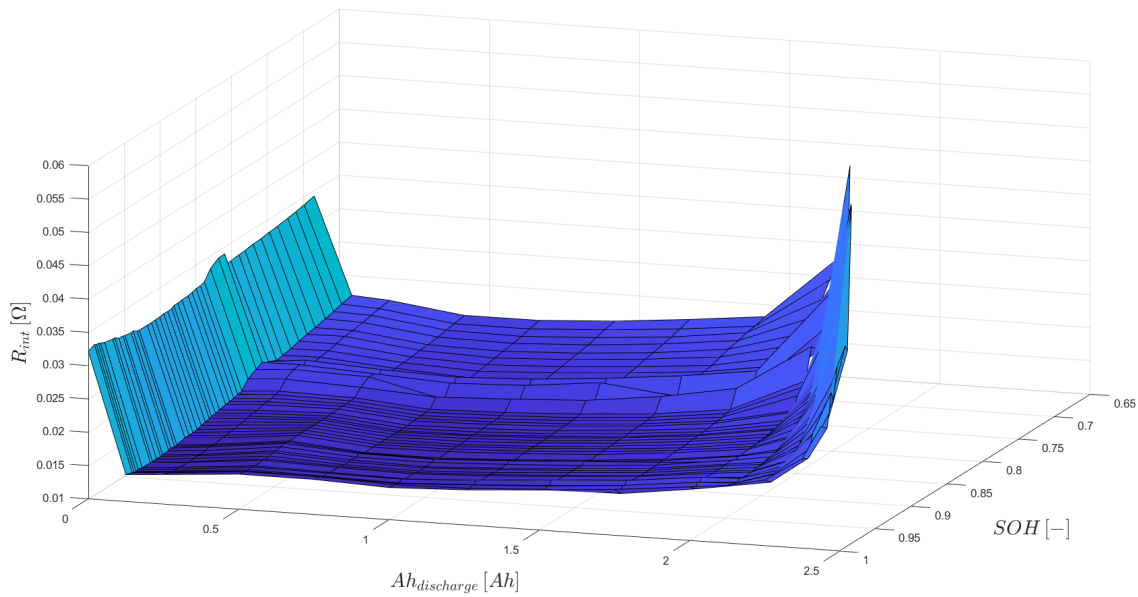


Figure 42: Internal resistance battery characteristic surface - Simulink[®] look-up-table

When examining Figure 41 and Figure 42, the domain of these two surfaces is defined by two axes. One axis represents the State of Health (SOH), where an SOH of 1 corresponds to a brand-new battery, and lower values indicate increased battery aging. While this description may suffice for now, it's important to note that this battery index will be thoroughly discussed in the following paragraphs. The other axis displays discharging curves for various SOH values. When $Ah_{discharge} = 0$, it indicates that the battery is fully charged. The variable $Ah_{discharge}$ represents the charge extracted from the battery starting from its fully charged state. In summary, as the battery discharges, this value increases until it reaches a certain upper threshold, which, depending on the battery's state of health, represents the maximum capacity of the battery at that moment. Another crucial aspect not yet highlighted is that, in the developed model, all cells within the battery pack behave identically.

4.2 Battery fading model

After designing the battery, the next crucial step, preceding the development of the HVAC power management strategy, was enabling battery degradation prediction. The literature is replete with research and papers devoted to studying battery fading and attempting to develop a comprehensive predictive model for it. A thorough examination of the various damaging mechanisms associated with battery degradation led to the identification of several key processes, including:

- capacity fade
This involves the reduction in a battery's ability to store and deliver electrical energy.
- cycle life degradation
Referring to the decrease in the round-trip cycles a battery can undergo before its capacity significantly diminishes.
- thermo-mechanical stress
Temperature fluctuations and mechanical stresses experienced during BEV operation can accelerate degradation processes.
- state of charge (SOC)
The SOC of a battery during operation plays a critical role in its degradation. Operating a battery at high or low SOC extremes, can lead to faster capacity fade.

The methodological approach to account for these processes can have various foundations, including electro-chemical, empirical, semi-empirical, and statistical methods.

For this project, we chose a semi-empirical formulation, which became possible by utilizing the data from [19]. These data specifically pertain to the cells used within this battery model. Among the processes listed earlier, our degradation model addresses only the first two and the battery temperature effect. Two central parameters in this model are the battery *SOH* and the battery *C-rate*. Essentially, the first parameter quantifies the amount of capacity still available for use in the cell, so it is used to identify capacity loss. This index is commonly employed to characterize battery aging, and is defined as follows:

$$SOH = \frac{Ah_{actual}}{Ah_{initial}} \quad [-] \quad (27)$$

The second one is an operating parameter, meaning that it depends on how the battery is working instantaneously. It is related to the discharge rate:

$$c = \left| \frac{i_{cell}}{Ah_{initial,cell}} \right| \quad [h^{-1}] \quad (28)$$

The higher the *C-rate*, the faster the battery will charge or discharge. This parameter significantly influences the chemical processes within a battery, and so it plays a key-role in battery deterioration.

Going further into the proposed model, it is worth noting its scientific foundation, which is the Arrhenius equation.

$$k = A \cdot e^{-\frac{E_A}{RT}} \quad (29)$$

This equation is largely used in chemistry to determine the velocity of a chemical reaction. Indeed, the term k is the *rate constant* for the reaction. Instead, A is a *pre-exponential factor*

that represents the fraction of collisions between reactants having enough energy to overcome the activation barrier, and E_A is the energy needed to make the reaction happening.

Building upon this, the model used in this project assumes the battery capacity degradation being a direct consequence of chemical reactions. Starting from this, it takes the Arrhenius formulation as a frame to be tuned in order to fit experimental results acquired from the exact cell under the study. That is the reason why it is reported under the class of semi-empirical formulations. Then, one can recognize a huge similitude with equation (29) in the following formulation:

$$Ah_{loss,\%} = B(c) \cdot e^{-\frac{A_f(c)}{T_{bat}}} \cdot Ah_{tp}^z \quad (30)$$

This equation predicts, for a given C-rate, i.e. c , and battery temperature, the percentage of capacity loss after a certain Ah-throughput, that is so defined:

$$Ah_{tp} = \frac{1}{3600} \cdot \int_{t=0}^{t_{EOL}} |i_{cell}| \cdot dt \quad [Ah] \quad (31)$$

The two terms depending on the C-rate are summarized in equation (32) and Table 5.

$$A_f(c) = 3814.7 - 44.6 \cdot c \quad (32)$$

c [1/h]	2	6	10	20
B(c)	21681	12934	15512	15512

Table 5: Pre-exponential factor table

In general, for automotive applications, a battery is considered worn out if its capacity falls below 80% of the initial battery capacity. Then, by managing the formula and considering our assumption to maintain the temperature constantly at 25°C, for each C-rate, one can calculate the respective Ah_{tp} . From this knowledge, it is possible to compute the number of lifetime round-trip cycles for the specified operating conditions:

$$N(c, T_{bat}) = \frac{Ah_{tp}(c, T_{bat})}{2 \cdot Ah_{cell, rated}} \quad (33)$$

Once completed this step, the rate of capacity degradation can be easily determined as follows:

$$SOH = 0.2 \cdot \frac{c}{3600 \cdot N(c, T_{bat})} \quad [1/s] \quad (34)$$

In this way, the battery capacity can be updated at each instant, assuming, as emphasised earlier, all the cells works similarly.

$$Ah_{bat}(t^*) = N_{parallel} \cdot Ah_{rated, cell} \cdot \left(SOH_0 - \int_{t=0}^{t=t^*} SOH(t) \cdot dt \right) \quad (35)$$

In conclusion, this model does not introduce novelties in its formulation, but it can leverage the knowledge of the battery characteristic curves over its lifetime, namely internal resistance and open-circuit-voltage. This enables a better precision in the model, taking into consideration that as the battery degrades, its behavior changes.

In the following image, Figure 43, it is displayed the final battery model scheme in Simulink[®]. Compared to the one shown in Figure 39, it can be observed the presence of an additional subsystem responsible for evaluating the battery SOH. The output of this subsystem, i.e. SoH, is fed back to the *SoC Estimation* subsystem, where it is exploited for updating the residual battery capacity.

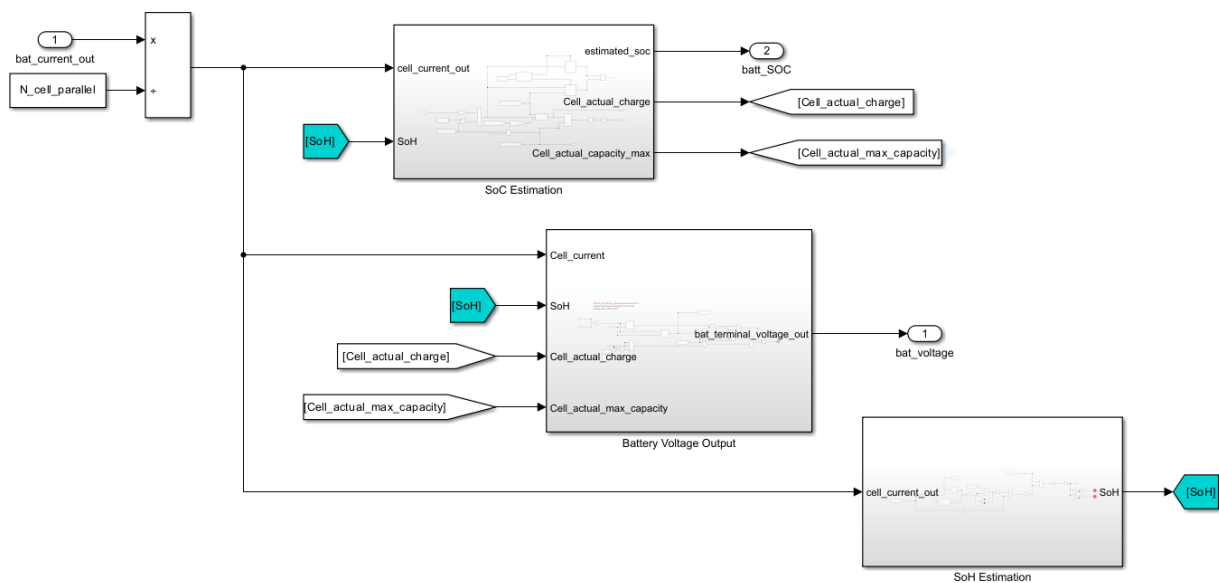


Figure 43: Final battery pack model - Simulink[®] flowchart

In Figure 44, is reported the profile of battery capacity over the course of a single drive cycle, both WLTP and EPA. Although the capacity decrease appears minimal when considering the y-scale, it is important to note that the distances traveled are relatively short. For one WLTP cycle, it covers 23.25 km, while an EPA cycle spans 28.50 km. However, regardless of the minimum amount of deterioration, it is worth highlighting that at the end of the WLTP cycle, the battery exhibits lower remaining capacity compared to the same battery subjected to an EPA cycle. As mentioned in the previous chapter, the WLTP is a more aggressive driving schedule than the EPA, resulting in higher power demands on the battery for propulsion. This justifies the curves displayed in Figure 44, and validates as well the model's effectiveness.

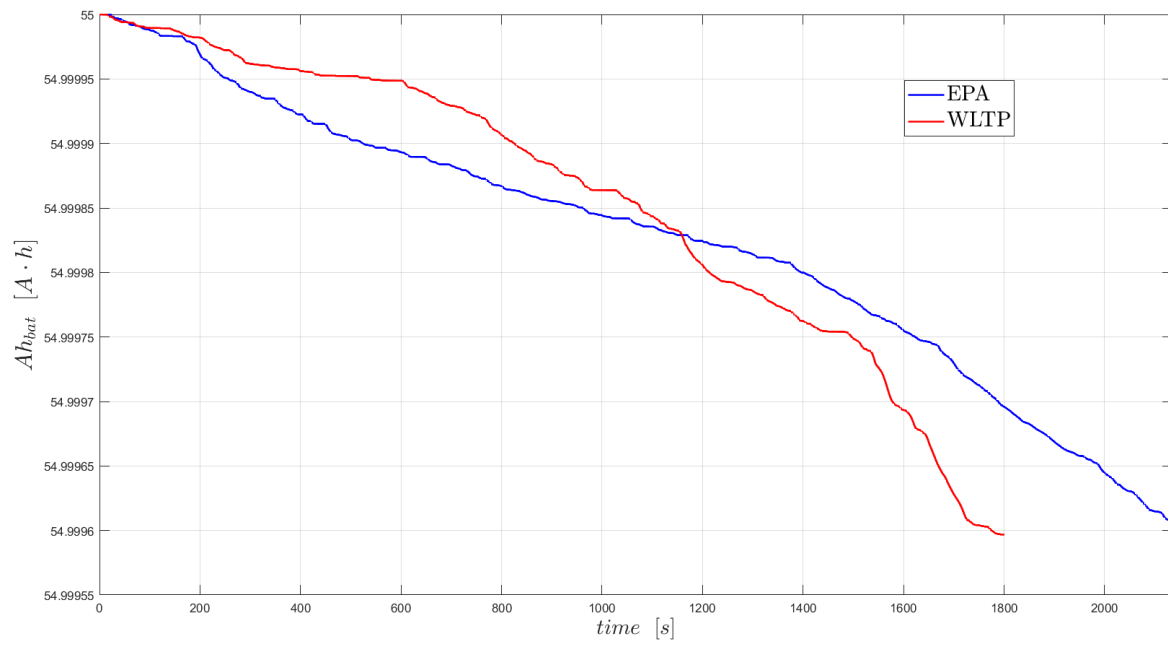


Figure 44: Battery capacity degradation along one cycle: WLTP vs. EPA

5 IETM strategy

After developing all the preliminary models, including the cabin, HVAC, and battery models, they were integrated into a single comprehensive Simulink[®] model of the Chevrolet e-Spark 2015. The rationale for the HVAC control strategy has been discussed in the introduction but is worth reiterating now.

When the vehicle is in motion and needs to follow a specific velocity trajectory, it requires power from the powertrain. In a battery electric vehicle, this powertrain relies solely on the battery pack. However, the same battery is also responsible for supplying power to all the auxiliary systems. Referring to equation (34), it becomes apparent that this situation could lead to critical conditions for the battery when both the traction and auxiliary systems demand peak power simultaneously. The SOH model for the battery implemented in this project does not distinguish between battery charge and discharge in terms of the damaging effects of different currents.

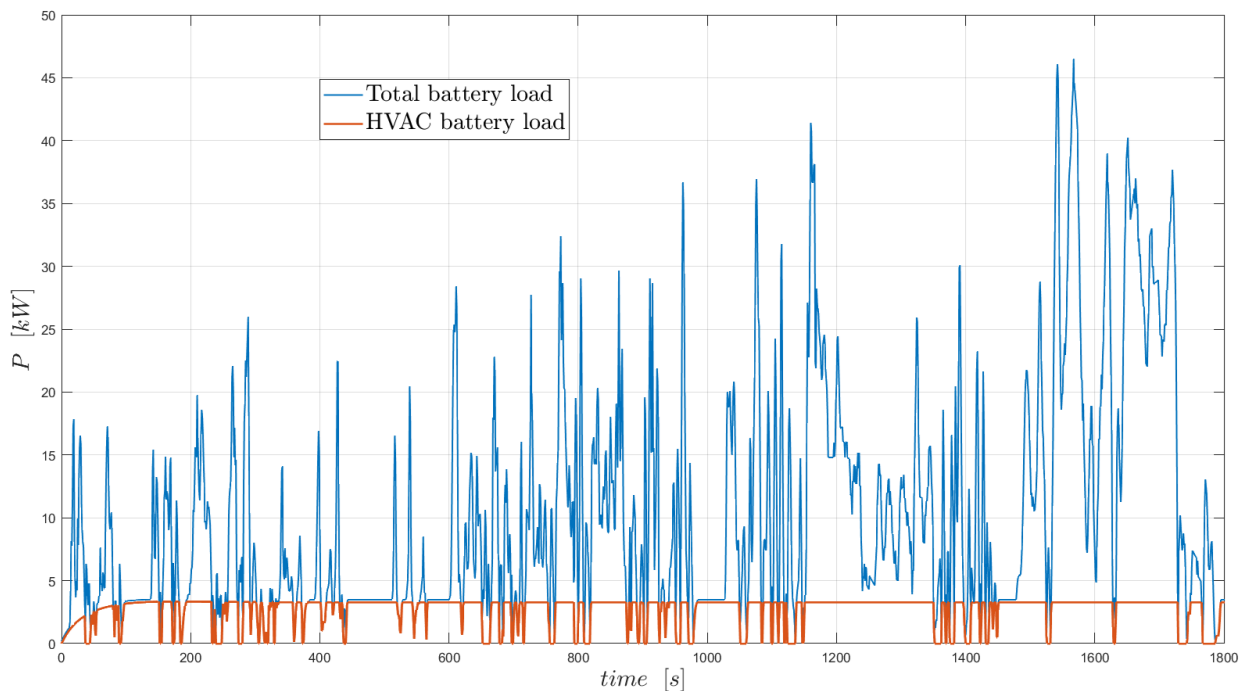


Figure 45: Battery loads along a WLTP cycle. Total battery load (blue) and HVAC battery load (red) to keep the cabin temperature at 18°C

Figure 45 illustrates the power loads on the battery when the studied vehicle follows a WLTP cycle, and the HVAC maintains a cabin temperature of 18°C . The blue profile represents the absolute value of the total power either drawn from or supplied to the battery. To identify the most critical conditions for the battery, it is not necessary to distinguish between charging and

discharging, as just specified. Instead, when assessing the HVAC's impact on the battery's power load, it is crucial to consider the power request in the context of the overall power demand on the battery. Except for the HVAC, all other auxiliary systems have been modeled with a constant power request of 200 W . When the vehicle is braking, the traction power component has a negative sign, while the HVAC's power demand remains positive. In such conditions, the load of the HVAC on the battery can be considered reduced, and supplying power to the HVAC might even be beneficial for the battery. The figure reported refers to a cabin temperature kept at $18\text{ }^\circ\text{C}$, but the situation slightly improves increasing the temperature inside the cabin because of the lower power required by the HVAC. Additionally, another adverse consequence of intense battery loading is battery pack heating. It has been previously mentioned that, in this project, the focus was primarily on various aspects, and the thermal management of the battery pack was assumed to be able to keep its temperature constant at $T_{bat} = 25\text{ }^\circ\text{C}$. Although not considered within this thesis work, battery overheating is a critical aspect for the battery health. Having a strategy like the one that is about to be explained, it can also mitigate this problem by smoothing the battery peak power requests. Reducing battery load peaks, consequently means enhancing the problem of battery thermal stress. This beneficial side effect further credits the implementation of the strategy presented in this chapter.

The expected benefits coming from such a strategy were a significant reduction in the battery degradation, to be quantified relying on the results given by the battery model developed.

Once the motivation for the work carried out has been plenty explained, it is the moment to delve inside the model of the controller developed, first presenting the overall control architecture it belongs to, and then showing the relative analytical foundation.

5.1 IETM controller integration in HVAC control architecture

Throughout this work, the importance of such a strategy that intelligently manages the heating power to be removed from the cabin acting on the HVAC control has been emphasized; this ensures consistent temperature control while extending the battery's useful life. The complete architecture of the final system controlling cabin thermal comfort is depicted in Figure 46. To fulfill its requirements, the IETM controller must work between the PI controller (discussed in Section 3.2) and the HVAC system. It acts as a filter for the commands that the PI controller intends to transmit to the HVAC system, simultaneously taking care of the battery's health. This means that the control architecture presented in previous chapters, designed to ensure cabin thermal comfort, remains largely intact but with some modifications. The IETM controller receives inputs for the desired heating capacity to be removed from the cabin (\dot{Q}_{HVAC}^{des}) and the battery power allocated to traction and other auxiliaries ($P_{tract+aux}$). With these inputs, it shapes the desired power for the HVAC, requested by the PI controller, in a manner that also

considers battery health. As a result, the heat rejected from the cabin is no longer \dot{Q}_{HVAC}^{des} , but rather \dot{Q}_{HVAC} . It is now the responsibility of the HVAC system's internal logic to convert this heating capacity into a real mass flow rate with a specific temperature, respectively denoted as \dot{m}_{HVAC} and $T_{HVAC,out}$. However, apart from the IETM controller, the architecture is the same compared to the one presented in Figure 30.

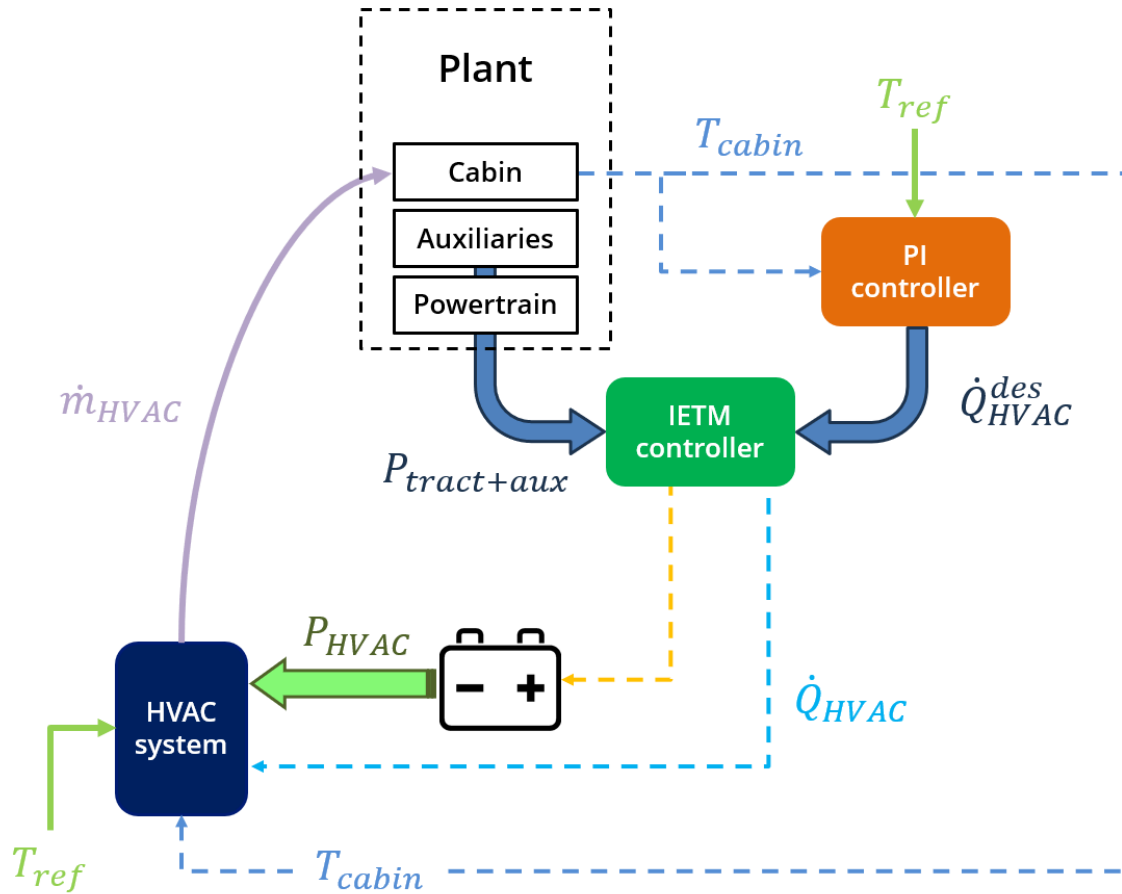


Figure 46: Cabin thermal comfort control architecture including IETM controller

5.2 Mathematical formulation

If one were to categorize this intelligent HVAC control strategy, it would fall under the classification of an “*instantaneous optimization*” strategy. What needs to be controlled in order to achieve the predefined objectives is the HVAC power, denoted as P_{HVAC} . The impact of this variable on cabin temperature evolution and battery degradation has been extensively discussed respectively in Section 3.2 and Section 4.2.

At each time instant, as already described before while presenting how the IETM controller is integrated into the existing cabin plant control architecture, the power to allocate by the battery

to the HVAC ranges between zero and P_{HVAC}^{des} :

$$0 \leq P_{HVAC} \leq P_{HVAC}^{des} \quad (36)$$

The left side boundary corresponds to the HVAC turned off, while the right side boundary is the power that the PI controller would like the battery to allocate to the HVAC. However, not necessarily one expect to find a proportionality among the power delivered to the HVAC and the heating capacity removed from the cabin. Nevertheless, if one look at equation (15) and equation (12), is evident that both this two power quantity are directly proportional to the air mass flow rate blown into the cabin, meaning \dot{m}_{HVAC} . Moreover, all the remaining terms present into the same equations, as a result of the low-control logic implemented for the HVAC, they are independent from the air flux blown into the cabin. Indeed, the only variability of such terms to underline is the one with the reference temperature and the current cabin temperature; but, these two values are constant working on a single time step. Then, considering what just stated, it turns out as:

$$\dot{Q}_{HVAC} \propto \dot{m}_{HVAC} \quad (37)$$

$$P_{HVAC} \propto \dot{m}_{HVAC} \quad (38)$$

These two relationships can be leveraged inside the IETM controller to find a direct link between the battery power allocated to the HVAC, and the respective heating capacity removed from the cabin, as follows:

$$\dot{Q}_{HVAC} = \dot{Q}_{HVAC}^{des} \cdot \frac{P_{HVAC}}{P_{HVAC}^{des}} \quad (39)$$

This means that, the domain of the battery power allocated to the HVAC has a one-to-one correspondence to the heating capacity removed from the cabin, resulting in such interval:

$$0 \leq \dot{Q}_{HVAC} \leq \dot{Q}_{HVAC}^{des} \quad (40)$$

Now, mathematically speaking it still misses what would be to optimize. The states, identified to instantaneously keep track of the system's objectives under the study, are:

- $T_{cabin} - T_{ref}$

This state stores an information about the compliance of the cabin thermal conditions with the temperature target. The more this state is close to zero, the better the comfort for passengers.

- SOH

It keeps track of the battery health conditions. This state is monotonically decreasing over the time. Although is impossible to hold it on its maximum value, acting on the control variable, its decreasing rate can be limited.

Given the vector of the states, i.e. $x^{(k)}$, and the respective control variable, i.e. $u^{(k)}$, of the system at time instant $t^{(k)}$, the following **cost function** was selected for the optimization problem:

$$F(u^{(k)}, x^{(k)}, t^{(k)}) = \gamma \cdot (1 - \beta) \cdot \left(\Delta SOH^{(k)} - \Delta SOH_{min}^{(k)} \right)^2 + \beta \cdot \left(\Delta T^{(k)} - \Delta T_{min}^{(k)} \right)^2 \quad (41)$$

Practically, the one reported is an instantaneous *multi-objective* function. The final cost is set up considering two differently weighted objectives: battery state of health (first term on the right side of equation (41)), and passengers thermal comfort (second term on the right side of equation (41)).

All the terms participating to the total cost are now explained:

- $\Delta SOH^{(k)} = SOH^{(k)} - SOH^{(k+1)} > 0$

This is the drop in *SOH* that occurs across one time step.

- $\Delta SOH_{min}^{(k)} = \left(SOH^{(k)} - SOH^{(k+1)} \right)_{min} > 0$

This is the smallest drop in *SOH* that could verify across that time step. It would be impossible, passing from instant $t^{(k)}$ to instant $t^{(k+1)}$, to further minimize the battery degradation below this threshold.

- $\Delta T^{(k)} = T_{cabin}^{(k+1)} - T_{cabin}^{(k)}$

It is the temperature difference in cabin occurring during a time instant. Considering the state of the system, the difference in T_{ref} should be considered as well. However, this is null.

- $\Delta T_{min}^{(k)} = \left(T_{cabin}^{(k+1)} - T_{cabin}^{(k)} \right) |_{P_{HVAC}^{des}} < 0$

This is the maximum temperature drop that happens if the command given by the PI controller is directly fed to the HVAC system. Here is reported as *min*, because it is a negative amount.

- γ

It is the *scaling factor*. This is crucial to fill the gap in magnitude existing among the two costs involved by the objective function, and it requires tuning.

- β

It is the *weighting factor*, that is used to ponder the weight to assign to the two costs of the objective function. This factor ranges between zero and one, and its value can be arbitrarily chosen depending on the effect that one want to get.

One element of the list shown above, in particular $\Delta SOH_{min}^{(k)}$, can be determined at each instant and its definition is not always the same. Depending on the load applied to the battery by the auxiliaries and traction or braking, one can leverage this knowledge to determine which is the

best amount of P_{HVAC} that can minimize the battery capacity reduction across one time step. It has already been claimed as, concerning battery loads, it is necessary to consider the incoming or out-coming battery power budget in absolute value. This may result in the following scenarios:

- $P_{trac} + P_{aux} < 0 \quad \wedge \quad |P_{trac} + P_{aux}| \geq P_{HVAC}^{des}$

The vehicle is braking but the maximum limit battery power to allocate to the HVAC is lower than the rest of power leaving the battery. In this condition, to reduce the battery load it would be necessary to send entirely the P_{HVAC}^{des} to the HVAC.

- $P_{trac} + P_{aux} < 0 \quad \wedge \quad |P_{trac} + P_{aux}| < P_{HVAC}^{des}$

Here the vehicle is braking and the maximum possible battery power to allocate to the HVAC is greater than the remaining power leaving the battery. To reduce the battery load, it must be $P_{HVAC} = |P_{trac} + P_{aux}|$.

- $P_{trac} \geq 0$

If the vehicle powertrain demands power to the battery, to minimize the battery degradation across one time step no power should be delivered to the HVAC, meaning $P_{HVAC} = 0$.

After these important considerations, it is worth underlining that the cost function expressed in equation (41) is convex. This is an excellent property for a cost function, because it means that the optimization problem has one single minimum, that is the same optimum cost. The convexity of the cost function has been carefully verified, and it can find a undeniable prove in the linearity of the two contributions accounted under square. After getting this information, beneficial consequences derived. As a matter of fact, it was possible to use the *Golden Section Search* algorithm to reduce the computational cost required at each time instant. This is an iterative algorithm whom, exploiting the so called *golden ratio* ($\frac{1+\sqrt{5}}{2}$), is able to find the minimum of a convex function with a very reduced number of iterations as compared to a simple minimum-search algorithm. This number reduces accordingly to the tolerance given to stop the iterations. Figure 47 shows the number of iterations executed by the GSS algorithm along a drive cycle operated at constant reference temperature. The results, depending on the tuning carried out for the final tolerance below which the value is considered as solution, clearly evidence as the number of iterations generally ranges between 8 and 14.

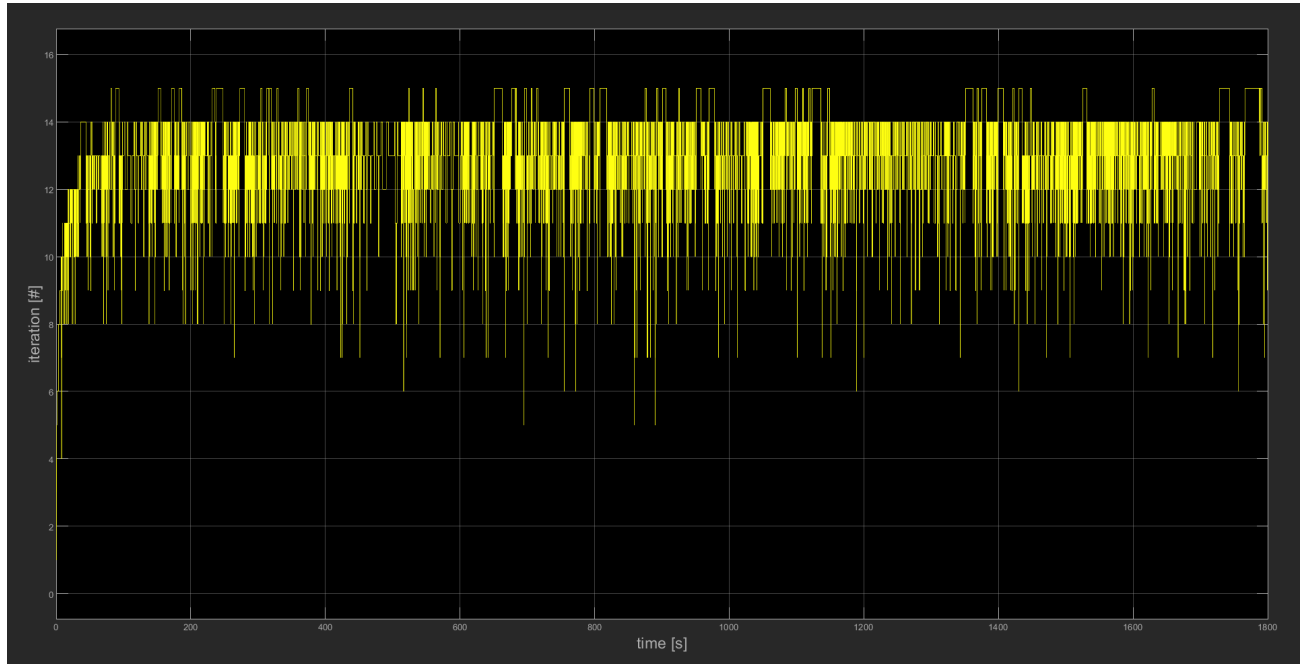


Figure 47: Number of iterations undergone by the GSS algorithm to find the minimum of the cost function along a WLTP cycle

The tuning for the scaling factor, whose need has been discussed before, ended up with a value of $\gamma = 6.43 \cdot 10^{15}$.

For what concerns the tuning of the weighting factor, called beta, it is important to remark that there is no a right value. On the contrary, the tuning depends on the importance that one want to assign to one term of the cost over the other one. Within this project, the tuning has been carried out admitting, over one of the two drive cycles considered, namely WLTP and EPA, a maximum amplitude for the cabin temperature to oscillate around the reference of $1.5 \text{ }^\circ\text{C}$. During the tuning, it turns out as the need for a β varying with the reference temperature. Actually, this fact is more than obvious. To understand this passage it is important to remind Table 4; this clearly shows that, given a set of boundary conditions for the temperature evolution problem, the lower the temperature kept inside, the higher the consumption related to the HVAC. Having an higher consumption means having instantaneously an higher power allocated by the battery to the HVAC, and so being more impacting in terms of battery degradation. Considering that the scaling factor is a constant, if for every reference temperature asked by the user we would like to guarantee an acceptable range for the temperature oscillation that meets the passengers' needs, it is necessary to consider a β -variability. Less importance must be given to the battery health if a lower reference temperature is set, and conversely. This way of proceeding is necessary if one want to keep, regardless of the target set, the temperature of the cabin within a fixed range. The value chosen for the weighting factor are reported in Table 6 and graphically represented in Figure 48.

T_{ref} [$^{\circ}C$]	18	19	20	21	22	23	24	25	26	27
β [-]	0.78	0.74	0.70	0.66	0.62	0.55	0.50	0.46	0.40	0.33

Table 6: Tuned weighting factor vector values

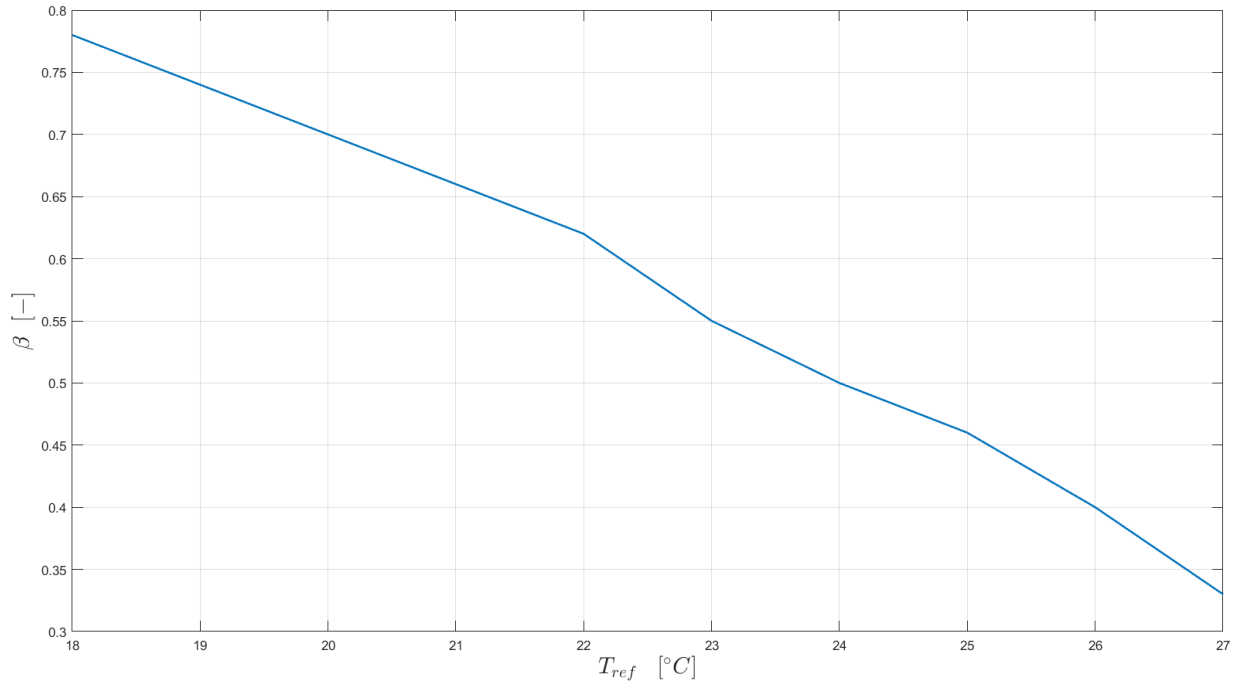


Figure 48: Weighting factor profile as function of the reference temperature

At the end of this explanation, it is worth emphasizing as the value of the final tolerance of the GSS and the value of the scaling factor are strictly linked to the working frequency of the IETM controller. This comes from the dependency, for the terms involved in the definition of the cost function, on the sampling time considered. The results presented and all the tuned variables refer to a IETM working frequency of 10 Hz .

5.3 Tuned IETM results

Once the parameters requiring tuning were found, the IETM controller was tested along the two drive schedules already mentioned before, namely WLTP cycle and EPA (UDDS + HWFET) cycle. To be sure about the effectiveness and robustness of the strategy, the simulations were run for any reference temperature, from 18 $^{\circ}C$ to 27 $^{\circ}C$, with a step of 1 $^{\circ}C$. In order to end up with comparable results, the same boundary conditions were considered for all these tests. All of them are reported in the table below.

T_{ext} [$^{\circ}\text{C}$]	$T_{\text{cabin},0}$ [$^{\circ}\text{C}$]	q_{sun} [W/m^2]	n_p [-]
32	T_{ref}	1000	1

Table 7: Boundary conditions for the set of simulations conducted for checking the effectiveness of the IETM controller

To better explain the leading thread of the simulation, here some conditions mentioned in Table 7 can be further clarified. The main purpose of all these simulations, as already discussed, was to understand the behaviour of the IETM controller in maintaining different temperatures inside the cabin. To do this, for each test we assumed to start from the same temperature as the target that has been set. Then, according to the reason that had led to design the controller, we expected to see oscillations in the temperature profile and in the power allocated to the HVAC as well. Before plotting all the results, it is worth representing the traction power required to the vehicle to follow the two different drive cycles, reported in Figure 49 and Figure 50. These latter will be very helpful to carefully explain the features of the trends found.

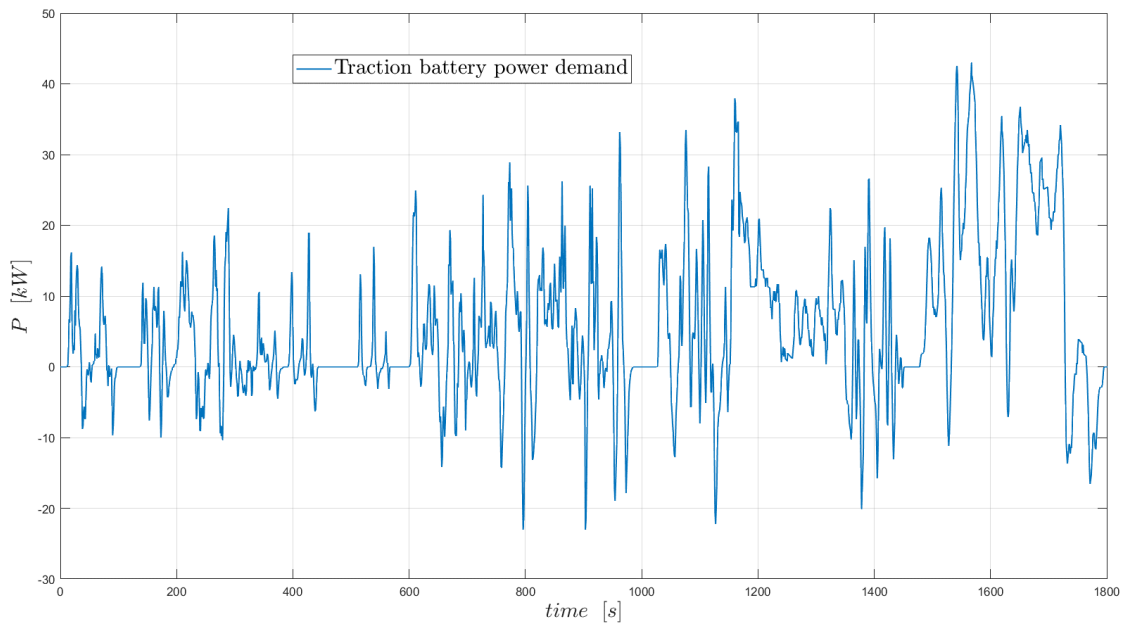


Figure 49: WLTP traction power request to the battery

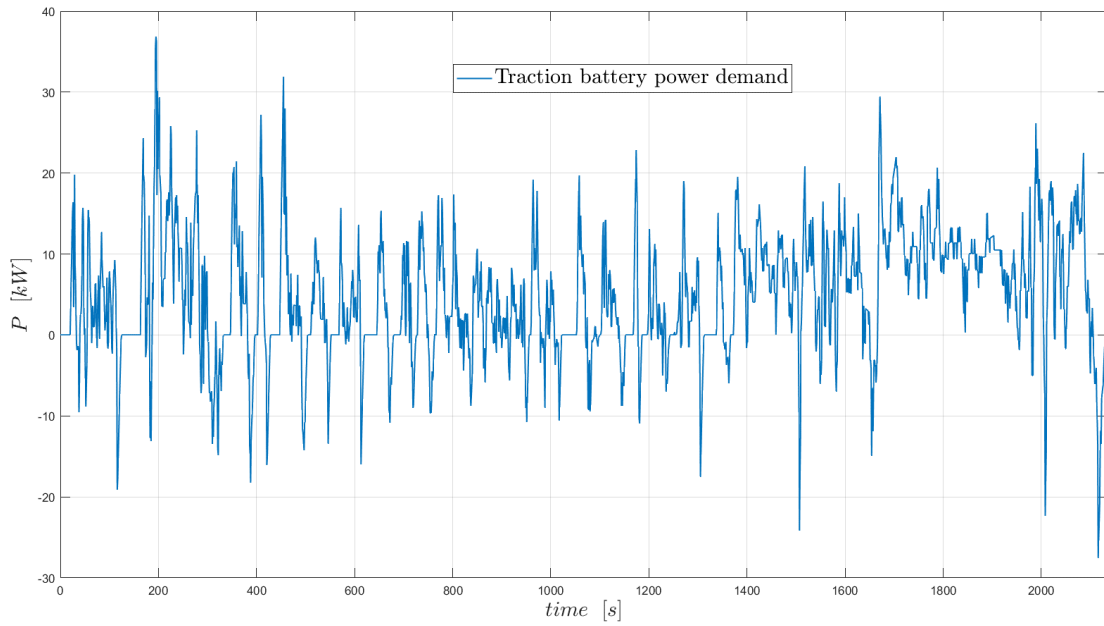


Figure 50: EPA traction power request to the battery

5.3.1 WLTP-based results

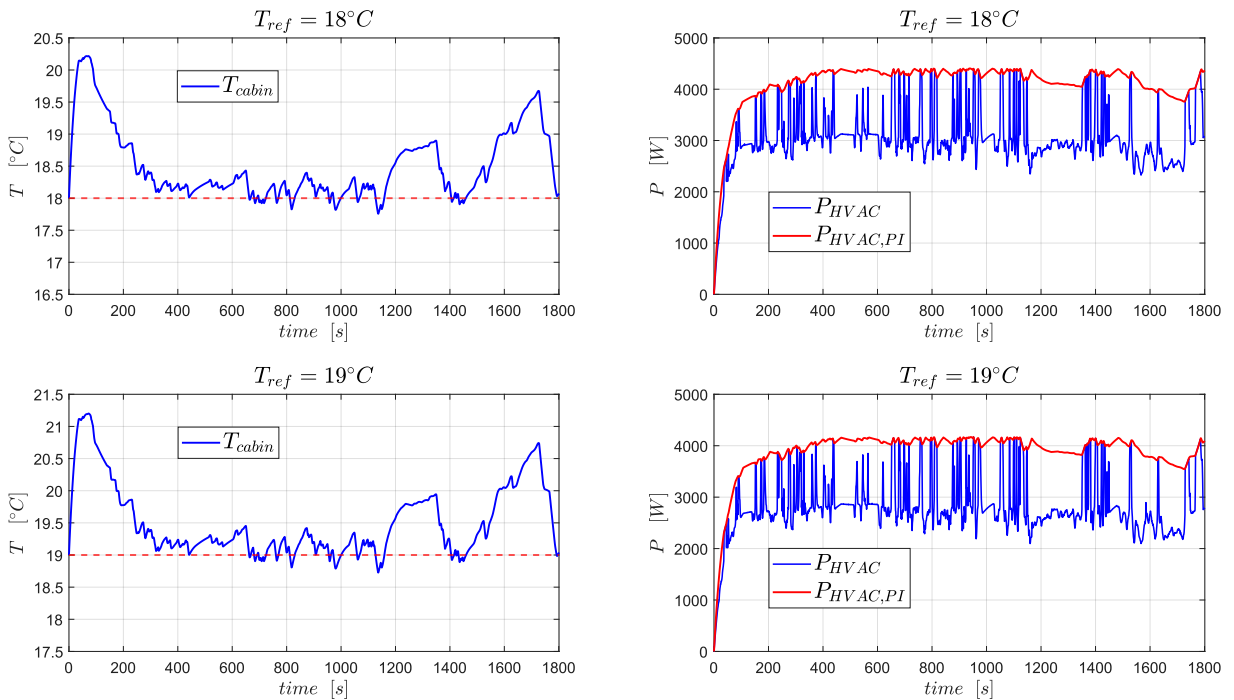


Figure 51: Temperature and HVAC battery power profiles with a target temperature of $18^{\circ}C$ (upper panel) and $19^{\circ}C$ (lower panel) along the WLTP cycle

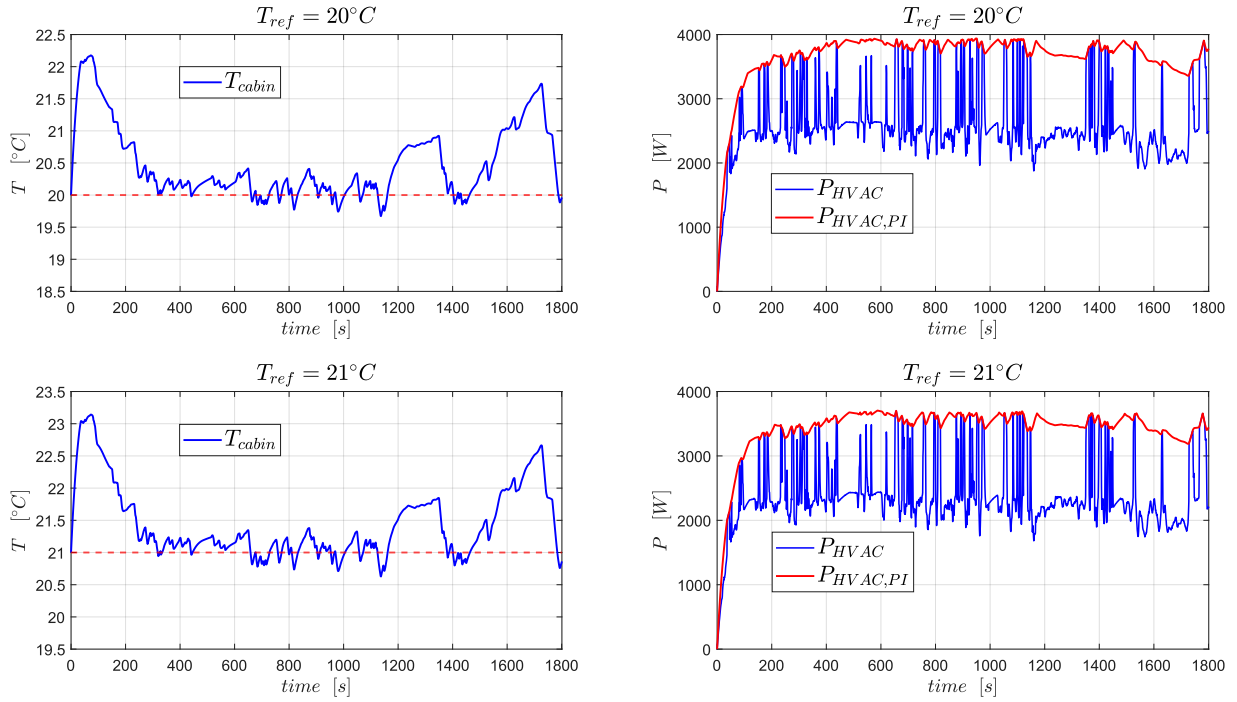


Figure 52: Temperature and HVAC battery power profiles with a target temperature of $20^\circ C$ (upper panel) and $21^\circ C$ (lower panel) along the WLTP cycle

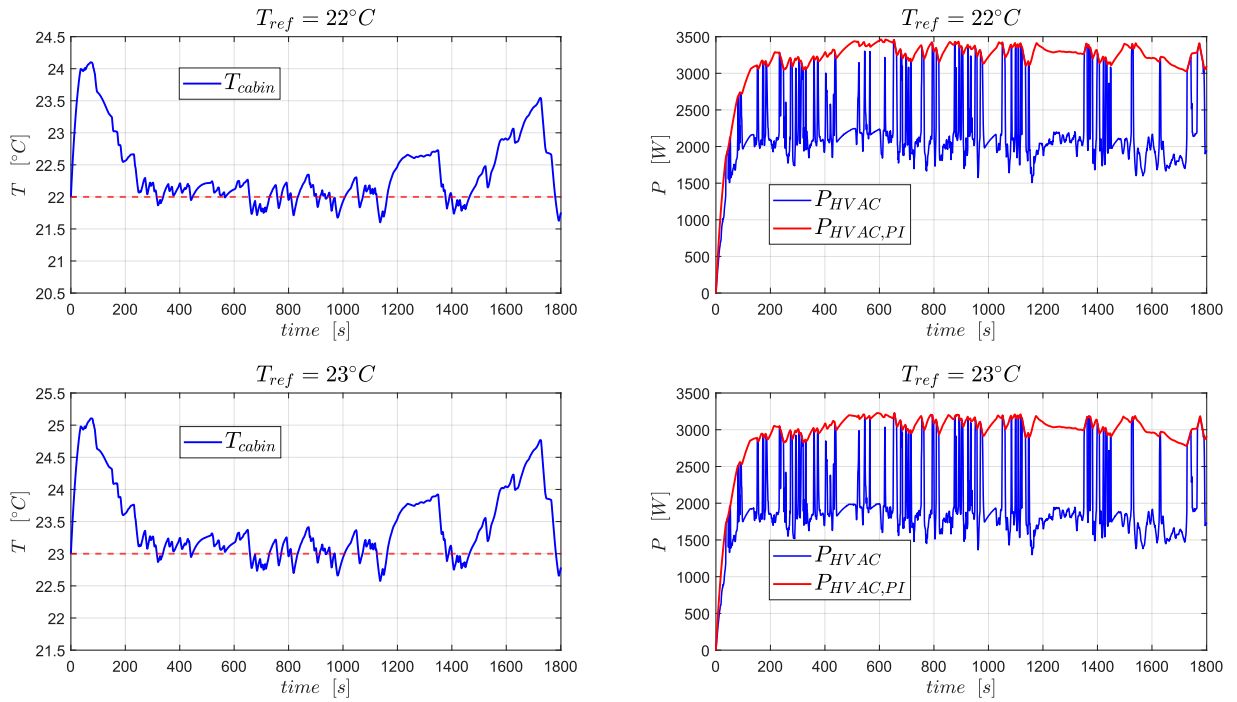


Figure 53: Temperature and HVAC battery power profiles with a target temperature of $22^\circ C$ (upper panel) and $23^\circ C$ (lower panel) along the WLTP cycle

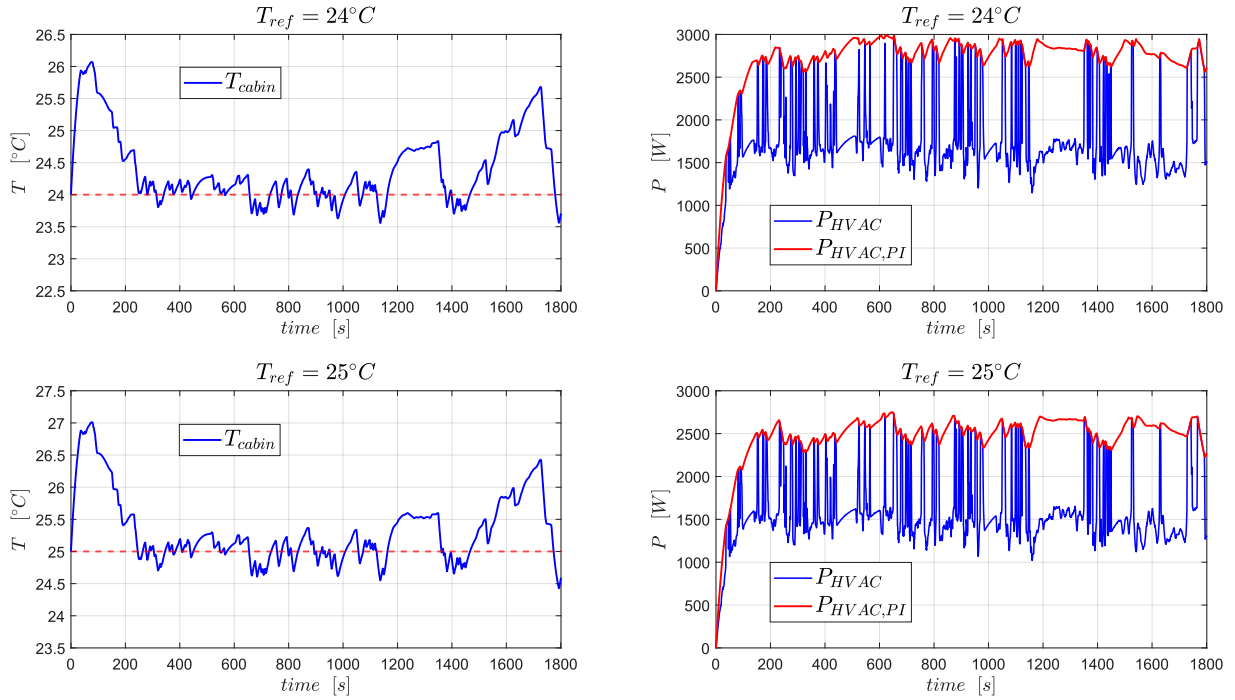


Figure 54: Temperature and HVAC battery power profiles with a target temperature of $24^\circ C$ (upper panel) and $25^\circ C$ (lower panel) along the WLTP cycle

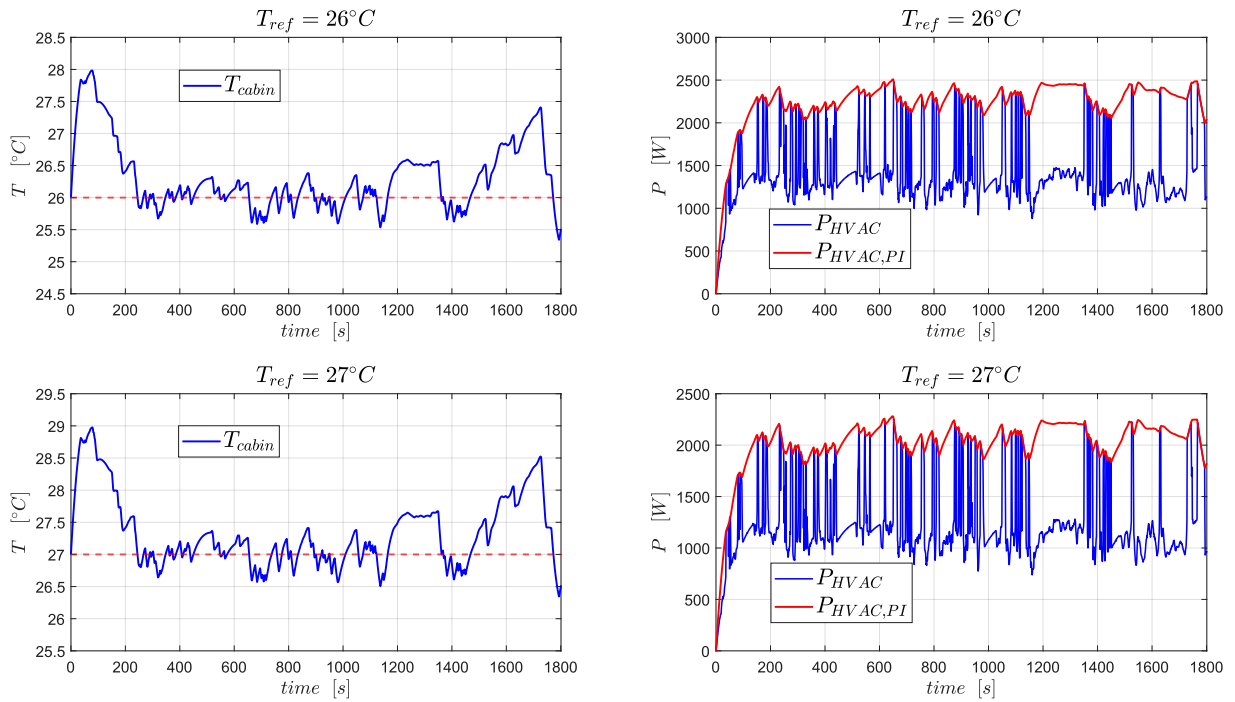


Figure 55: Temperature and HVAC battery power profiles with a target temperature of $26^\circ C$ (upper panel) and $27^\circ C$ (lower panel) along the WLTP cycle

5.3.2 EPA-based results

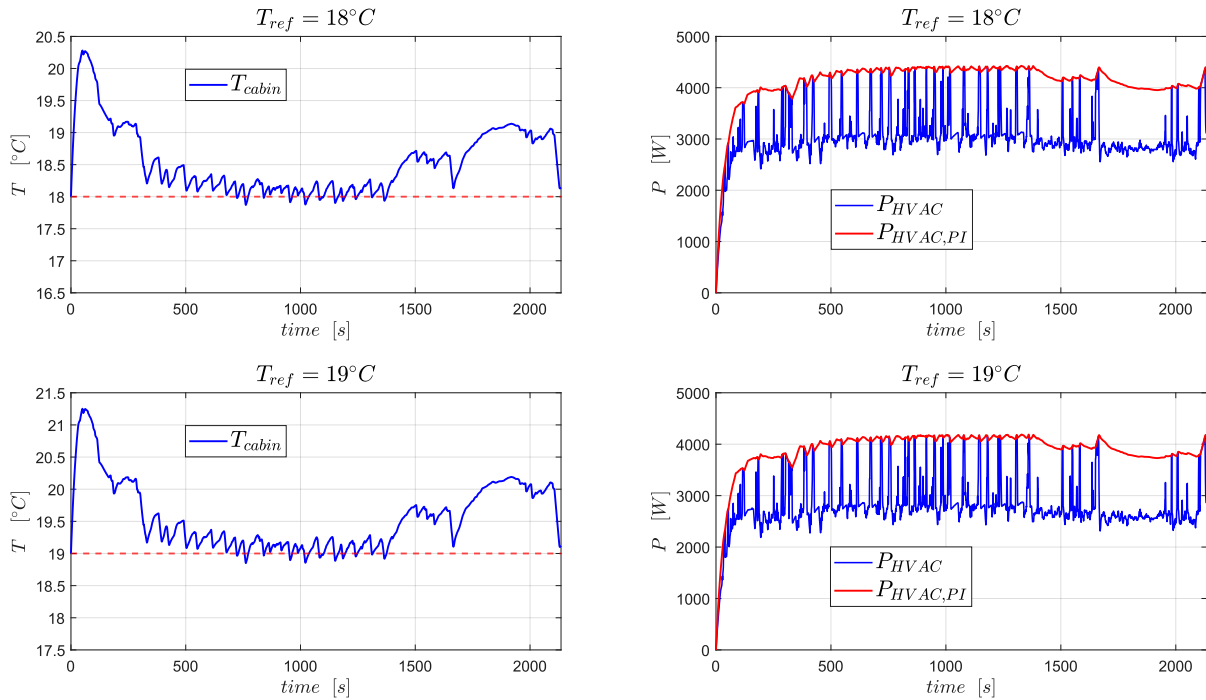


Figure 56: Temperature and HVAC battery power profiles with a target temperature of $18^\circ C$ (upper panel) and $19^\circ C$ (lower panel) along the EPA cycle

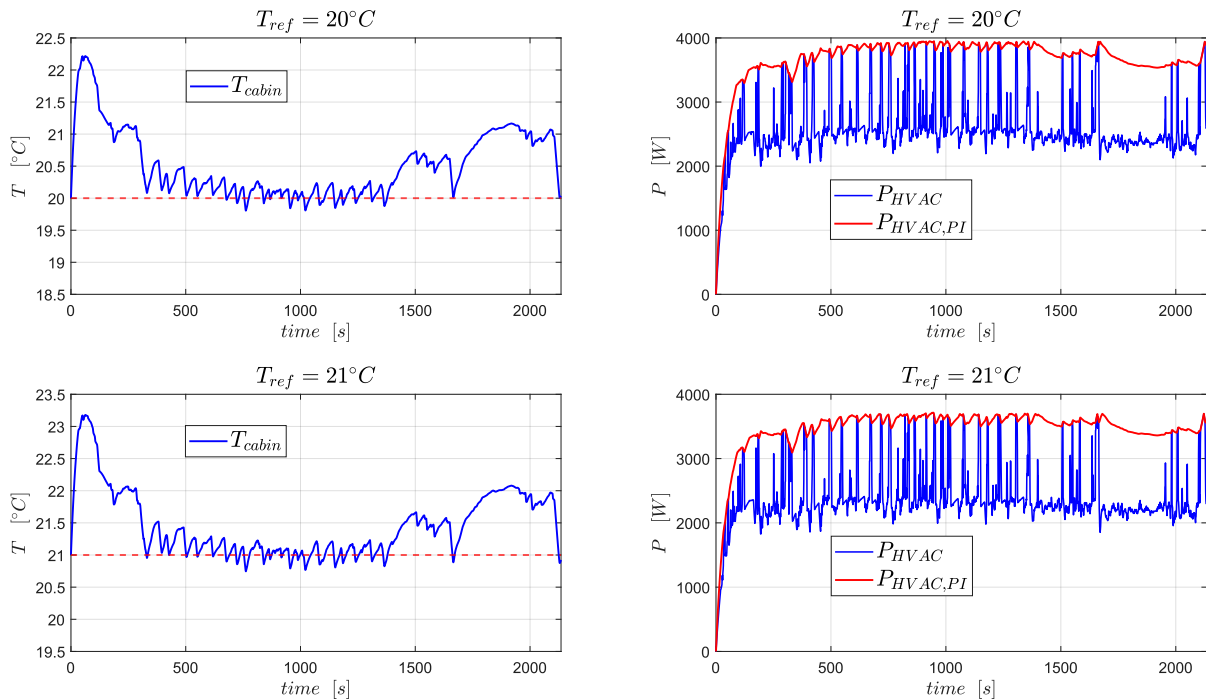


Figure 57: Temperature and HVAC battery power profiles with a target temperature of $20^\circ C$ (upper panel) and $21^\circ C$ (lower panel) along the EPA cycle

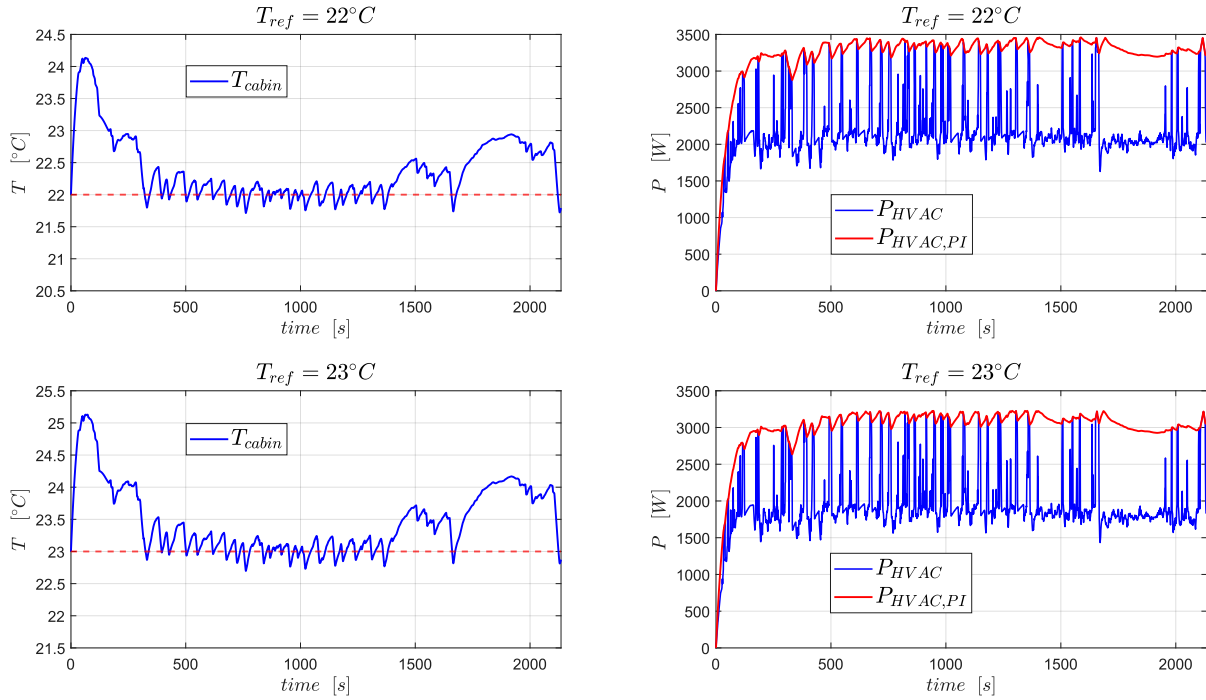


Figure 58: Temperature and HVAC battery power profiles with a target temperature of $22^\circ C$ (upper panel) and $23^\circ C$ (lower panel) along the EPA cycle

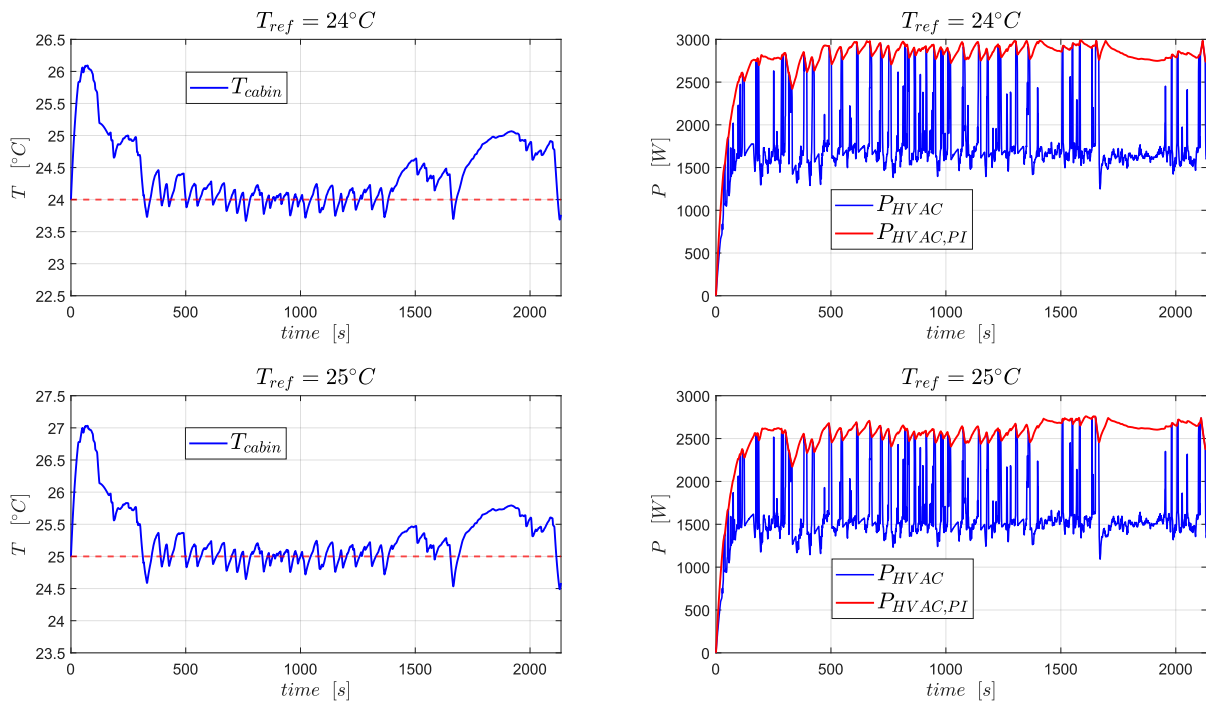


Figure 59: Temperature and HVAC battery power profiles with a target temperature of $24^\circ C$ (upper panel) and $25^\circ C$ (lower panel) along the EPA cycle

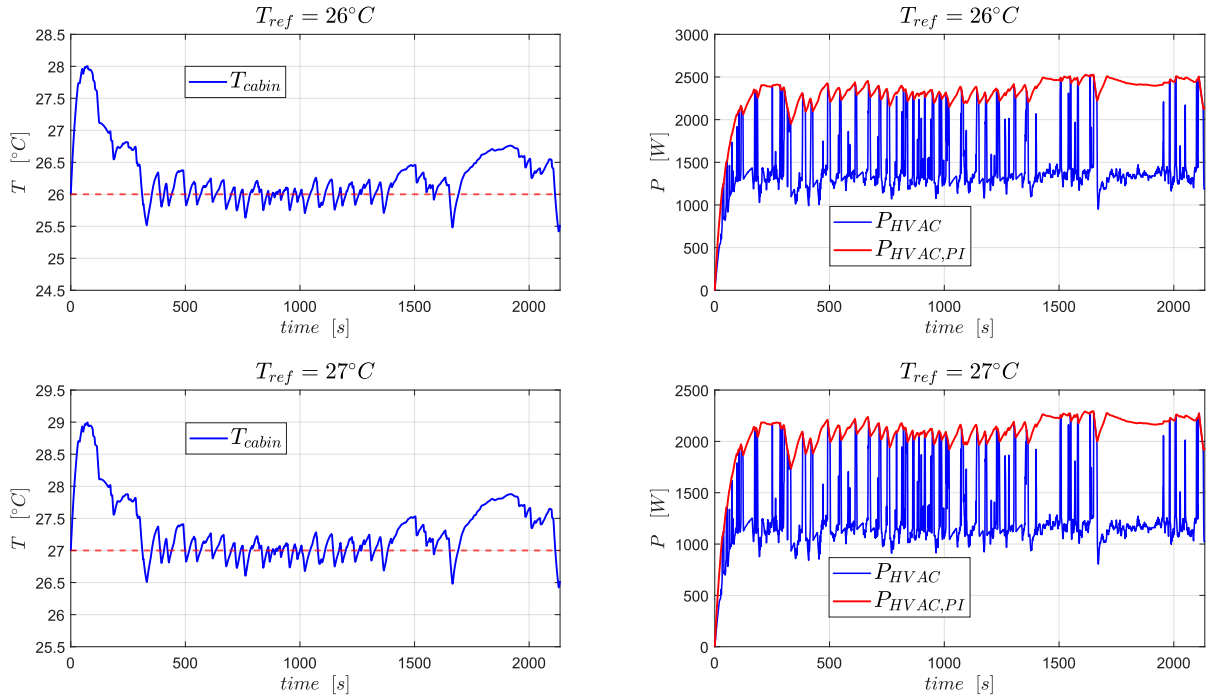


Figure 60: Temperature and HVAC battery power profiles with a target temperature of $26^\circ C$ (upper panel) and $27^\circ C$ (lower panel) along the EPA cycle

5.3.3 Results comment

Before delving into the analysis of the benefits carried by the IETM strategy, it is important to note that the initial temperature overshoot, occurring in the early part of the time scale, is not representative of the controller’s performance. This overshoot is a common feature in all the temperature profiles resulting from the dynamic response of the PI controller, as shown from Figure 51 to Figure 60. This simply happens because, since the tests started with a cabin’s temperature exactly equal to the reference temperature, the PI controller needs to accumulate some error before commanding a suitable response. As a matter of fact, if another cycle were followed in succession, this systematic temperature deviation from the target in the early part of the cycle would not occur.

To critically evaluate the results, let’s begin by analyzing the battery loads due to traction in the two different drive scenarios. Comparing Figure 49 and Figure 50, it is evident that the average power required during the EPA cycle is lower. The peak traction power request occurs in the initial part of the cycle, after about 200 seconds, and it does not even reach 40 kW. The remaining part of the cycle appears relatively regular, and the power stays on average values. In contrast, the WLTP drive schedule has a different power demand pattern. In the initial “low” phase, the power requirement is very low, mostly below 20 kW. Subsequently, there is a gradual increase in power demand through the “medium”, “high”, and “extra-high” phases. During

the “extra-high phase”, a peak power demand of over 40 kW is reached. These differences in power demand naturally affect the signals controlled by the IETM controller. If one compares the figures related to the WLTP cycle shown in 5.3.1, after the initial overshoot where the HVAC power allocation matches the reference power commanded by the PI controller, it can be observed an increase in temperature oscillation amplitude. The oscillating behavior in cabin temperature profiles, albeit with slower dynamics, arises from the rapid adjustment of HVAC power in response to traction conditions. The results for the EPA scenario as well, they align with the traction requests, especially for lower target temperatures. In the first 500 seconds, there is a reversal in the temperature trend, with the temperature rising up again after the initial overshoot. This behavior is influenced by the high-power demands observed during that time-frame, as shown in Figure 50. Furthermore, it is essential to note the direct relationship between temperature profiles and HVAC power profiles. Comparing the frequency of temperature oscillations (left panels) to that of HVAC power (right panels), one can see that the temperature oscillation frequency is orders of magnitude lower than the frequency of power delivered to the HVAC ($f = 10 \text{ Hz}$). This result is significant because the project’s foundations were based on this observation. The cabin’s temperature dynamics are relatively insensitive to rapid variations in the heat removed from the cabin if this happens over a small time window. Therefore, these results are consistent with the assumptions made in the project’s introduction.

5.4 IETM-related benefits

Once the response capability of the IETM controller has been verified, the last step to take on is the assessment of the benefits that it could bring. In order to evaluate the benefits coming from such a HVAC control strategy, the first thing to do is to set a baseline over which computes advantages or disadvantages deriving from using it. The results have been gathered both running over WLTP and EPA cycle. The baseline chosen assumes that inside the vehicle the target temperature is kept relying on the standard HVAC control, which is the PI-based control architecture. The test has been performed for several reference temperatures included between 18°C and 27°C . The battery degradation effect has been evaluated making the vehicle travelling 160,000 *km* over the same drive cycle repeated in succession, and looking at the final battery capacity. Instead, regarding the energy consumption advantages, these have been determined on the base of one single drive cycle travelled. For both the assessment scenarios, the respective boundary conditions can be found in Table 7.

5.4.1 Battery degradation improvements

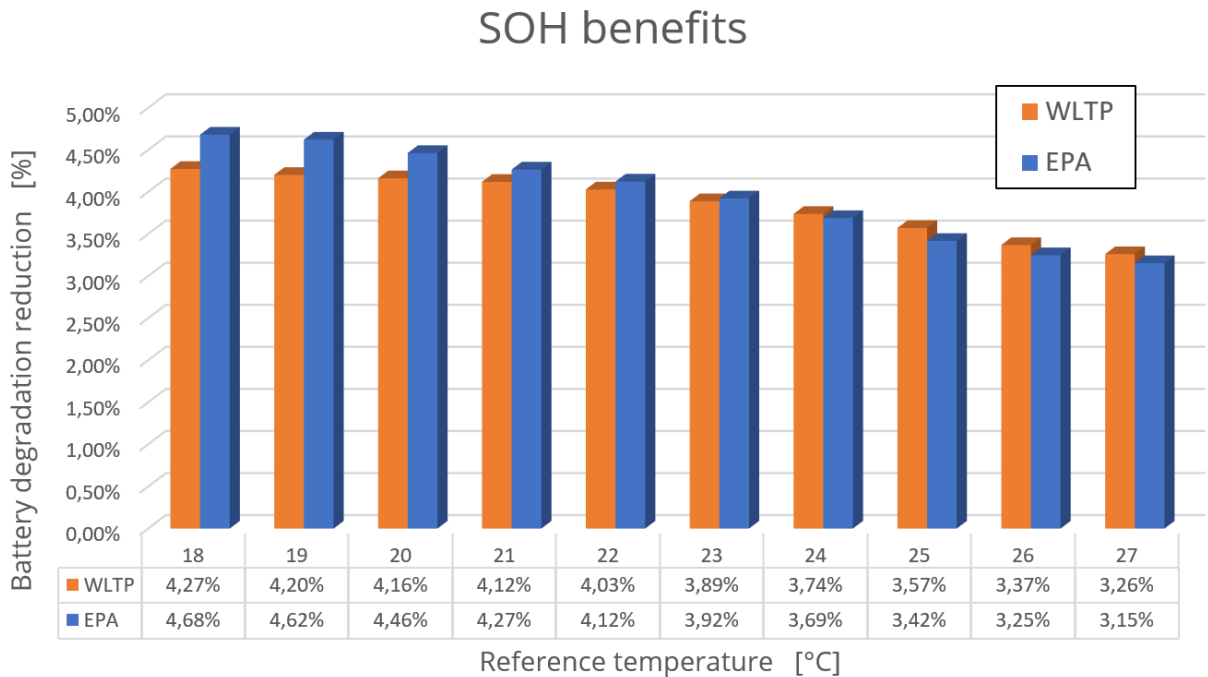


Figure 61: Battery degradation benefits with HVAC controlled through IETM controller rather than PI controller

The results, expressed in percentage, represent the additional battery capacity found for the battery pack at the end of the 160,000 *km* using the IETM strategy, as compared to the same distance travelled without the assistance of the controller. The improvements, ranging in the

interval between 3.1 % and 4.5 %, are in line with what one could have expected by such a strategy. Indeed, this is neither a strategy acting on the driving style, nor some improvement in powertrain efficiency. These last could have returned higher improvements, minimizing the traction power, which would have meant having a range of values of power to act on, that would be far larger than the one required by the HVAC. Aiming to explain the decreasing trend that occurs as the reference temperature within the cabin increases, this is due to the HVAC system's increased energy consumption necessary to maintain lower temperatures inside the cabin. Then, the IETM control can work on a higher power margin, limiting the damaging effect on the battery when needed, thus leading to greater improvements.

5.4.2 Energy consumption improvements

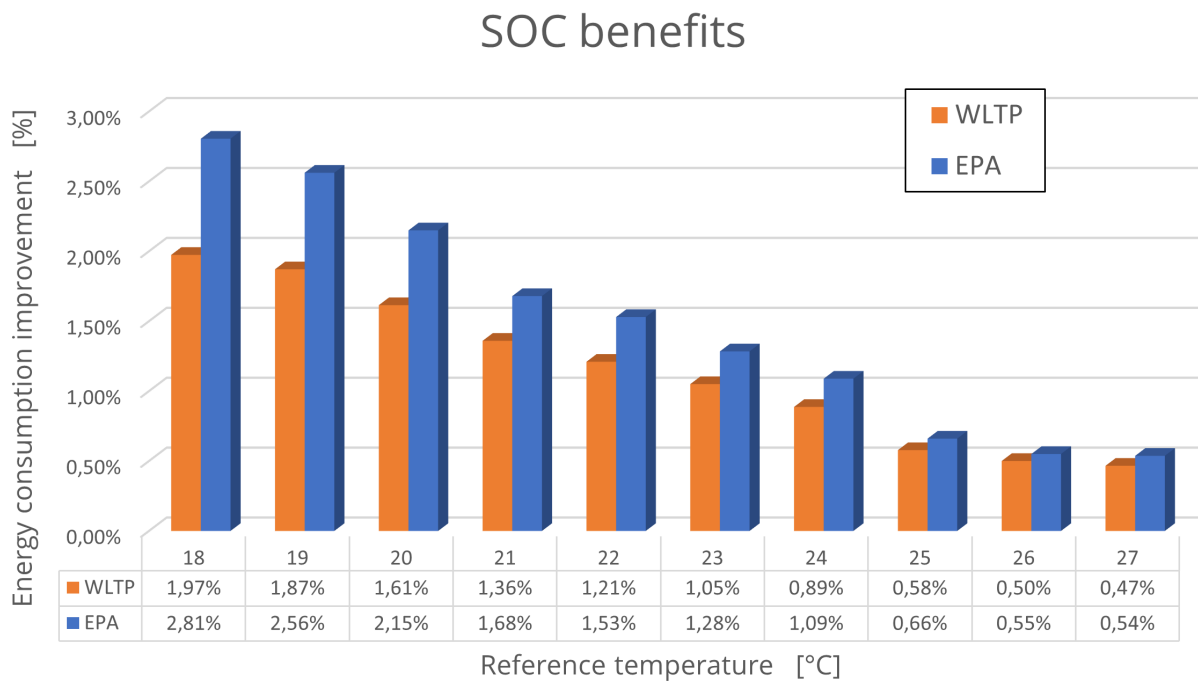


Figure 62: Energy consumption benefits with HVAC controlled through IETM controller rather than PI controller

It is worth noting that the strategy has been developed with the aim of increasing the battery lifespan, acting on the instantaneous minimization of the degradation undergone by the battery. According to this, even if one could imagine an improvement in energy consumption, this latter was not obvious, and it is to be considered as a side beneficial effect. The battery energy required to complete one cycle reduces of an amount included between 0.5 % and 2.8 %. Conversely to the trend showed for the battery degradation improvements, when it comes to energy consumption improvements it is naturally reversed. The further one is from the ambient temperature, the

faster the cabin's temperature dynamics evolves, causing it to rise rapidly. Since thermal comfort for passengers must also be ensured, larger and faster temperature fluctuations at lower reference temperatures lead to higher power demands to bring the temperature back to the target level. That is the same reason why the strategy shows lower benefits over the WLTP. Being more aggressive than EPA cycle, on the WLTP there will be more and larger oscillations.

6 Combined effect of eco-driving and IETM strategies

At the end, after the assessment of the IETM strategy, that was the target of this thesis project, we decided to quantify the advantages coming from using a combination of the two strategies whose development was involved in the broader project with Stellantis partnership: IETM strategy, and eco-driving strategy. The *eco-driving strategy* has been referred as **Cooperative Adaptive Cruise Control** (CACC), and it consists in an automated vehicle following longitudinal control. Namely, this type of control developed allows the ego vehicle to monitor and autonomously control its distance from the preceding vehicle, i.e. leading vehicle, acting on the acceleration command. This results in a smoothed velocity profile for the ego vehicle, that enables a reduced energy consumption. Here a brief description is given about the CACC, whose detailed design is accurately explained in [20].

The CACC is based on a model predictive control (MPC) algorithm. Essentially, with a period equal to the control horizon, the CACC of the ego vehicle receives relative velocity and relative position of the leading vehicle, and exploiting a certain predictive function, it can test different acceleration commands over a defined predictive horizon. Then, based on a cost function, the controller can check unfeasible conditions that may arise from some control actions, and evaluates the total cost over the predictive horizon for every admissible acceleration command. The one associated to the lower cost is taken, and applied to the vehicle over a certain control horizon before the command will be refreshed again.

It is important to anticipate as, though the main target of such strategy was the one of making the ego vehicle following the leading vehicle velocity pathway with a resulting improved energy efficiency, this strategy leads as well to a notable reduction in battery degradation. Like has been emphasized earlier, this strategy has direct consequences on the traction power required, that is the highest load on the battery. Thus, relevant improvements have been found for battery health as well. Before showing the results coming by merging the two strategies, it is worth noting that the two strategies are not fully independent one each other. The IETM controller takes decisions on the base of the current traction power demanded to the battery. Then, because the CACC directly affects the traction power demand, also the IETM control will return a different controlled power for the HVAC over the same drive cycle as without CACC turned on. However, merging the two strategies no synergy effect can be evidenced, but simply the benefits coming from both ones add up almost entirely. The results, shown as follows in Figure 63 and Figure 64, refer exactly to the same baseline as the one explained in Section 5.4.

6.1 Battery degradation improvements

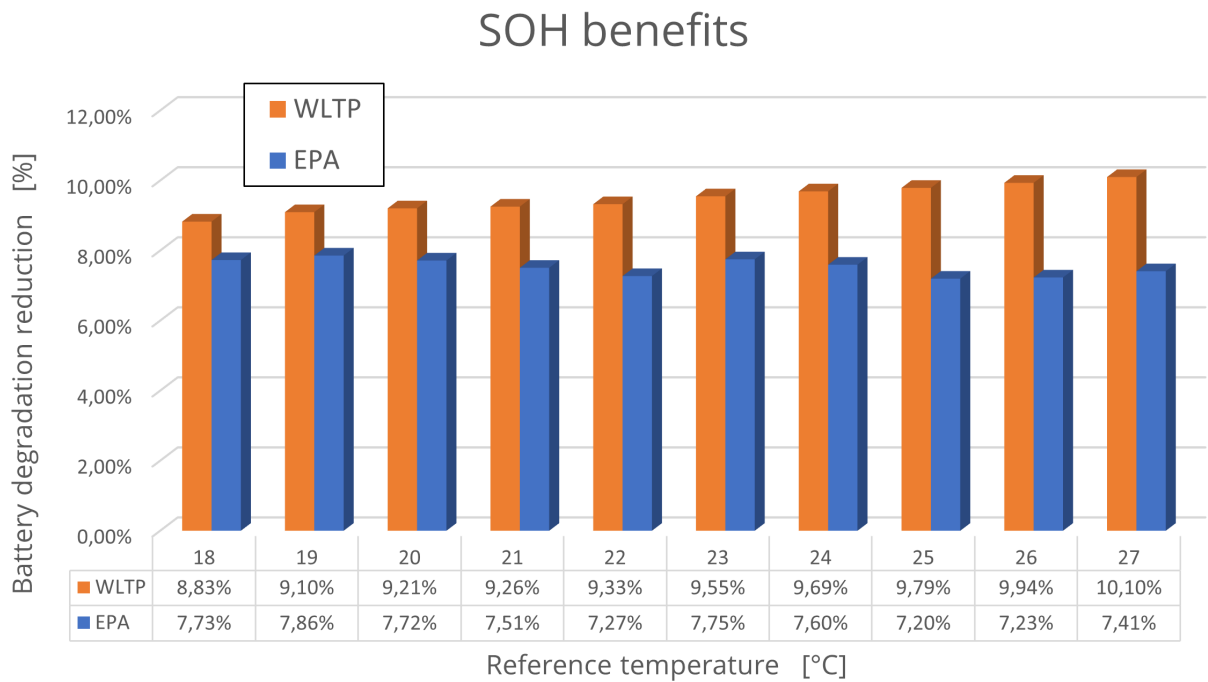


Figure 63: Battery degradation benefits with HVAC controlled through IETM controller and CACC enabled over HVAC controlled through PI controller and CACC disabled

The first thing to do is a comparison between the benefits found in terms of battery capacity saving and the ones in Figure 61. One can appreciate that, as it could have been possible to figure out a priori the improvements are higher and significant. After 160,000 *km* the battery capacity saved is between 7.2 % and 10.1 %. Another thing that stands out is the completely different trend for the improvements with the cabin comfort conditions variation, as compared to the one in Figure 61. This different result in trend comes from the superimposition of the two separated benefits: the one from the IETM strategy, and the one from the CACC. When they add up, it will result in a trend that will be decided by the most prevalent one of the two. Furthermore, the improvements over the WLTP cycle are lower than the one over the EPA for the same reference temperature, differently from what has been evidenced for the IETM-related benefits. This is a direct consequence of using the CACC. Indeed, being the WLTP a more aggressive drive schedule, the eco-driving strategy can actively smooth the velocity profile over an higher number of instants, resulting in a higher improvement.

6.2 Energy consumption improvements

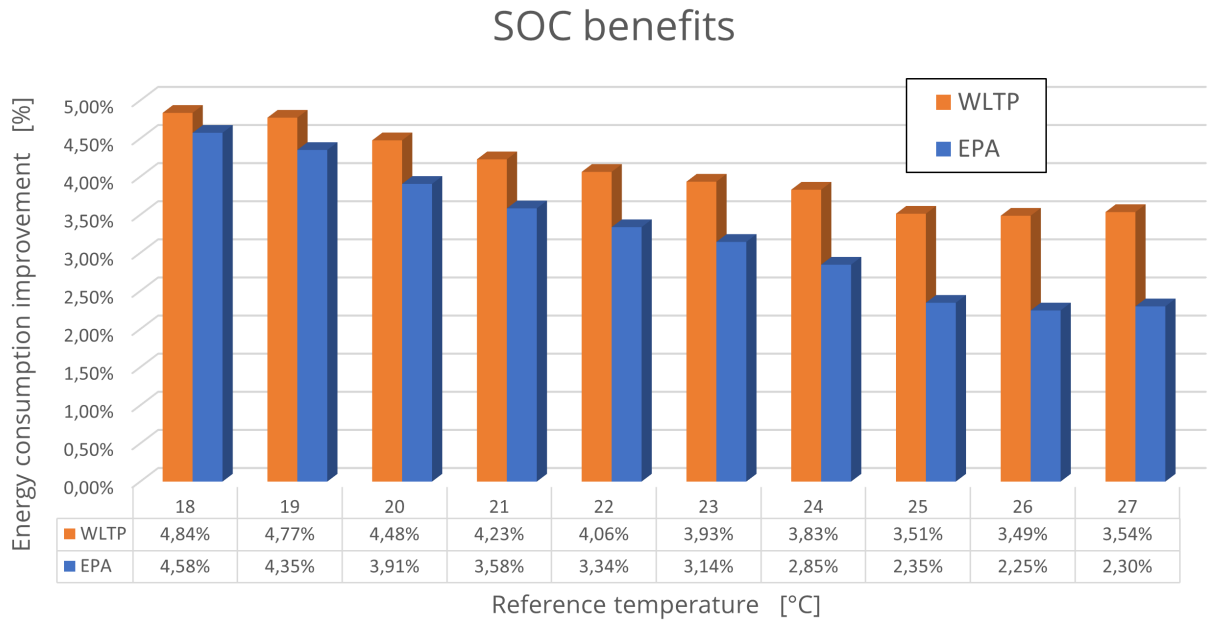


Figure 64: Energy consumption benefits with HVAC controlled through IETM controller and CACC enabled over HVAC controlled through PI controller and CACC disabled

The figure reported above clearly shows which are the advantages for the energy consumption deriving from a combined usage of both the strategies. A comparison arises spontaneously between the benefits here reported, ranging almost from 2.3 % to 4.8 %, and the ones coming from applying only the IETM controller, i.e. Figure 62. Apart from low temperature levels maintained inside the cabin, the driving effect for energy consumption improvements is brought by the CACC. Indeed, the latter mentioned strategy was specifically developed to achieve this result. The leading role of the CACC, as compared to the IETM controller, in providing energy efficiency improvements, can be also captured comparing the results over WLTC rather than EPA cycle. These are inverted with respect to what shown in Figure 62, meaning that CACC, capable of enhancing better results over more aggressive drive schedules, takes the lead in reducing the consumption.

7 Future developments

In the realm of future work, several promising avenues for further research activities emerge. Firstly, exploring the feasibility of real-time implementation and assessment of the IETM strategy using onboard vehicle systems represents a critical next step. This approach would provide insights into the real-world applicability and performance of the IETM controller under dynamic driving conditions. This possibility also would enable to check how far the real advantages coming from IETM application could set far from the ideal one outlined within this thesis project. Additionally, an in-depth analysis could be conducted to identify and prioritize the most impacting input parameters influencing the effectiveness of the IETM controller. Factors such as solar radiation, external temperature, and other environmental variables could be investigated to determine how their prediction could affect the strategy's outcomes. Understanding these key input variables would enable the fine-tuning of the IETM controller, that may arise the need for a MPC strategy for achieving better results and further enhance its benefits. These future research directions hold the potential to advance the field of battery electric vehicles' technology, and contribute to the ongoing development of sustainable and efficient transportation solutions.

8 Conclusions

In conclusion, this thesis project has made significant strides in enhancing the durability and energy efficiency of battery electric vehicles, by introducing the innovative Integrated Energy and Thermal Management (IETM) strategy. The positive results obtained underscore the potential of intelligent control systems to address critical challenges in the transition to sustainable transportation. This work not only provides valuable insights for the current state of battery electric vehicles, but also paves the way for continued advancements in this exciting field.

References

- [1] Alizadeh M., Dhale S., Emadi A., “Model Predictive Control of HVAC System in a Battery Electric Vehicle with Fan Power Adaptation for Improved Efficiency and Online Estimation of Ambient Temperature”, *IEEE*, 2021
- [2] Alizadeh M., Dhale S., Emadi A., “Real-Time Ambient Temperature Estimation Using Kalman Filter and Traction Power-Aware Cabin Climate Control in Battery Electric Vehicles”, *IEEE*, 2022
- [3] Haskara I., Hegde B., Chang C.F., “Reinforcement Learning Based EV Energy Management for Integrated Traction and Cabin Thermal Management Considering Battery Aging”, *IFAC-PapersOnLine*, vol. 55, Issue 24, pp. 348-353, 2022
- [4] IEA, “Energy and Air Pollution”, *IEA, Paris*, 2016
- [5] Buis A., “Sizing Up Humanity’s Impacts on Earth’s Changing Atmosphere: A Five-Part Series”, *NASA news*, 2019
- [6] IEA, “Global CO2 emissions from energy combustion and industrial processes, 1900-2022”, *IEA, Paris*, 2023
- [7] IEA, “The role of CCUS in low-carbon power systems”, *IEA, Paris*, 2020
- [8] IEA, “Global energy-related CO2 emissions by sector”, *IEA, Paris*, 2020
- [9] IEA, “Global CO2 emissions from transport by sub-sector in the Net Zero Scenario, 2000-2030”, *IEA, Paris*, 2022
- [10] IEA, “CCUS in Clean Energy Transitions”, *IEA, Paris*, 2020
- [11] IEA, “Electric car sales, 2016-2023”, *IEA, Paris*, 2023
- [12] IEA, “World gross electricity production by source, 2019”, *IEA, Paris*, 2020
- [13] “International Conference of Electrical and Electronic Technologies for Automotive”, 2017
- [14] Afrasiabian E., Douglas R., Best R., “Dynamic Modelling and Performance Prediction of a Multi-unit Baseline Air Conditioning System for a Generic Bus under Part-Load Conditions”, *SAE International Journal of Commercial Vehicles*, 2021
- [15] Rehan Mohsin Rashid, “Thermal Management of Vehicle Interior Temperature for Improvement of Fuel Economy”, *University of Windsor*, 2018
- [16] He H., Jia H., Sun C., Sun F., “Stochastic Model Predictive Control of Air Conditioning System for Electric Vehicles: Sensitivity Study, Comparison, and Improvement”, *IEEE*, 2018

-
- [17] Vemuri A. T., Stauder K., “How to Design Heating and Cooling Systems for HEV/EVs”, *Texas Instruments*, 2020
 - [18] Shaut S., Sawodny O., “Thermal Management for the Cabin of a Battery Electric Vehicle Considering Passengers’ Comfort”, *IEEE*, 2020
 - [19] Anselma P.G., Kollmeyer P., Lempert J., Zhao Z., Belingardi G., Emadi A., “Battery state-of-health sensitive energy management of hybrid electric vehicles: Lifetime prediction and ageing experimental validation”, *Applied Energy*, 2021
 - [20] Fiorillo C., “Energy optimization based on ADAS sensors and connectivity in electric vehicles”, *Politecnico di Torino*, 2023